TARGETED DELIVERY OF CARBON NANOTUBES TO CANCER CELLS

by

PAVITRA CHAKRAVARTY

Presented to the Faculty of the Graduate School of

The University of Texas at Arlington in Partial Fulfillment

of the Requirements

for the Degree of

DOCTOR OF PHILOSOPHY

THE UNIVERSITY OF TEXAS AT ARLINGTON

May 2010

To my “scientific mother” Ellen Vitetta,

who taught me not just to survive in chaos, but to actually *thrive* in it

(ES Vitetta, *J. Immunol*. 1994; 153; 1407-1420).

ACKNOWLEDGEMENTS

I would like to thank my mentor Dr. Ellen Vitetta for being a constant source of inspiration and for providing one of the primary reasons to persist in this project – the sheer joy of sitting in her room and gloating over a challenge that was overcome. She taught me how empowering freedom of thought could be and how setting the mind free truly enabled you to walk among giants. Her humility and appreciation of the ridiculous belie her greatness as a scientist.

I thank my dissertation committee members Drs. Robert Eberhart, Philip Thorpe, Padmakar Kulkarni and Liping Tang for their valuable input to my work. My project had different challenges that matched areas of interest specific to each of them and I have benefitted tremendously from this.

I thank Drs. Laurentiu Pop and Radu Marches, two wonderful scientists who have been a big help. Dr. Pop trained me initially when I joined the lab and still continues to provide technical assistance whenever asked, interspersed with some very serious efforts at eliminating me from this planet. Dr. Marches was my co-mentor on my project and I am incredibly lucky to have worked with such a knowledgable biochemist. His common sense and practicality have been instrumental in solving many challenges on the project.

I thank our collaborators Drs. Rockford Draper, Pantano, Winston Layne, Hadi Yehia, Pooja Bajaj and Robert Azad from UT Dallas. They taught me techniques that have been key to finishing this project. Drs. Draper and Pantano in particular, have been incredibly helpful, motivating and supportive of all my activities at UT Dallas.

I thank my mommies on the floor, Linda Berry, Catherine Holloway and Rhonda McCracken of the administrative staff in the Cancer Immunobiology Center for providing such a helpful and warm atmosphere – they have always been the solid pillars of support that I have

leaned on so many times. I thank Kay Emerson for her constant support and love and her patience in bailing me out of many troublesome situations that I have landed myself in during the course of graduate school.

I thank Kelly Mapes for being such a great buddy in addition to being a wonderful scientific resource who has helped me troubleshoot problems on my project. I thank Drew Ivey who does such a thankless tough job with such a phenomenal sense of humour. I thank Ayesha Ahmed, Ryan Willingham and Dr. John Gu for all their help in the laboratory.

I thank my wonderful fellow students at the CIC, Dr. Kimberly Brooks for her scientific accumen and common sense, Dr. Lydia Tsai for her incredible cheeriness and grit in the face of seemingly insurmountable problems, Andrew Bitmansour for showing me how a guy can cook and clean better than a woman and still look macho doing it, soon-to-be Dr. Praveena Marconescu for being a source of knowledge, scientific and otherwise and for her peppy personality, Allison Case for her strength of character and kindness, Megan Wachsmann whose youth belies her wisdom and maturity and the two Angelas – young, bright and immensely capable. I want to be like all you guys when I grow up.

I thank my friends and family who have supported and encouraged me all these years. My uncle, Sreedharan, who has been instrumental in ensuring that I had a good life and career and sacrificed so much to make that happen, my aunt Vijayanthi, who showed by example how sweet the human spirit can be and how giving, my mother Kausalya who is one of the toughest women I know and my most devoted cheerleader, my inlaws Sridevi and Sreenivasan who are so loving and supportive and genuinely proud of what I have accomplished and my cousin Vikram who is one of the nicest and smartest guys I have ever had the good fortune of growing up with.

I thank my husband Srinath Chakravarty for his support of this very long journey that I undertook – a journey where I mistakenly thought the ends would justify the means. I thank him

for opening my eyes to the wonder of Hindu philosophy, for his intelligence, sense of humour and strong values.

Finally, I thank my son Raman Chakravarty for showing me that sweetness such as what I experience with him can exist. For me he is truly “the one for whom the sun does shine” (Ramesses II of his wife Nefertari).

March 29, 2010

ABSTRACT

TARGETED DELIVERY OF CARBON NANOTUBES

TO CANCER CELLS

Pavitra Chakravarty, PhD

The University of Texas at Arlington, 2010

Supervising Professor: Ellen S. Vitetta

CD22 is broadly expressed on human B cell lymphomas. Monoclonal anti-CD22 antibodies (MAbs) alone, or coupled to toxins, have been used to selectively target these tumors both in severe combined immunodeficient (SCID) mice with xenografted human lymphomas and in patients. Single-walled carbon nanotubes (CNTs) attached to antibodies or peptides represent another approach to targeting cancer cells. CNTs convert absorbed near-infrared (NIR) light into heat, which can thermally ablate cells in the vicinity of the CNTs.

We have made MAb-CNT constructs where the MAb was either noncovalently or covalently coupled to CNTs, and investigated their ability to bind specifically to cells and to thermally ablate them after exposure to NIR light. The specific binding of these MAb-CNT constructs to antigen-positive and antigen-negative cells was demonstrated *in vitro* by using $CD22^{+}CD25^{-}$ Daudi cells, $CD22^{-}CD25^{+}$ phytohemagglutinin (PHA)-activated normal human peripheral blood mononuclear cells (PBMCs) and CNTs coupled non-covalently or covalently to either anti-CD22 or anti-CD25. We then demonstrated that the MAb-CNTs could bind to tumor cells expressing the relevant antigen but not to cells

lacking the antigen. Furthermore we showed that, following exposure to NIR light, the cells could be thermally ablated. We also determined the stability of the MAb-CNTs in conditions designed to mimic the *in vivo* environment, *i.e.* mouse serum at 37^{o}C.

We then use the intrinsic Raman signature of CNTs to study the circulation and tissue distribution of intravenously injected MAb-CNTs in a murine xenograft model of lymphoma *in vivo* over a period of 24 hrs. We demonstrated that the MAb-CNTs have a short half-life in blood and that most of them are cleared by the reticuloendothelial system (RES). In the current embodiment, these constructs would therefore be of limited effectiveness *in vivo*

TABLE OF CONTENTS

LIST OF FIGURES

LIST OF TABLES

LIST OF ABBREVIATIONS

ABTS	2, 2'-azino-bis(3-ethylbenzothiazoline-6-sulfonic acid)
AFM	Atomic Force Microscopy
ATCC	American Type Culture Collection
B-CNT	Biotinylated CNT
B-HRP	Biotinylated horseradish peroxidase
BCA	Bicinchoninic acid
BL	Burkitt's lymphoma
B/NA	Biotin/Neutravidin
BSA	Bovine serum albumin
CIC	Cancer Immunobiology Center
c-CNT	Carboxylated CNT
CNT	Carbon nanotube
CPM	Counts per minute
DAPI	4',6-diamidino-2-phenylindole
DI	Deionized
DNA	Deoxyribonucleic acid
DOTA	1,4,7,10-tetraazacyclododecane-1,4,7,10-tetraacetic acid
Dox	Doxorubicin
DSPE-PEG (2000)-amine	1,2-distearoyl-*sn*-glycero-3-phosphoethanolamine-*N*-[amino(polyethylene glycol) 2000]
DSPE-PEG (2000)-biotin	1,2-distearoyl-*sn*-glycero-3-phosphoethanolamine-*N*-[biotinyl(polyethylene glycol) 2000]

DTPA	Diethylenetriaminepentaacetic acid
DTT	Dithiothreitol
ECL	Enhanced chemiluminescence
EDC	1-ethyl-3-[3-dimethylaminopropyl]carbodiimide hydrochloride
EGFP	Enhanced green fluorescent protein
ELISA	Enzyme-Linked Immunosorbent Assay
FCS	Fetal calf serum
FITC	Fluorescein-isothiocyanate
Gd	Gadolinium
GNP	GNR-embedded polymeric nanoparticles
HD	Hydrodynamic diameter
Hr	Hour
GAMIg	Goat anti-mouse Immunoglobulin
HBSS	Hanks' Buffered Salt Solution
HiPCO	High-pressure Carbon Monoxide
ICP-MS	Inductively coupled plasma-mass spectrometry
i.p.	Intraperitoneal
i.v.	Intravenous
MAb	Monoclonal antibody
MAb-NA	Monoclonal antibody-Neutravidin
Mab-NA-B-CNTs	Mab-NA coupled to B-CNTs
MAb-c-CNTs	MAb coupled to c-CNTs
MBS	m-maleimidobenzoyl-N-hydroxysuccinimide ester
MES	2-[*N*-morpholino]ethane sulfonic acid
Min	Minute

MRI	Magnetic Resonance Imaging
NA	Neutralite Avidin
NCI	National Cancer Institute
NHS	N-hydroxysuccinimide
NIR	Near-infrared
PAGE	Polyacrylamide gel electrophoresis
PBMC	Peripheral blood mononuclear cells
PBS	Phosphate-buffered saline, pH 7.4
PBST	Phosphate-buffered saline Tween-20
PDT	Photodynamic therapy
PE-SA	Phycoerythrin-Streptavidin
PFA	Paraformaldehyde
PHA	Phytohemagglutinin
p.i.	Postinjection
PPM	Parts per million
PVDF	Polyvinylidene difluoride
RBM	Radial breathing mode
RES	Reticuloendothelial system
RPMI	Roswell Park Memorial Institute
SCID/NOD	Severe combined immunodeficient/Nonobese diabetic
SDS	Sodium dodecyl sulfate
Sec	Second
TBST	Tris buffered saline Tween-20
TEM	Transmission electron microscopy
TEMED	N,N,N',N'-Tetramethylethylenediamine

TGA	Thermal Gravimetric Analysis
UTSWMC	University of Texas Southwestern Medical Center
UV-Vis-NIR	UV-Visible-Near-infrared
V	Volts
WB	Western blot
WST-1	4-[3-(4-iodophenyl)-2-(4-nitrophenyl)-2H-5-tetrazolio]-1,3-benzene disulfonate

CHAPTER 1

INTRODUCTION

1.1 Cancer as a disease

A total of 1,479,350 new cancer cases and 562,340 deaths from cancer were estimated to occur in the United States in 2009. Cancer death rates decreased in men by 19.2% between 1990 and 2005 and in women, rates decreased by 11.4% between 1991 and 2005 [1]. Although progress has been made in reducing the incidence and mortality rates and improving survival, cancer still kills more people than heart disease in persons younger than 85 years of age. Expenditures for oncology-related products today represent almost 10% of the $430 billion worldwide market for pharmaceuticals and the market is expected to exceed $60 billion[2]. It is important that further progress be accelerated in cancer prevention, early detection, diagnosis and treatment.

1.1.1 Surgery

Surgery is the oldest form of cancer treatment and is highly effective. It is sometimes used to reduce a tumor size (a procedure called debulking) so that radiation and chemotherapy can be more effective. It is also performed when the tumor has not spread to other areas of the body (curative surgery). It can also be used to remove a tumor that is causing pain or other symptoms and to restore comfort and quality of life without affording a cure (palliative surgery). Surgery is not highly effective once a cancer has metastasized. While surgery is an effective cancer treatment for many types of cancer, the location of the cancer and its growth pattern will determine whether it is the most effective approach. General risks include trauma, bleeding, infection and reactions to anesthesia [3].

1.1.2 Radiation

Radiation has been used for cancer treatment for decades and is available in several different forms[4]. Radiation is generally targeted locally, either to primary tumors or to large, well-defined metastases. While radiation is capable of eliminating some tumors on its own, it is used in combination with chemotherapy to shrink tumors prior to surgical resection or to provide palliation. However, the hypoxic nature of tumors can reduce the effectiveness of radiation therapy since it works best under oxygenated conditions. Radiation therapy is associated with both acute effects such as skin irritation and myeloablation, as well as chronic effects that occur months to years later, such as nerve injury, renal failure, fibrosis and an increased risk of developing other cancers [5].

1.1.3 Chemotherapy

Chemotherapy or “chemical treatment” has been used since the days of the ancient Greeks. However, chemotherapy for the treatment of cancer began in the 1940s with the use of nitrogen mustard [6]. Cancer-related chemotherapy drugs and biological treatments comprise 48% and 15% of the total market of oncology-related products. The major classes of chemotherapeutic agents based on their chemical structures are deoxyribonucleic acid (DNA) alkylating agents, anti-metabolites, platinum compounds, topoisomerase interactive agents and anti-microtubule agents. Most chemotherapeutic drugs such as doxorubicin, vincristine, cyclophosphamide, topotecan and paclitaxel target rapidly growing cancer cells by interfering with DNA replication or cell division. However, because these agents affect all rapidly proliferating cells, they are associated with a variety of side effects such as fatigue, nausea, diarrhea, mouth sores, hair loss, anemia and sometimes, death [7]. It has also become apparent that human cancers of any given histological type have great genetic diversity and only a subset of patients are responsive to any new agent. Even among those that respond, human tumors can contain sub-clones that become drug-resistant. Because of resistance to single agents,

combination therapy is essential for tumor eradication and cure. Trials should combine targeted drugs and cytotoxics in a more effective manner [2].

1.1.4 Hypothermia

Dr Temple Fay (1895-1963) [8] hypothesized that differences in location of cancer growths was due to temperature and found a decrease of 12–22 °F below the knees and elbows while common cancerous sites, were mostly located in areas with higher temperatures [9]. He found that local hypothermia applied to involved areas, controlled pain, retarded malignant cellular metabolism and was bacteriostatic and anti-inflammatory [10]. It was found that in dogs treated with alkylating agents, there was hypoplasia in the bone marrow of the control animals while in the hypothermic animals, the levels were considered normoblastic [11]. Other treatments found the disappearance of tumors in hypothermic conditions [12-13]. In normal rat brains, it was found that hypothermia in combination with photodynamic therapy (PDT) reduced the damage to normal tissue relative to hyperthermia or normal conditions in combination with PDT. *In vitro* studies found that a combination of hyper-, hypothermic therapy (HIT) worked better than either treatment alone on cancer cells. Five cycles of HIT killed all colon cancer, human basal cell carcinoma and melanoma cells. In addition it was also found that HIT enhanced the susceptibility of the melanoma cells to a chemotherapeutic agent [14]. However, HIT has not always been effective in the treatment of cancer and it has been thought that competing physiological mechanisms of hypo- and hyperthermia might be the cause. If one considers the extremely complex processes involved in thermoregulation (heat transfer by conduction, convection, radiation and evaporation, metabolic rate, etc) [15] this is not surprising. Treatment in rats showed that manipulation of tumor physiology – using hypothermia to reduce tumoral interstitial fluid pressure (IFP), could reduce the efflux rate of a chemotherapeutic drug from the tumor, thereby increasing the mean residence time of the drug [16].

1.1.5 Hyperthermia

Hyperthermia is a therapeutic procedure used to raise the temperature of a region of the body affected by cancer. One of the means to accomplishing this was using the hot water suit developed by the National Cancer Institute (NCI) in 1970s-1980s [17]. A synergistic interaction between heat and radiation dose as well as various cytostatic treatments have been validated in preclinical studies [18-20].For the combination of radiotherapy and hyperthermia, the effect is greatest for simultaneous application. With chemotherapeutic drugs, several types of effects are seen with the interaction of heat with drugs such as, supra-additive (alkylating agents, platinum compounds), threshold behavior (doxorubicin) and independent or additive (fluorouracil, taxanes and vinca alkaloids). Hyperthermia can be induced locally, regionally, interstitially and on the whole body [21]. The concept of heat-induced tumor cell destruction should be viewed from the perspective of the critical temperature threshold of about 43^{o}C [22]. Chromosomal protein inactivation and nuclear damage may be of minor importance when heat is the only therapy; however, it can contribute to the improved tumor control after combined therapy with hyperthermia and chemotherapy/radiotherapy [23-24]. Primary cytoplasmic destruction is observed where hyperthermic treatment stimulates increased lysosomal activity in the cytoplasm [25]. The second important heat-induced alteration is inhibition of respiratory metabolism without a similar depression of anaerobic glycolysis. This leads to a higher amount of lactic acid, and because solid tumors have a slow exchange between intracellular fluid and blood, the acidity will increase, intensifying the activity of lysosomal enzymes [26]. Also, massive hemorrhage, coagulative necrosis and rupture of blood vessels were evident and this became progressively severe *in situ* [27-28]. Also, some membrane lipids begin to melt at 43^{o}C [29].

1.1.6 Targeted therapy

Targeted therapy is the use of special drugs and other substances to attack specific molecular features or pathways involved in the development of cancer. Unlike chemotherapy drugs, targeted therapies can often destroy cancer cells with less damage to surrounding healthy tissue [30]. Kinases have become one of the most intensively pursued classes of drug targets with 30 distinct kinase targets entering Phase I clinical trials. Deregulation of kinase function has been implicated in several disorders and hence there is a great deal of interest in the development of small molecule kinase inhibitors. Small molecule inhibitors or tyrosine kinase inhibitors (TKI) such as Imatinib Mesylate (Glivec™) that compete with adenosine triphosphate (ATP) and inhibit kinase activity have been effective in the treatment of chronic myeloid leukemia (CML, kinase: breakpoint cluster region-V-abl Abelson murine leukemia (BCR-ABL)) and gastrointestinal stromal tumors (GIST, kinase: KIT). In spite of a high degree of conservation in the ATP binding site, highly selective small molecules can be developed. Inhibition of kinase activity in normal cells can be tolerated, presenting a therapeutic window for the selective killing of tumor cells [31]. The epidermal growth factor receptor (EGFR) is also a rational target for small-molecule inhibitors such as gefitinib (Iressa™) and erlotinib (Tarceva™). Sorafenib (Nexavar) and sunitinib malate (Sutent™) are new dual-action kinase inhibitors [32] .

MAb therapies have been approved for the treatment of lymphoma (anti-CD20 Rituxan™), breast cancer (anti-human epidermal growth factor receptor 2 (ERBB2) Herceptin™), colon cancer (anti-EGFR Erbitux™, anti-vascular endothelial growth factor (VEGF) Avastin™), leukemia (anti-CD52 Campath™) to name a few [32] . Putative mechanisms of antibody-based therapy can be subcategorized into direct and indirect actions. The first mechanism includes blocking the binding of a ligand to its receptor (Avastin™ binding to VEGF [33]), targeting epitopes on the extracellular domain of cell-

surface receptors such as EGFR and interfering with its activation (Erbitux™ and Vectibix™ [34]), inducing apoptosis (Rituxan™ bound to two CD20 molecules or cross-linked by other anti-antibodies [33]), inhibiting cell proliferation (Herceptin™ and Erbitux™ [33]) and providing additional functionality of the MAb conjugated to radionuclides (anti-CD20/^{90}Yttrium: Zevalin™, anti-CD20/^{131}Iodine: Bexxar™), toxins (anti-Interleukin-2 receptor/diphtheria toxin: Denileukin diftitox or Ontak™), drugs (anti-CD33/ calicheamicin: Mylotarg™) or enzymes (anti-carcinoembryonic antigen (CEA) F(ab')$_2$/carboxypeptidase G2) [35-36]. The second mechanism is mediated by the immune system and includes complement-dependent cytotoxicity (CDC, anti-CD52 Campath™ [34]) and antibody-dependent cellular cytotoxicity (ADCC, Rituxan™ and Herceptin™ engage both activation (FcγRIII) and inhibitory (FcγRIIB) antibody receptors on myeloid cells, thus modulating their cytotoxic potential [37]). Studies have shown the benefit of combining antibody therapy with chemotherapy [33, 38].

Although the development of therapeutic MAb therapies requires a relatively complex process and high costs, chimeric and humanized MAbs have higher marketing approval rates (18% and 24% respectively) than small-molecule agents (5%). The molecular weight (MW) of MAbs (150 kDa) is larger than TKI (500 Da), resulting in inefficient delivery and poor tissue penetration, tumor retention and clearance. MAbs also cannot pass though the cell membrane (like small molecules can) and can only act with high specificity on molecules expressed on the cell surface (and then be internalized) or secreted. MAbs are frequently used for hematological malignancies while small molecule inhibitors are used for solid tumors [32]. Antibody engineering is also used for improving the structure of MAbs such as developing largely human or fully human MAbs, manipulating the affinity of FcR for the Fc domains, improving the affinity of the MAb for its antigen and altering valence and size [34].

Another problem with MAb therapy is the nonspecific uptake of the antibody molecules into the RES such as the liver, spleen and lung. Cell-surface binding peptides are useful alternatives for targeting cancer cells. Peptides smaller than MAbs, are generally not cleared by the RES. They are chemically stable and easy to derivatize. They are however, susceptible to proteolytic degradation *in vivo*. Octreotide is a somatostatin cyclic octapeptide analog that inhibits growth hormone secretion. It was evaluated in rats and humans and found to have resulted in a substantial improvement of hormonal symptoms in more than 90% of patients with tumors [39] .

1.2 Nanotechnology in cancer

While the Food and Drug Administration (FDA) stipulates that the currently accepted dimensions of nanoparticle therapeutics be in the range of 10-100 nm [4], this definition excludes numerous devices of micrometer dimensions, a scale that is included within the definition of nanotechnology. A more practical definition of nanotechnology, unconstrained by arbitrary size limitations has been proposed: *The design, characterization, production and application of structures, devices and systems by controlled manipulation of size and shape at the nanometer scale (atomic, molecular and macromolecular scale) produces structures, devices and systems with at least one superior characteristic or property* [40]. The first-pass elimination by the kidneys (sieving coefficients for the glomerular capillary wall) is a threshold hydrodynamic diameter of 10 nm for deformable, neutral polymers [41], 5-6 nm for globular proteins [42] and 5.5 nm for zwitterionic inorganic metal-containing nanoparticles [42]. The vasculature in tumors is leaky to macromolecules, lymphoid drainage is poor and macromolecules accumulate by a process called “enhanced permeation and retention (EPR) effect” [43]. Nanoparticles in the size range of 50-100 nm will be restricted from exiting normal vasculature (that requires the size to be between 1 – 2 nm) and only exit tumor vasculature. They are characterized by high surface-to-volume ratios (carbon nanotubes, for example) and so it

is critical to control their surface properties. Their ultimate fate in the body is determined by their interactions with their local environment which depends on a combination of size and surface properties. Nanoparticles that have been sterically stabilized by polyethylene glycol (PEG) and have surface charges that tend to be slightly positive, negative or neutral, tend to have minimal homotypic and heterotypic interactions. Larger surface charges increases macrophage scavenging which in turn leads to greater clearance by the RES [44].

The addition of targeting ligands provides specific interactions with cell-surface receptors which are known to be increased in number on cancer cells [45]. The targeting ligands bind to the receptors and enter the cell by receptor-mediated endocytosis. Recent work has shown that specific targeting and receptor-mediated endocytosis did not change the levels of accumulation or retention of the nanoparticles at the tumor site; however, it did improve the localization of the nanoparticles within cancer cells and led to more pronounced treatment efficacy and better anti-tumor effects, relative to untargeted nanoparticles [46-51] .

In theory, nanoparticles can carry large quantities of therapeutic (drugs of any type and number) or imaging payloads and protect them from degradation. Their constituent materials might provide image-enhancement properties such as iron oxide for magnetic resonance imaging (MRI) and quantum dots for imaging [52]. They can contain multiple targeting ligands that can allow multivalent binding to cell-surface receptors – this multivalency can lead to increased avidities even though the affinity of the targeting moiety might not be very high. Nanoparticles can also carry multiple types of drug molecules so as to permit combination therapy. Drug release kinetics can be designed to match the properties of the nanoparticles. They also have the ability to bypass multidrug resistance mechanisms since they can bypass protein pumps (glycoprotein P, for example) and be endocytosed [44, 53].

1.2.1 Liposomes

Liposomes (~ 100 nm and larger) are self-assembling closed colloidal structures composed of lipid bilayers, in which the outer lipid bilayer surrounds a central aqueous space. The unmodified phospholipid surface of liposomes can attract plasma proteins and thus the recognition by the RES system and their rapid clearance from the circulation. Stealth liposomes have solved this problem, yielding liposomes with a significantly increased half-life [54-55]. Currently, several cancer drugs are being carried by liposomal-based systems such as the anthracyclines doxorubicin (Doxil™, Myocet™) and daunorubicin (DaunoXome™). They have both been approved for the treatment of metastatic breast cancer and Kaposi's sarcoma [44]. They are mainly used to solubilize drugs and provide a longer half-life than the free drug. However, they do not provide control for the time of drug release, and in most cases, do not achieve effective intracellular delivery of the drug molecules. They appear to have reduced toxicity relative to the free drug; however, there has been the emergence of other toxicities [44]. There is also a trend towards higher liposomal uptake by smaller tumors, suggesting that the tumor volume (or stage of development) is important for liposomal uptake [56]. The next generation of liposomes will be immunoliposomes that can selectively deliver the drugs to the desired site [44, 53]. The only targeted liposomes in the clinic are MBP-426 which contains cytotoxic platinum-based oxaliplatin and SGT-53, a liposome coding for the tumor suppressor P53. MCC-465 which is an immunoliposome-encapsulated doxorubicin tagged with PEG and the $F(ab')_2$ fragment of the MAb, GAH is also being evaluated in clinical studies [57]. Liposomes are constantly being refined for novel and more efficacious drug-delivery at the tumor site [52].

1.2.2 Polymeric nanoparticles

Covering nanoparticles with a hydrophilic coating protects them from macrophage uptake. The increased hydration makes the nanoparticles more water-

soluble and less sensitive to enzymatic degradation [58-59]. Polymer-based drug delivery has grown exponentially over the past decade with the advent of biodegradable polymers. In polymers, drugs are dissolved, entrapped, encapsulated and covalently attached to the polymer matrix. An advantage of polymer therapeutics is the versatility of synthetic chemistry which allows the tailoring of molecular weight, addition of biomimetic features and even the possibility of including bioresponsive elements. Generally, polymers that are used for the preparation of nanoparticles fall into 2 major categories: natural (albumin, chitosan, heparin, etc) and synthetic (poly-L-lactide (PLLA), poly-L-glutamate (PLGA), poly-[D,L-lactide-co-glycolide], PEG, etc) [60].

1.2.2.1 Polymer – drugs

Polymer formuation of paclitaxel bound to albumin (Abraxane™ or ABI-007) was approved for the treatment of metastatic breast cancer [61-62].

1.2.2.2 Polymer – PEGylated protein

Several PEGylated proteins (enzymes, cytokines) have been approved or are in clinical trials. PEGylation of proteins provides a way to improve solubility, reduce immunogenicity, prevent rapid renal clearance and prolong plasma half-life [63]. PEG-L-asparaginase (Oncospar™) [64], PEG-granulocyte colony-stimulating factor (GCSF) (Neulasta™) [65], styrene maleic anhydride-neocarzinostatin (SMANCS™) [43, 66] and PEG-recombinanant arginine deaminase (PEG-rhArg) [67] are being used for the treatment of acute lymphoblastic leukemia and lymphoma, prevention of neutropenia, hepatoceullar carcinoma and hepatocellular carcinoma respectively. PEG-inteferon (IFN)-α2a (PEGASYS™), PEG- inteferon-α2b (PEGINTRON™) have been clinically approved for hepatitis C therapy [68]. Because of the advantage of prolonged half-life of PEG-IFN-α conjugates, they can be given by subcutaneous injection every 12 weeks instead of 3 times per week for free IFNs.

1.2.2.3 Synthetic polymer – drugs

Since the conjugation of PEG to proteins was so successful, it was also used for conjugation to drugs. PEG-conjugated chemotherapeutics such as PEG-irinotecan, PEG-SN-38 and in Phase I clinical trials [69]. However, because of the limited number of drug molecules that can be conjugated to PEG, other polymers have been considered. These include poly-L-glutamic acid (PG) and *N*-(2-hydroxypropyl) methacrylamide (HPMA). PG improved the half-life of paclitaxel and topothecan (an analogue of camptothecin) from 21.8 and 3 hrs to 70-120 hrs (PG-Paclitaxel, Xyotax™) and 65-99 hrs (PG-Camptothecin) respectively and are now in clinical trials [70-71]. The PG-drug conjugates have high drug loading capacity, better solubility, endocytic uptake and drug efficacy. HPMA has also been used to prepare polymer-drug conjugates. HPMA-Gly-Phe-Leu-Gly-doxorubicin (PK1) entered Phase I studies but along with other HPMA-drug conjugates showed disappointing results and has been abandoned. The HPMA-platinum containing drug, AP5346 is the only one that remains in clinical development [72]. HPMA-Gly-Phe-Leu-Gly-doxorubicin (PK2) which also contains the sugar galactosamine was the first ligand-targeted nanoparticle to reach the clinic. The galactose-based ligand targeted the asialoglycoprotein receptor (ASGPR) which was also unfortunately expressed on healthy hepatocytes [73-74]. The only targeted polymer-based conjugate in the clinic is CALAA-01, a polymer-siRNA composite [75].

1.2.2.4 Synthetic polymer micelle – drugs

Self-assembling block copolymer micelles have long been explored as drug carriers. A Pluronic™ block copolymer micelle incorporating doxorubicin and able to circumvent p-glycoprotein-mediated resistance has shown promising results [76]. NK911 is a self-assembling polymeric micelle of PEG 5000 - poly(aspartic acid) which has doxorubicin both covalently bound and in the free form [77] with the free doxorubicin escaping over an 8 -24 hr period. SP1049C which has two non-ionic Pluronic™ block co-

polymers and doxorubicin, showed a slower clearance than has been observed for free doxorubicin [78]. Genexol-PM™, a polymeric micelle containing paclitaxel, has received approval in South Korea. A Phase II trial in patients with metastatic breast cancer has been reported in the United States [79]. Multifunctional nanoparticles such as IT-101, a conjugate of camptothecin and cyclodextrin-based polymer, have increased circulation times, enter tumor cells and allow slow release of the drug [80]. Initial results from Phase I trial showed that patients receiving IT-101 had long-term stable disease and low side-effect profile and were able to overcome certain kinds of multi-drug resistance (MDR) [81].

1.2.2.5 Dendrimers

These polymers are synthesized as well-defined spherical structures ranging from 1 to 10 nm in diameter. Molecular weight and number of terminal groups increase exponentially as a function of generation of the polymer. Poly(amidoamine) spherical dendrimers (PAMAM) with ethylene-diamine (EDA) as a tetravalent initiator core are used [82]. One of the major applications of dendrimers is as a delivery vehicle for various anticancer drugs. PAMAM dendrimers were conjugated to doxorubicin [83], cisplatin [84], 1-bromoacetyl-5-fluorouracil (5-FU) [85], PEG or polyethylene oxide (PEO) and doxorubicin (dox) [86] and PEG and 5-FU [87]. In all cases, it was found that the dendrimer lead to higher drug-loading capacity, stability of the systems in the body and controlled release. Dox-coupled dendrimers could substantially inhibit the progression of dox-insensitive tumors. Dendrimers were also targeted to the folate receptor using folate and could deliver the drug methotrexate and provide imaging with fluorescein [88-89]. They could be targeted to tumors using a targeting moiety and could be attached to gadolinium-based MRI agents to enable imaging [90] thus providing a means to target, image and treat with the same nanoparticle.

1.2.3 Quantum dots

Semiconductor quantum dots (QD) are rapidly emerging as a popular luminescence probes for many biological and biomedical applications owing to their extremely small size (approximately 10 nm in diameter), high photostability, tunable optical properties and multimodality [91-93]. Such inorganic-organic composite nanomaterials have shown efficiency in cancer diagnosis *in vivo*, with their small size and large surface area which facilitates targeting, imaging and therapy [94-97]. Researchers have now extended the emission wavelength of the QDs into the near infrared (NIR, 650 - 950 nm) to take advantage of the improved tissue penetration depth and reduced background fluorescence [98]. QDs have also been linked with Fe_2O_3 and FePt to generate dual-function nanoparticles [99-100]. Dual-modality nanoparticles have been created by attaching paramagnetic gadolinium (Gd) chelates to polymer-coated QDs. *In vivo* imaging with QDs has been used to determine how surface coating of QDs with PEG would affect their circulation time [101]. QDs and two-photon excitation have been used to image small blood vessels [102-103]. Ballou et al. [104] prepared novel QDs and observed uptake into lymph nodes and clear imaging of the sentinel nodes. *In vivo* cancer targeting and imaging in living animals was demonstrated by Gao et al. [105] using subcutaneous injection of QD-tagged prostate cancer cells and systemic injection of multifunctional QDs and by Bagalkot et al. [106] using QD-aptamer-Dox conjugate for targeted cancer therapy, imaging and sensing.

One of the major problems with QDs is their inherent toxicity, where Cadmium-Selenium (CdSe) particles might leak cytotoxic cadmium ions after long-term exposure to ultraviolet (UV) light while Cadmium-Telluride (CdTe) particles produce reactive oxygen species (ROS) after long-term circulation [107-110]. Ballou et al. confirmed the nontoxic nature of stably protected QDs [101].

1.2.4 Gold nanostructures

Noble metal nanostructures have recently become very useful agents for cancer therapeutics. While many approaches are being developed for nanotechnology-enabled cancer diagnostics and therapeutics, a remarkably promising strategy involves the combination of noble metal nanoparticles and light. The uniquely vivid colors of metallic nanoparticles such as gold or silver are a result of their strong optical interferences and resonances [111]. When illuminated by light, metal nanoparticles support coherent oscillations of their valence electrons known as surface plasmons. The plasmon resonance wavelength strongly depends on the shape, size and type of metal of the nanoparticle, in addition to the local environment [112]. There is very strong enhancement of absorption or scattering at the plasmon wavelength of the nanoparticle, depending on the size of the nanoparticle: smaller nanoparticles are better absorbers at the plasmonic wavelength, while increasing the size increases the scattering cross section by the nanoparticle [113]. However, nanoparticles in the 100 nm diameter size range can possess both resonant absorption and scattering characteristics. The resonant absorption properties of metal nanoparticles result in strong, highly localized photothermal heating after laser illumination, an effect that can be exploited to induce cancer death. This effect is known as photothermal therapy (PTT) in which photothermal agents are employed to achieve the selective heating of the local environment. When the PTT agent absorbs light, electrons make transitions from the ground to the excited state. They subsequently relax through nonradiative decay channels, resulting in an increase in the kinetic energy in the local environment surrounding the light-absorbing species [114-116]. The photoabsorbing agents can be natural chromophores in the tissue [117] or externally added dye molecules such as indocyanine green [118-119]. However, they suffer from low absorption cross sections, inefficient light-to-heat conversion requiring large amounts of laser energy and can photobleach. Noble metal nanostructures are

useful agents for PTT because of their enhanced absorption cross sections ensuring laser therapy at lower energies, higher photostability and no photobleaching.

1.2.4.1 Gold nanoparticles

In addition to the local heating of the surrounding environment that leads to irreversible cell destruction, there is also vapor formation around gold nanoparticles, in the case of short pulses, that imposes internal mechanical stress leading to membrane rupture and cell damage [120-124]. MAb-based targeting can be employed to target the gold nanoparticles to EGFRs [125-129] and then therapeutically treat the cancer cells or image them.

1.2.4.2 Gold nanoshells

The goal of thermal ablation is to conform a lethal dose of heat to a prescribed tissue volume with as little damage to surrounding tissue as possible, which is hard to do with most of the techniques under investigation. *In vitro* studies with nanoshells bound to breast cancer cells showed effective destruction of cells following exposure to NIR light with nanoshells (either with or without a targeting moiety) providing a dual imaging/therapy approach [130-134]. These studies showed rapid heating of nanoshell-laden tissues upon exposure to the NIR light, with little to no damage to the surrounding tissue.

In vivo studies showed that nanoshells injected interstitially into the tumor were capable of inducing irreversible tissue damage such as coagulation, cell shrinkage and loss of nuclear staining [135] with magnetic resonance guidance revealing average maximum temperatures reached in the tumor. *In vivo* studies done with PEG-coated nanoshells injected intravenously and then the tumor irradiated, ablated the tumors and the mice appeared healthy and tumor-free 90 days after treatment, while the control mice (not treated with nanoshells) were euthanized 6-19 days after treatment [136].

1.2.4.3 Gold nanorods (GNR)

To use the long-wavelength laser irradiation that penetrates tissue for *in vivo* photothermal treatment (650 - 900 nm), the absorption band of the nanoparticles must to be in the NIR region. CNTs absorb naturally in this region; however, it is predicted that the surface plasmon field enhancement of the absorption of the GNRs is the strongest of all the different shapes of gold and silver nanoparticles [137-138]. *In vitro* studies showed that EGFR-targeted GNRs could be used for dual molecular imaging and selective photothermal therapy [139]. Biocompatible GNR-embedded polymeric nanoparticles (GPN) have been used as photothermal agents which absorb NIR light [140]. GNRs have been targeted with folate to tumor cells and then ablated with a laser tuned to the plasmon resonance at 765 nm. There was photoactivation damage and loss of membrane integrity, accompanied by extensive and irreversible membrane blebbing [141]. *In vivo* studies have shown that PEGylated GNR can be injected i.t. or i.v. and following NIR ablation, all PEG-GNR injected mice had no recurrence of tumor 50 days following treatment, whereas the control mice (no GNR + laser, GNR - laser) had to be euthanized by day 33 [142]. GNRs have been used in a cooperative nanomaterial system consisting of two discrete nanomaterials, the first being a GNR “activator” that populates tumor vessels and acts as a photothermal antenna to heat the tumor. This heating then accelerates the recruitment of the second component: a targeted nanoparticle containing doxorubicin-loaded liposomes. Mice containing tumors and treated with the cooperative nanomaterial system displayed significant reductions in tumor volume [143].

1.2.5 Carbon nanotubes (CNTs)

CNTs are rolled up cylinders of graphene sheets, exhibiting unparalleled physical, mechanical and chemical properties [144-148]. Depending on the number of graphene layers, CNTs can be classified as single-walled CNTs (SWNTs) or multi-walled CNTs (MWNTs). With diameters of 1-2 nm and lengths ranging from 50 nm up to 1 cm,

SWNTs are quasi one-dimensional (1D) cylindrical nanomaterials which may behave differently from spherical nanoparticles.

SWNTs are quasi I-D quantum wires with sharp densities of states (DOS) at the van Hove singularities, which imparts distinctive optical properties to them [149]. They absorb in the NIR region and can be used for photothermal therapy [150-152] and photoacoustic imaging [153]. Semiconducting SWNTs, with small band gaps, exhibit photoluminescence in the NIR range between 800 – 2000 nm [154-163]. SWNTs also have distinct resonance-enhanced Raman signatures for Raman detection/imaging, with large scattering cross-sections for single tubes [157, 164-165].

SWNTs can be functionalized either non-covalently or covalently to solubilize them, to render biocompatibility and to reduce toxicity. Covalent functionalization can be achieved by oxidation and cycloaddition reactions [166-174]. However, the intensities of Raman scattering and photoluminescence are reduced following covalent coupling [175]. In contrast, the structure and optical properties of the CNTs can be maintained when noncovalent functionalization is carried out by coating the CNTs with amphiphilic polymers. The surface of the CNTs can be coated with pyrene derivatives [176-178], DNA ([179-182], porphyrin [183-184], tween-20 and Pluronic™ [185] Pluronic™ [158], surfactant [186-188], PL-PEG [155, 179, 189-196], peptide [197-199] and serum proteins [200].

Cell culture experiments and *in vivo* pilot studies conducted by various groups observed no toxicity of properly functionalized CNTs [150, 154, 157, 160, 178, 189, 191, 193, 200-209], while raw CNTs were toxic to mice after inhalation and in cell culture [210-218]. It should be noted that some of the studies where the authors claim toxicity of the CNTs, the CNTs were <u>not</u> functionalized and hence the results are not relevant since they were not biocompatible. It is important to note the type of test that is used to assess viability of cells in cell culture after incubation with the CNTs. CNTs have been shown to

interact with certain dyes [219-220]. Also, the interactions between administered CNTs and the immune complement system, whose activation is an important line of defense against foreign species, should be examined [221].

It has been shown that functionalized CNTs can enter cells without toxicity by endocytosis [157, 160, 199, 208, 222] or by non-endocytic means [223-225].

Different cargoes have been shuttled by CNTs into cells and include drugs [189, 205, 226-232], fullerenes, cesium, metallocenes [233-236], proteins [150, 208], DNA [237-239] and RNA [190-191, 228, 240-241].

CNTs have been targeted to cells using small molecules such as folic acid [150, 242], peptides [189, 194] and MAbs [155, 243-244].

In vivo biodistribution and pharmacokinetic studies have been carried out by groups using different CNT materials, different surface functionalizations and different tracking methodologies, thus obtaining varying and sometimes contradicting results. However, some common themes did emerge. It appears that better covalent functionalization of CNTs of short lengths in dispersions of individual tubes resulted in urinary excretion and low organ accumulation [243, 245-252], whereas CNTs that had been non-covalently coated were more likely to accumulate in the RES for long durations with slow excretion of non-degraded CNTs through the bile and fecal pathways [158, 193-194, 201, 206, 253-256] .

1.3 Study Objectives

The goal of this study was to test a new targeting strategy ie, using CNTs attached to MAbs, followed by thermal ablation of tumor cells by exposure of the cells to NIR light. Once this was determined, we studied the pharmacokinetics and biodistribution of these constructs in mice. The specific aims of this study were: 1) to design and characterize non-covalent and covalent anti-CD22 and anti-CD25-targeted CNT constructs, 2) to determine the binding of the non-covalent and covalent MAb-CNT

constructs *in vitro,* 3) to investigate the killing properties of the non-covalent and covalent MAb-CNT constructs *in vitro,* 4) to determine the behavior of the non-covalent MAb-CNT constructs *in vivo.*

CHAPTER 2

MATERIALS AND METHODS

2.1 Culture of human tumor cell lines

Daudi cells from the American Type Culture Collection (ATCC, CCL-213, Manassas, VA) were cultured in complete medium. Complete medium consisted of Roswell Park Memorial Institute (RPMI)-1640 medium (Sigma-Aldrich, St Louis, MO) containing 1% antibiotic-antimycotic mixture (Pencillin/Streptomycin/Amphotericin B) (Sigma-Alrich), 10% heat-inactivated fetal calf serum (FCS) (52^{o}C for 30 min) (HyClone, Logan, UT) and 2 mM L-glutamine (Sigma-Aldrich). PBMCs from normal healthy donors were isolated from fresh heparinized blood by Ficoll-Plaque PLUS (GE Healthcare, Piscataway, NJ) density gradient centrifugation. Normal activated $CD25^{+}$ cells were generated by culturing the PBMCs for 72 hrs at 1 x 10^{6} cells/ml in complete medium supplemented with 5 µg/ml phytohaemagglutinin (PHA) (Sigma-Aldrich). Both cell types were incubated at 37^{o}C in a water-humidified incubator (NapCo. 5200, NapCo, Portland, OR) under conditions of 95% air – 5% CO_2.

2.2 Cell proliferation: Incorporation of ^{3}H-Thymidine

10^{5} Daudi cells or PBMCs were dispensed in triplicate wells in a sterile, flat-bottomed 96-well culture plate (Corning Life Sciences, Lowell, MA) in 200 µl complete medium, and incubated for the required duration. Twelve hrs prior to the end of plate incubation, 10 µL of 1 mCi/mL ^{3}H-thymidine (GE Healthcare), diluted 1:10 in complete medium was added to each well. The plate was returned to the incubator. At the end of incubation, cells were collected onto FilterMAT harvester paper (Skatron Instruments, Sterling, VA) using a cell harvester (Skatron Instruments). The filter paper was air dried and the perforated circles on the filter paper were

placed into individual scintillation vials (Research Products International Corp., Mount Prospect, IL). CytoScint scintillation fluid (MP Biomedicals, Solon, OH) was added to each vial in a volume of 2 mL and allowed to saturate the filter paper for about 30 min. The radioactivity in the vials was determined using a Tri-Carb 2900 TR (PerkinElmer, Waltham, MA) liquid scintillation analyzer. Radioactivity in counts per minute (cpm) of the triplicate wells for each condition was averaged and represented as % proliferation relative to that of untreated cells.

2.3 Preparation of CNT dispersions

CNT dispersions were prepared in the following manner for the non-covalent and covalent linkage to MAbs.

2.3.1 Non-covalent approach

Degassed ultrapure deionized (DI) water was used for all solutions. Purified High-pressure carbon monoxide (HiPCO) CNTs (0.3 mg, Carbon Nanotechnologies, Inc., Houston, TX) were suspended in 1 ml of 166 µM 1,2-distearoyl-sn-glycero-3-phosphoethanolamine-N-[biotinyl(polyethylene glycol) 2000] (DSPE-PEG (2000)-biotin) (Avanti Polar Lipids, Inc., Alabaster, AL). The mixture was sonicated with a 2 mm probe tip connected to a Branson Sonifier 250 (VWR, West Chester, PA) for 10 min at a power level of 10 W, with the sample immersed in an ice water bath. To remove excess DSPE-PEG-biotin, samples were washed twice in DI water by centrifugation for 15 min at 90,000 x g at 4°C in a TL-100 ultracentrifuge (Beckman Coulter, Fullerton, CA). The supernatant was discarded, the pellet was resuspended in 1 ml of DI water, and the entire wash procedure was repeated once more. The samples were then centrifuged two times in an Eppendorf 5417C (Eppendorf, Westbury. NY) for 10 min at 16,000 x g at room temperature and the upper 70% of the supernatant containing the biotinylated CNTs (B-CNTs) was recovered. In order to obtain more concentrated samples, the B-CNT suspension was centrifuged for 60 min at 16,000 x g at 4°C, the supernatant discarded, and the pellet was resuspended in 0.2 ml of DI water.

2.3.2 Covalent approach

Carboxyl-functionalized CNTs (0.5 mg, Sigma-Aldrich) were dispersed in 1 ml of 0.1 M 2-[*N*-morpholino]ethane sulfonic acid (MES, Pierce Endogen, Rockford, IL) buffer, pH 4.5 with 0.2% Tween-20 (Sigma-Aldrich) (activation buffer) by sonication with a 2 mm probe tip connected to a Branson Sonifier 250 (VWR) for 5 min at a power level of 10 W, with the sample immersed in ice. The mixture was then centrifuged at 16,000x *g* for 15 min to remove non-dispersed material. The supernatant containing the dispersed CNTs was recovered.

2.4 Characterization of CNT dispersions

Characterization of the CNT dispersions was carried out in a similar manner for both the non-covalent and covalent conjugates unless otherwise noted and as described below.

2.4.1 Atomic force microscopy (AFM)

AFM was performed in air under ambient conditions using a Digital Instruments Nanoscope III Multimode scanning probe microscope (Veeco Metrology, Inc., Santa Barbara, CA). Images were acquired in the TappingMode using cantilevers with 0.9 Nm^{-1} force constants as described earlier [197, 200]. In order to image the CNTs, 5 µl of the prepared solutions were spun-cast on freshly cleaved mica (Asheville-Schoonmaker Mica Co., Newport News, VA) at ~ 800 *x g* for 30 sec. All samples were dried at room temperature in a desiccator for 12 hrs prior to imaging. During imaging, a 125 µm long rectangular silicon cantilever/tip assembly was used with a spring constant of 40 N/m, resonance frequency of 315–352 kHz and a tip radius of 5–10 nm. The images were generated by the change in amplitude of the free oscillation of the cantilever as it interacted with the sample.

2.4.2 Thermal gravimetric analysis (TGA)

TGA was performed as described previously [200] with modifications. A Pyris-1 thermal gravimetric analyzer (PerkinElmer) equipped with a high temperature furnace and sample thermocouple was used. Samples were flash-frozen in liquid nitrogen and then lyophilized (Flexi-Dry MP Freeze-dryer, FTS Systems, Stone Ridge, NY) for 48 hrs before being transferred

to the platinum pan of the analyzer. The samples were heated from 100 to 1000 °C at 10°C/min in >99.9% O_2 using a flow rate of 20 mL/min. A baseline was generated for each scan and baseline-subtracted thermograms were converted into % weight. Thermal oxidation temperatures were identified by the peaks from the derivative of weight percent curves. Weight loss due to CNT burning was determined by subtracting the weights of the CNT peak at the onset and at the end of the procedure.

2.4.3 Inductively coupled plasma – mass spectrometry (ICP-MS)

Elemental analysis was performed using a ThermoElectron X-Series inductively coupled plasma mass spectrometer (Thermo Fisher Scientific Inc., Waltham, MA). Samples (1 mg of as-received CNT powder, 100 µL of a DSPE-PEG-biotin CNT dispersion or 100 µL of a DSPE-PEG-amine CNT dispersion) were acid - digested using a protocol developed in association with PreciLab Inc. (Addison, TX). In brief, a solution of 100 µL of 37% HCl and 100 µL of 69% HNO_3 was added to samples which were then ultrasonicated for 20 min. Next, the samples were diluted with a 2% HNO_3 blank to a total volume of 10 mL (100 mL for Fe detection). All samples and standard solutions were sprayed into flowing argon and passed into the torch, the plasma core of which was inductively heated to ~10,000 °C. Ni and Fe were calibrated using a blank, 0.25-, 1.0-, and 5.0-parts per billion (ppb) standard solutions at 590 watts (additional 50.0-ppb for Fe for the CNT powder) and Ti was calibrated using blank, 0.25-, 1.0- and 5.0-ppb standard solutions at 1200 watts.

2.4.4 UV-Vis-NIR spectroscopy

A dual-beam Lambda 900 UV-Vis-NIR spectrophotometer (PerkinElmer) was used for absorption spectra. Background correction was carried out using DI water. Scans were performed from 400-861 nm with a scan speed of 125 nm/min and a 0.44-sec integration time and from 861-1350 nm with a scan speed of 125 nm/min and a 0.48-sec integration time. The wavelength of the instrument was calibrated on a quarterly basis using Holmium standards.

2.4.5 Raman spectroscopy

Raman spectroscopy at 632.8 and 785 nm excitation was performed with a LabRAM high-resolution confocal Raman microscope system (Jobin Yvon Horiba, Edison, NJ) as described previously [200]. Wavenumber calibration was performed using the 520.5 cm^{-1} line of a silicon wafer; the spectral resolution was ~1 cm^{-1}. The power distribution over the sample was Gaussian, so it was fairly uniform.

The 632.8-nm laser excitation was provided by a 127 helium-neon laser operated at 35 mW (Spectra-Physics, Mountain View, CA). The laser power at the sample was < 5 mW using either a 10x or 50x microscope objective. The entrance slit was 500 µm, and the confocal pinhole was 1100 µm; the acquisition time for a 250 cm^{-1} spectral region was 90 sec.

The 785-nm laser excitation was provided by a HPNIR785 diode laser operated at 300 mW (Renishaw Inc., Gloucestershire, UK). The laser power at the sample was ~ 73 mW using a 10x microscope objective. The entrance slit was 450 µm, and the confocal pinhole was 1100 µm; the acquisition time for a 250 cm^{-1} spectral region was 90 sec. Sixty-five µl of the CNT samples were placed in 35 mm uncoated glass bottom "imaging" dishes (MatTek Corporation, Ashland, MA) under the objective (x10) of the Raman microscope.

2.4.6 Transmission electron microscopy (TEM)

A 1:1 dilution of CNT to incubation buffer (Gold Conjugate dilution buffer, Kirkegaard & Perry Laboratories, Gaithersburg, Maryland) was prepared and 3 µl was added to a 200 mesh nickel Formvar grid (Electron Microscopy Systems, Hatfield, PA). The CNT dilution was allowed to remain on the grid for 30 sec, after which the excess CNT solution was removed using a filter paper. Blocking buffer was prepared by adding 500 mg of bovine serum albumin (BSA, Sigma-Aldrich) to 0.02 M phosphate-buffered saline (PBS) [1X PBS (0.01 M): 1.2 g NaH_2PO_4, 1.4 g Na_2HPO_4, DI water to 1 L and pH 7.2; add 8.77 g NaCl]. Ten µl of coldwater fish skin gelatin (CWFS gelatin, Electron Microscopy Systems) was added to the 0.02 M PBS. The blocking buffer was then filtered such that no aggregates were present. One hundred µl of blocking

buffer was then added to a plastic dish. The grid was submerged in the blocking buffer for 90 min. The blocking buffer was again removed using filter paper. One hundred µl of the 5 nm diameter gold-labeled anti-biotin (Kirkegaard & Perry Laboratories) at a dilution of 1:50 in the incubation buffer was added to the grid and allowed to incubate for 3 hrs. Following this, the liquid on the grid was wicked off using filter paper and the grid was washed with 3 µl of DI water. TEM was performed using a JEOL JEM-1200EX II (JEOL Ltd., Tokyo, Japan) electron microscope.

2.4.7 Enzyme-linked immunosorbent assay (ELISA)

Neutralite Avidin (NA, Accurate Chemical and Scientific Corp., Westbury, NY) at a concentration of 4 µg/ml was prepared in coating buffer [8.4 g of $NaHCO_3$, 3.56 g of Na_2CO_3, DI water to 1 L, pH 9.5]. One hundred µl of this NA solution was added to wells on a 96-well ELISA plate (Nunc Maxisorp, Nunc, Rochester, NY). Controls consisted of wells to which 100 µl of coating buffer (lacking NA) only was added. The plates were covered with saran wrap and incubated at 4^oC for 12 hrs. Following the incubation, the plate was inverted to remove the NA solution. Two hundred µl of blocking buffer [1% BSA in 0.01 M PBS pH 7.2, filtered before use] was added to each well and incubated at room temperature for 1 hr. The plates were washed three times with washing buffer, phosphate-buffered saline Tween-20 (PBST) [0.05% Tween-20 in 0.01 M PBS, pH 7.2]. Dilutions of B-CNTs or MAb-NA were added to each well along with biotinylated horseradish peroxidase (B-HRP, Vector Labs, Burlingame, CA) and incubated for 1 hr at room temperature. After washing 5 times with PBST, 100 µl of the substrate 2, 2'-azino-bis(3-ethylbenzothiazoline-6-sulfonic acid) (ABTS, Sigma-Aldrich) was added and incubated for 5 min at room temperature. The absorbance was measured at 405 nm. The amount of B/NA present was calculated using a standard curve constructed by plotting optical density (OD) against increasing amounts of B/NA in the presence of a constant amount of B-HRP.

2.4.8 Toxicity to cells

3.6 µg of B-CNTs was added to a million Daudi cells. 10^5 of these Daudi cells were then dispensed in triplicate wells in a sterile, flat-bottomed 96-well culture plate (Corning Life Sciences) in 200 µl complete medium, and incubated for 24 hrs. Cells were pulsed for the last 12 hrs with 1 µCi [^{3}H]-thymidine/well (GE Healthcare) and the incorporated radioactivity was measured by liquid scintillation counting. The incorporated radioactivity for each sample was calculated relative to the corresponding untreated samples.

2.5 Preparation of MAb-NA conjugates

To couple the B-CNTs to MAbs, we used a protocol modified from that of Schnyder et al. [257]. Briefly, 10 mg of RFB4 (Mouse IgG1 anti-human CD22, [258]) or RFT5 (mouse IgG anti-human CD25, [259]) in 1 ml of IgG activation buffer [0.15 M borate buffer, 0.1 mM ethylenediaminetetraacetic acid (EDTA), pH 8.5] were thiolated by incubation for 1 hr at room temperature with a 20:1 molar excess of 2-iminothiolane (Traut's reagent, Pierce Endogen). After incubation, the reaction was quenched with 0.1 M glycine. In parallel, 10 mg of NA dissolved in 1 ml of NA activation buffer [0.01 M PBS, 0.1 mM EDTA, pH 7.4] was activated by a 30 min incubation at room temperature using a 6:1 molar excess of m-maleimidobenzoyl-N-hydroxysuccinimide ester (MBS, Pierce Endogen). The unreacted Traut's reagent and MBS were removed by gel-filtration on Sephadex G-25 columns with elution buffer [0.01 M PBS, 0.1 mM EDTA, pH 7.4]. The thiolated MAb was conjugated to the activated NA at a molar ratio of 1:2 for 2 hrs at room temperature by gentle shaking. The resultant conjugate was purified by gel-filtration on a Sephacryl S-300 HR column (GE Healthcare) using another elution buffer [0.05% Tween-20 in 0.1 M PBS, pH 7.4]. The protein concentration of the purified conjugate was quantified using the bicinchoninic acid assay (BCA, Pierce Endogen).

2.6 Characterization of MAb-NA conjugates

MAb-NA conjugates were characterized as described below.

2.6.1 Western blot

The size and integrity of the MAb-NA conjugate was analyzed by western blot (WB). A 7.5% non-denaturing polyacrylamide gel (PA) was poured. The 7.5% separating gel [DI water 4.85 ml, Acrylamide/Bis (30% stock, Bio-Rad Laboratories, Hercules, CA) 2.5 ml, 1.5 M Tris-HCl pH 8.8 2.5 ml, DI water 100 µl, 10% ammonium persulfate (Bio-Rad) 100 µl, N,N,N',N'-Tetramethylethylenediamine (TEMED) (Bio-Rad) 5 µl] was allowed to set for 30 min. The 4% stacking gel [DI water 6.1 ml, Acrylamide/Bis (30% stock) 1.3 ml, 0.5 M Tris-HCl pH 6.8 2.5 ml, DI water 100 µl, 10% ammonium persulfate 50 µl, TEMED 10 µl] was allowed to set for 30 min. Running buffer [dilute 10X stock: 30 g Trizma Base pH 8.3, 144 g glycine 1:10 with DI water to 1 L] was added to the top of the gel. The samples were loaded into wells with a 1:1 dilution of the loading buffer [1 ml 0.5 M Trizma Base pH 6.8, 4 ml DI water, 0.8 ml glycerol, 1.6 ml 10% sodium dodecyl sulfate (SDS), 0.2 ml 1% bromophenol blue]. The samples were electrophoresed at 150 V for 70 min. A polyvinylidene difluoride membrane (PVDF, Bio-Rad) was soaked in methanol and transferred to the 1X transfer buffer [dilute 10X stock: 30 g Trizma Base pH 8.3, 144 g glycine 1:10 with DI water to 0.8 L, 0.2 L methanol]. The gel was placed on the PVDF membrane and the transfer performed at 100 V for 60 min. Following the transfer, the PVDF membrane was washed with 1X Tris buffered saline Tween-20 (TBST) buffer [dilute 10X TBS stock: 24 g Trizma Base pH 7.5, 87 g NaCl 1:10 with DI water to 1L, 0.05% Tween-20] once for 15 min. The PVDF membrane was then blocked with the blocking buffer [3% BSA in 1X TBST] for 2 hrs. The PVDF membrane was washed with TBST two times for 10 min per wash. Sheep anti-mouse IgG-HRP (to detect MAb) (GE Healthcare) and B-HRP (to detect NA) (Vector Labs) dilutions (1:3000 and 1:10000 respectively) in TBST were added to the PVDF membrane and incubated for 1 hr at room temperature. The PVDF membrane was washed three times with TBST for 15 min and once with TBS for 15 min. 3 ml of a 50:50 mixture of

enhanced chemiluminescence system (ECL, GE Healthcare) Reagent A and Reagent B was added to the PVDF membrane for 1 min, the excess liquid removed and the PVDF membrane visualized.

2.6.2 Toxicity to cells

Ten µg/ml of RFB4-NA were added to a million Daudi cells. Similar concentrations of unconjugated RFB4 and NA were used as negative controls and goat anti-IgM was used as the positive control. 10^5 Daudi cells were then dispensed in triplicate wells in a 96-well plate in 200 µl complete medium, and incubated for 24 hrs. Cells were pulsed for 12 hrs with 1 µCi [^{3}H]-thymidine/well (GE Healthcare) and the incorporated radioactivity was measured by liquid scintillation counting as described above. The incorporated radioactivity for each sample was calculated relative to the corresponding untreated samples.

2.7 Preparation of MAb-CNT conjugates

MAb-CNT conjugates were prepared as described below.

2.7.1 Non-covalent approach

Fresh MAb-CNTs were prepared immediately before use by mixing B-CNT with MAb-NA in a 1:2 (w/w) ratio. The mixture was placed on a mixer (BD Clay Adams Nutator Mixer, BD, Franklin Lakes, NJ) for 35 min at room temperature and gently vortexed (American Scientific Products S/P Vortex Mixer) every 5 min. After coupling, the mixture was centrifuged for 5 min at 16,000 *x g* at 4°C. The supernatant containing unreacted MAb-NA was discarded, and the pellet was resuspended in 40 µl of PBS for every 3.6 µg B-CNT and used immediately. Following the coupling, the optical properties of the MAb-CNTs were tested by UV-Vis-NIR and Raman Spectroscopy.

2.7.2 Covalent approach

The carboxyl groups on the dispersed CNTs were activated by incubation for 30 min at room temperature with 2 mM 1-ethyl-3-[3-dimethylaminopropyl]carbodiimide hydrochloride (EDC, Pierce Endogen) and 5 mM N-hydroxysuccinimide (NHS, Pierce Endogen). The excess

reagents were removed by centrifugation in an Amicon Ultra-4 centrifugal filter unit (Millipore, Billerica, MA) and rinsed with binding buffer (0.1 M PBS pH 7.2, 0.2% Tween-20). The activated CNTs were recovered in 1 ml binding buffer and reacted with 10 mg RFB4 or RFT5 MAbs for 2 hrs at room temperature by gentle rocking. The control for covalent coupling was a mixture of MAb and non-activated, carboxyl-functionalized CNTs. The unreacted MAb was washed by centrifugation at 16,000 x *g* for 30 min. The supernatant containing unreacted MAb was discarded, the pellet resuspended in 1 ml of PBS buffer and the wash procedure repeated two more times. After each wash, the MAb-CNTs were briefly sonicated in 1 ml of PBS for 10 sec at a power level of 10 W. Following the coupling, the optical properties of the MAb-CNTs were tested by UV-Vis-NIR, AFM and Raman Spectroscopy.

2.8 Preparation of MAb-CNT-EGFP conjugates

2.8.1 Covalent approach

The carboxyl groups on the dispersed CNTs were activated by incubation for 30 min at room temperature with 2 mM 1-ethyl-3-[3-dimethylaminopropyl] carbodiimide hydrochloride (EDC, Pierce Endogen) and 5 mM N-hydroxysuccinimide (NHS, Pierce Endogen). The excess reagents were removed by centrifugation in Amicon Ultra-4 centrifugal filter units (Millipore) and rinsed with binding buffer (0.2% Tween-20 in 0.1 M PBS, pH 7.2). The activated CNTs were recovered in 1 ml binding buffer and reacted with 10 mg RFB4 or RFT5 MAb and 100 µg EGFP (BioVision Inc., Mountain View, CA) for 2 hrs at room temperature by gentle rocking. The unreacted MAb and EGFP were washed by centrifugation in an Eppendorf 5417C (Eppendorf) at 16000 x *g* for 30 min. The supernatant containing unreacted MAb and EGFP was discarded, the pellet resuspended in 1 ml of PBS, and the wash procedure repeated two more times. After each wash, the MAb-EGFP-CNTs were briefly sonicated for 10 sec in 1 ml of PBS at a power level of 10 W.

2.9 Stability of MAb-CNT conjugates

The stability of the MAb-CNTs of the non-covalent and covalent conjugates was determined as described below.

2.9.1 Non-covalent approach

2.9.1.1 Incubation in mouse serum

The MAb-CNTs were prepared as described above. MAb-CNTs (containing 3.6 µg CNT) were suspended in 0.1 ml of filtered mouse serum (not heat-inactivated, Sigma-Aldrich) and incubated at 37^{o}C for 0-72 hrs. At each the time point, the suspension was washed by centrifugation in an Eppendorf 5417C (Eppendorf) at 16,000 x *g* for 5 min and the pellet was resuspended in 40 µl of PBS. Following this, the ablation of MAb-CNT-coated cells with NIR light was tested as described below.

2.9.2 Covalent approach

2.9.2.1 Sodium dodecyl sulfate – polyacrylamide gel electrophoresis (SDS-PAGE)

Covalent MAb-CNTs were prepared as described above. RFB4-CNTs or a mixture of RFB4 and carboxylated CNTs (control) were subjected to SDS-PAGE. Samples containing 3 or 5 µg CNTs were loaded on the gel. The presence of dissociated RFB4 was detected by staining with Simply Blue SafeStain (Invitrogen Corporation, Carlsbad, CA).

2.9.2.2 Incubation in mouse-serum

RFB4-CNTs (containing 1 µg CNT) were suspended in 0.5 ml mouse serum (Sigma-Aldrich) and incubated at 37^{o}C for 0-24 hrs. At each time point, the RFB4-CNTs were recovered by centrifugation in an Eppendorf 5417C (Eppendorf) at 16,000 x *g* for 15 min. Following this, the binding of RFB4-CNTs to Daudi cells was determined by flow cytometry as described below.

2.10 Binding of MAb-CNTs to target cells

The binding of the MAb-CNTs to the target cells was done as described below.

2.10.1 Non-covalent approach

2.10.1.1 Flow Cytometry

A million Daudi cells or PHA-activated PBMCs (>95% $CD25^+$ cells) were incubated with 40 µl of the MAb-CNTs (containing 3.6 µg of CNTs) for 20 min at 4°C in PBS. Cells were washed two times with ice-cold PBS and then incubated with either Phycoerythrin-Streptavidin (PE-SA, Jackson ImmunoResearch Laboratories, Inc., West Grove, PA) or fluorescein-isothiocyanate (FITC)-labeled goat anti-mouse immunoglobulin (GAMIg) (FITC-GAMIg, Kirkegaard & Perry Laboratories) for 20 min at 4°C. The cells were washed two times with ice-cold PBS, resuspended in 0.5 ml of PBS and the bound fluorescence was analyzed on a FACScan (Becton Dickinson, San Jose, CA).

2.10.1.2 Ability to bind B-CNTs

A million Daudi cells were incubated with saturating amounts of RFB4-NA or RFT5-NA (1 µg) for 15 min at 4°C in PBS. Cells were washed twice with ice-cold PBS, incubated with incremental amounts of B-CNTs for 20 min at 4°C in PBS and then washed two times with ice-cold PBS. The amount of B-CNT bound to cells was determined by measuring the absorbance at 808 nm of the B-CNT suspension before and after incubation with Daudi cells. The amount of B-CNT bound per cell was determined using the extinction coefficient [$\varepsilon^{0.1\%}$= 25 $(mg/ml)^{-1}$] calculated from the linear fit (Beer-Lambert law) of absorbance at 808 nm vs. the B-CNT concentration.

2.10.2 Covalent approach

2.10.2.1 Flow Cytometry

A million Daudi cells or PHA-activated PBMCs (>95% $CD25^+$ cells as determined by flow cytometry) were incubated with the MAb-CNTs (containing 1 µg of CNTs) for 15 min at 4°C in PBS. Cells were washed two times with ice-cold PBS and then incubated with FITC-GAMIg

(Kirkegaard & Perry Laboratories) for 15 min at 4°C. The cells were washed two times with ice-cold PBS, resuspended in 0.5 ml of PBS and the bound fluorescence was analyzed on a FACScan (Becton Dickinson). Direct immunofluorescence staining was performed with EGFP-conjugated RFB4-CNTs for 15 min on ice, and washed two times with ice-cold PBS.

2.10.2.2 Fluorescence Microscopy

A million Daudi cells were incubated with RFB4-EGFP-CNTs (containing 1 µg CNTs) for 15 min at 4°C in PBS. Cells were washed two times with ice-cold PBS and allowed to adhere to poly-L-lysine-coated slides (Sigma-Aldrich) at room temperature for 20 min and fixed with 3% Paraformaldehyde (PFA) for 10 min. The slides were washed two times with PBS, rinsed with distilled water, air-dried and mounted with VECTASHIELD mounting medium (Vector Laboratories) containing 4',6-diamidino-2-phenylindole (DAPI) as counterstain. The slides were examined under a fluorescence microscope (Axiophot, Zeiss, Germany) under a 63x objective using single-pass filters for FITC (green) and DAPI (blue) or a dual-pass green/blue filter set.

2.10.2.3 Saturation Curve

A million Daudi cells were incubated with increasing amounts of MAb-CNTs for 15 min at 4^{o}C in PBS, washed two times with ice-cold PBS and stained with FITC-GAMIg. The amount of bound fluorescence was analyzed on a FACScan (Becton Dickinson).

2.11 Ablation by MAb-CNTs of target cells

The thermal ablation by the MAb-CNTs of target cells was carried out as described below.

2.11.1 Non-covalent approach

A million cells were incubated with 40 µl of the MAb-CNTs (containing 3.6 µg CNTs) in PBS for 20 min at 4°C. Cells were washed three times with ice-cold PBS, and then 10^5 cells were dispensed in triplicate wells in a 96-well plate in 200 µl complete medium. The cells were exposed to continuous NIR light using a FAP-Sys-30W 805-811 nm laser system (Coherent, Inc., Santa Clara, CA) for 7 min at 5 W/cm^2. Cell death was assessed by pulsing the cells for

the next 12 hrs with 1 μCi [^{3}H]-thymidine/well (GE Healthcare) and the incorporated radioactivity was measured by liquid scintillation counting. The incorporated radioactivity for each sample was calculated relative to the corresponding non-irradiated samples.

2.11.2 Covalent approach

A million cells were incubated with 100 μl of the MAb-CNTs (containing 3 μg CNTs) in PBS for 15 min at 4°C. Cells were washed three times with ice-cold PBS, and then 10^5 cells were dispensed in triplicate wells in a 96-well plate in 200 μl complete medium. The cells were exposed to continuous NIR light using a FAP-Sys-30W 805-811 nm laser system (Coherent, Inc.) for 4 min at 9.5 W/cm^2. Cell death was assessed by pulsing the cells for the next 12 hrs with 1 μCi [^{3}H]-thymidine/well (GE Healthcare) and the incorporated radioactivity was measured by liquid scintillation counting. The incorporated radioactivity for each sample was calculated relative to the corresponding non-irradiated samples.

2.12 Tumor xenograft model

2.12.1 Severe combined immunodeficient / nonobese diabetic (SCID/NOD) mice

For the xenograft experiments, inbred SCID/NOD mice were purchased from the University of Texas Southwestern Medical Center (UTSWMC) Mouse Breeding Core Facility. Female mice were used in the xenograft experiments. All mice were housed in sterilized cages with filter tops in accordance with institutional animal care policy. Mice were acclimated in the facility for a minimum of seven days prior to handling. All protocols were approved by our institutional protocol review committee. The mice were 7-8 weeks of age at the time of tumor cell inoculation. Following tumor inoculation, mice were followed for weight loss and for signs of the following: visible tumor and sickness.

2.12.2 Human Burkitt's lymphoma (BL) model

A solid tumor model of BL was generated by injecting 1 x 10^7 Daudi cells in 200 μL of sterile PBS subcutaneously (s.c.) into SCID/NOD mice. The mice were followed for the development of palpable tumors, and the tumors were measured using calipers. Tumor volume

was calculated using the formula Volume = W^2 x L ÷ 2, where L was the longest diameter and W was its perpendicular width. When the tumors reached 150 to 360 mm^3, 160 µl of non-covalent RFB4-CNT (containing 18.6 µg CNTs as determined by UV-Vis-NIR and Raman Spectroscopy) was injected i.v. into the tail vein of each mouse. The RFB4-CNT was prepared according to the method detailed earlier. A small sample of the RFB4-CNT was saved to be used for Raman spectroscopy later.

2.13 Sample preparation for Raman spectroscopy

2.13.1 Blood collection

A small nick was made in the sub-mandibular region using a 5.5 MM GoldenRod animal lancet (Medipoint, Mineola NY). A 75 MM heparinized hematocrit tube (Drummond Hemato-Clad, Drummond Scientific Company, Broomall, PA) to which a bulb had been attached, was placed parallel to the ground and the tip placed in the nick that was just made. Blood was drawn up by capillary action and forced into blood collection tubes (BD Microtainer Tubes with K_2EDTA, Becton Dickinson). The tubes were vortexed thoroughly and stored at 4^oC.

2.13.2 Blood processing

The blood was mixed thoroughly 1:1 with lysis buffer (1% SDS, 1% Triton X-100, 40 mM Tris Acetate, 10 mM EDTA, 10 mM Dithiothreitol (DTT)) and kept at 4^oC for 72 hrs prior to Raman spectroscopy.

2.13.3 Harvesting organs

The mouse was weighed and 200 µl of Nembutal sodium solution (50 mg/ml, Ovation Pharmaceuticals) injected i.p. The mouse was then perfused with 5 USP units/ml heparin (Heparin Sodium Injection, USP, Baxter Healthcare Corporation, Deerfield, IL) in saline (0.9% Sodium Chloride Irrigation USP, Braun Medical Inc., Irvine, CA) using a polystaltic pump (Buchler Instruments, Fort Lee, NJ) at a rate of 1.45 ml/min for 15 min. Following this, the liver, lung, spleen, kidney and tumor were removed and weighed. The organs were then cut into small pieces (3-4 per organ) and placed in 50 ml tubes. They were covered with parafilm and

placed at -80^{o}C for about 30 min. The tubes were then placed in a lyophilizer (Savant ModulyoD, Thermo Electron Corporation) for about 72 hrs after which they were stored at 4^{o}C.

2.13.4 Processing organs

The lyophilized organs were ground to a fine powder using a mortar and pestle. Collagenase Type I (250 units/mg, Invitrogen Corporation) was prepared at 10 mg/ml in Hanks' buffered salt solution (HBSS, Invitrogen Corporation) and added to the organs to suspend them in the following volumes: 1.5 ml for the liver and tumor and 0.5 ml for the lung, spleen and kidneys. The organs were then placed in the shaking incubator at 37^{o}C for 2 hrs and 45 min. They were then placed at 4^{o}C for 12 hrs, after which they were mixed 1:1 with lysis buffer (1% SDS, 1% Triton X-100, 40 mM Tris Acetate, 10 mM EDTA, 10 mM DTT) and then stored at 4^{o}C for 48 hrs. Following this, the organs were sonicated with a 2 mm probe tip connected to a Branson Sonifier 250 for 3 pulses at 15 sec each at a power level of 10 W. The samples were then passed through a 23G needle five times and stored at 4^{o}C for 24 hrs.

2.14 Raman Spectroscopy of MAb-CNTs

2.14.1 Calibration curves

RFB4-CNT conjugate was prepared fresh as described earlier. The organ lysates and blood were prepared as described in collecting and processing blood and collecting and processing organs. The concentration of the CNT component of the RFB4-CNT was determined by UV-Vis-NIR spectroscopy at a wavelength of 808 nm. RFB4-CNT dilutions, made in corresponding organ lysates from untreated mice (mice not injected with RFB4-CNT), ranged from 4 µg/ml to 0.063 µg/ml (4 – 0.25 µg/ml for blood, kidney and PBS). Sixty-five µl of each dilution was placed in imaging dishes and placed under the 10X objective. At least two Raman spectra were recorded at different locations in the imaging dish (90-sec acquisition time) for each dilution and the results averaged. For a given concentration of RFB4-CNT, the Raman intensity was obtained by averaging the CNT G-band peak area from 1572 cm^{-1} to 1610 cm^{-1} using a 785 nm laser with ~ 73 mW power at the sample. Calibration curves were obtained for

all the harvested organs and for blood and PBS. This experiment was repeated at least three times with a total of three untreated mice.

2.14.2 Detection of CNTs in blood

Blood was collected and processed at < 1 min, 8 and 24 hrs p.i. using the methods described earlier in Collecting and Processing Blood. Raman spectroscopy was carried out with 65 µl of the sample in imaging dishes under the 10X objective. The intensity was obtained by averaging the CNT G-band peak area from 1572 cm^{-1} to 1610 cm^{-1} using a 785 nm laser with ~ 73 mW power at the sample. The percent injected dose (%ID) was calculated by the following equation:

$$\%ID = \frac{[RFB4\text{-}CNT]_{blood\ lysate} \times V_{blood\ lysate}}{[RFB4\text{-}CNT]_{injected} \times V_{injected}} \times 100\%$$

The concentration of RFB4-CNT in the blood of the injected animal ($[RFB4\text{-}CNT]_{blood\ lysate}$) was determined from the Raman intensity of the blood lysate and the corresponding calibration curve. The volume of the blood lysate ($V_{blood\ lysate}$) was taken as 6% of the mouse body weight [260].

This experiment was repeated three times with five mice per experiment. We have data from only four mice as we could not measure a Raman signal of sufficient intensity from the remaining eleven mice. %ID from animals were compiled and then grouped; each dot represents one animal, the average of all animals in a group is represented by a horizontal line.

2.14.3 Biodistribution

Organs were collected and processed at 24 hrs p.i. using the methods described earlier in Harvesting and Processing organs. Raman spectroscopy was carried out and the intensity obtained by averaging the CNT G-band peak area from 1572 cm^{-1} to 1610 cm^{-1} using a 785 nm laser with ~ 73 mW power at the sample. The %ID was calculated by the following equation:

$$\%ID = \frac{[RFB4\text{-}CNT]_{tissue\ lysate} \times V_{tissue\ lysate}}{[RFB4\text{-}CNT]_{injected} \times V_{injected}} \times 100\%$$

The concentration of RFB4-CNTs was determined by measuring the intensity and using the calibration curve obtained from the corresponding organ. The volume of the tissue lysate was the total volume of buffer in which the organ had been suspended. This experiment was repeated three times with five mice per experiment. We have data from only six mice since we could not measure a Raman signal of sufficient intensity from the remaining nine mice. %ID from animals were compiled and then grouped; each dot represents one animal, the average of all animals in a group is represented by a horizontal line.

2.15 Statistical Analysis

Values for both *in vitro* and *in vivo* experiments were analyzed using a two-tailed t test unless otherwise noted. Samples were considered to be significantly different when $p < 0.05$.

CHAPTER 3

RESULTS

3.1 CNTs form stable suspensions which are characterized by various means

The first step in developing MAb-targeted CNTs was creating soluble and stable CNT dispersions that would enable the coupling of MAb and retain the thermal activity of the CNTs in serum at physiological temperatures. The non-covalent CNTs were dispersed by using biotinylated polar lipids that adsorbed to the surface of the CNTs, while the covalent CNTs, which already had carboxyl groups introduced on their surface by chemical means, were dispersed in surfactant which coated their entire surface.

3.1.1 Non-covalent approach

Well-dispersed single-walled CNTs were prepared by sonicating CNTs in the presence of DSPE-PEG (2000)-biotin or DSPE-PEG(2000)-amine. They were then characterized by a variety of methods. The CNT dispersion or raw CNT powder was agitated ultrasonically with 37% HCl and 69% HNO_3, ICP-MS was performed and the ratio of the metal content of the dispersion to the powder was obtained (certain methods of synthesizing CNTs require the use of metals as catalysts). It was observed that the CNT dispersion had ≤ 3 parts per million metal corresponding to less than 0.0003% of the dispersion. The levels of metals in the dispersion were significantly lower than the levels seen in the raw CNT powder (Table 1**)**. It should be noted that the toxicity threshold of Ni is 25 ppb [29] and our CNT dispersions contain ~ 45 ppb Ni. It is unknown if this level will have an impact on the toxicity profile of the CNT dispersions.

The dispersions were stable and did not aggregate at room temperature for > 120 days. Five µl of the B-CNT dispersion was spun-cast on mica, dried in a dessicator and then imaged

by AFM. AFM analysis demonstrated that the suspension was free of nontubular carbon structures and the CNTs were either individually dispersed or in small bundles. The CNTs could be seen coated by the biotinylated polar lipid, DSPE-PEG-biotin. The lengths of the CNTs ranged from 0.2 to 1.4 µm with an average of 0.59 µm (Figure 1.a). The B-CNTs were immunodetected with gold-labeled goat anti-biotin to determine the extent of distribution of the biotin (from the DSPE-PEG-biotin polymer) on the CNT following the sonication process. TEM analysis revealed that the biotin from the DSPE-PEG-biotin was distributed along the entire surface of the B-CNT with the inset showing the biotin distribution on the CNT at a higher magnification (Figure 1.b). UV-Vis-NIR spectroscopy was performed on the B-CNTs to determine the quality of the dispersion. Background subtraction was performed with DI water and the spectra from 400-1350 nm were acquired. The presence of electronic transitions between van Hove singularities suggested that the optical properties of the CNTs were maintained after the adsorption of DSPE-PEG-biotin (Figure 1.c). Raman spectroscopy carried out at 632.8 nm with a 10X objective showed a number of well characterized resonances such as the radial breathing mode (RBM) region between 100 and 300 cm^{-1} and the tangential (G-band) peak at 1590 cm^{-1}, confirming the presence of CNTs in the sample (Figure 1.d). To determine the inherent cytotoxicity of the B-CNTs (in the absence of NIR light and MAb-NA), cells from the IgM^{+} $CD22^{+}CD25^{-}$ Burkitt's lymphoma cell line Daudi, were incubated for 24 hrs with up to the highest amount of B-CNT used in binding and killing experiments (3.6 µg). Following this, the viability of the cells was determined by [^{3}H]-thymidine incorporation. It was found that the B-CNTs are not toxic to cells by themselves. As a positive control, 10 µg of goat anti-IgM was used which resulted in a 60% reduction in thymidine incorporation (Figure 1.e).

In conclusion, these data indicated that the non-covalent B-CNTs were well dispersed with the biotin present along their entire surface, optically active, relatively pure and non-cytotoxic to cells.

3.1.2 Covalent approach

Carboxyl-functionalized CNTs were sonicated in 0.1M MES buffer (pH 4.5) with 0.2% Tween-20 and then centrifuged to remove the large aggregates and bundles. The supernatant was collected and 20 µl was spun cast onto freshly cleaved mica, dessicated overnight and then AFM was employed to determine the quality of the dispersion. It was observed that the dispersion consisted of individual tubes and small bundles with the surfactant-coated CNTs (Figure 2.a). Raman spectra were acquired using a 785 nm diode laser and a 10X objective, with the sample contained in a 35 mm polylysine-coated glass bottom dish. The G-band, observed at ~ 1590 cm^{-1} exhibited a G^-/G^+ line shape that is characteristic of SWNTs. The D-band was observed at ~ 1310 cm^{-1} indicative of the disorder introduced during the carboxylation process (Figure 2.b).

In conclusion, these data indicated that the covalent c-CNTs were well dispersed with the surfactant coating their surface and were optically active as indicated by the presence of the G-band peak at ~ 1590 cm^{-1}.

Table 1. CNT dispersions contain less metal than the raw CNT powder

Metal	Raw CNT powder (ppb)	DSPE-PEG-biotin CNT (ppb)	DSPE-PEG-amine CNT (ppb)	% (DSPE-PEG-biotin CNT/Raw CNT)	% (DSPE-PEG-amine CNT/Raw CNT)
Fe	5,333,000	2,739	1,096	0.05	0.02
Ni	3,800	46.83	40.93	1.2	1.08
Ti	3,500	7.47	4.08	0.2	0.12

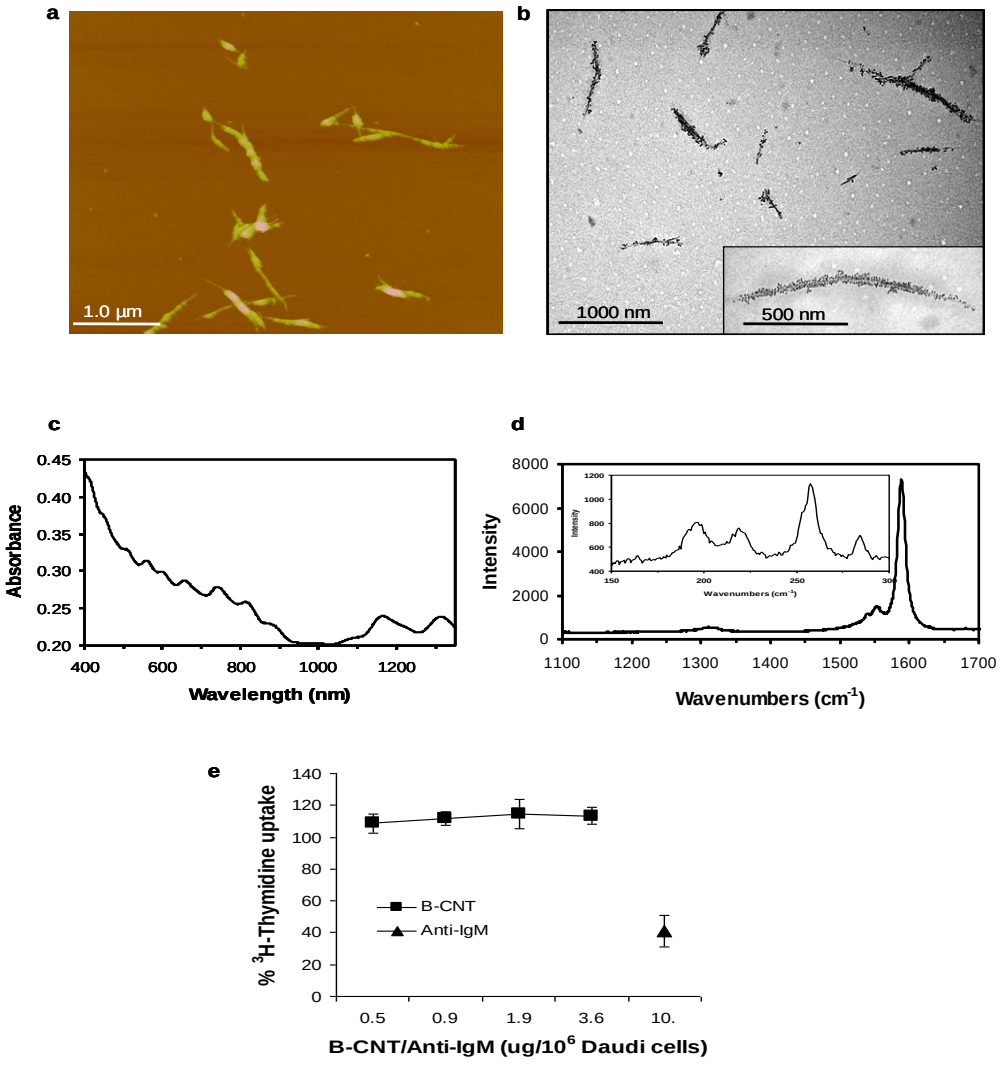

Figure 1. Characterization of CNTs non-covalently suspended by biotinylated polar lipids (B-CNTs). (a) AFM image of B-CNTs shows CNTs coated by the biotinylated polar lipid, DSPE-PEG-biotin. (b) TEM images of individual B-CNTs show uniform coverage of biotin after immunodetection with gold-labeled anti-biotin. Higher magnification of a B-CNT coated with gold-labeled anti-biotin (inset). (c) UV-Vis-NIR spectra of B-CNTs show a number of metallic and semi-conducting CNT absorbances consistent with the presence of individual tubes. (d) Raman spectra of B-CNTs show four predominant radial breathing modes (inset) and an intense G band (~1590 cm^{-1}) indicating the presence of CNTs. Data in a, b, c and d are representative of at least three independent experiments. (e) $5x10^4$ Daudi cells were incubated for 12 hr with the highest amount of B-CNTs used in the binding and killing assays and cytotoxicity was detected by [^{3}H]-Thymidine incorporation. 10 µg goat anti-IgM was used as a positive control. Data represent the mean ± S.D. of three independent experiments.

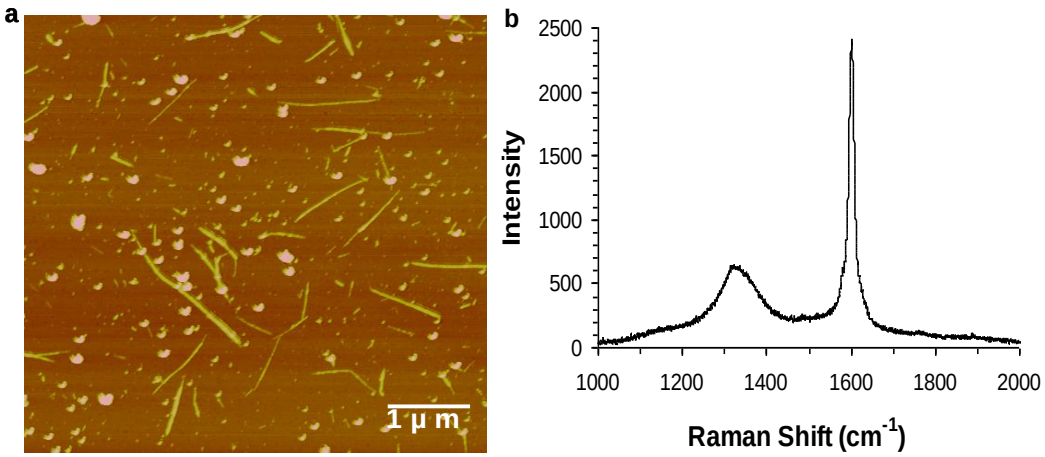

Figure 2. Characterization of carboxylated CNTs in a suspension of MES and Tween-20 surfactant (c-CNTs). (a) AFM image of c-CNTs shows CNTs dispersed by the MES and Tween-20 surfactant. (b) Representative Raman spectrum of CNTs showing the D-band at ~1310 cm^{-1} and the G-band at ~1590 cm^{-1}.

3.2 Characterization of MAb-NA conjugates

It was next important to derivatize the MAb for attachment to the B-CNTs. Our strategy was to attach NA to the MAb and biotin to the CNTs. NA binds biotin with high affinity [261]. The use of the MAb-NA with the B-CNTs provided the flexibility to "assemble" the targeted CNTs using any cell-binding MAb. To prepare the targeting agents, Mouse IgG anti-human CD22 (RFB4) or mouse IgG anti-human CD25 (RFT5) were thiolated with 2-iminithiolane (Traut's reagent). NA was activated with *m*-maleimidobenzoyl-*N*-hydroxysuccinimide ester (MBS). The purified thiolated IgG was mixed with MBS-activated NA at a 2:1 ratio as shown by preliminary experiments to give the best yields. The resulting conjugate was chromatographed on a Sephacryl S-300 HR column and fractions of the different peaks were pooled (Figure 3.a). Purity was determined by western blot analysis. Pooled and concentrated RFB4-NA, RFT5-NA and MAb alone were electrophoresed under nondenaturing conditions on a 7.5% polyacrylamide gel and immunoblotted with sheep anti-mouse IgG - HRP (to detect MAb) (Figure 3.b). The conjugate was of a higher molecular weight than MAb alone and had the MAb component as determined by the band seen with sheep anti-mouse IgG - HRP.

To determine the cytotoxicity of the MAb-NA conjugates, Daudi cells were incubated with up to 10 µg/ml of RFB4-NA; cytotoxicity was determined by [^{3}H]-thymidine incorporation. Similar concentrations of unconjugated RFB4 and NA were used as negative controls, and goat anti-IgM (which induces apoptosis of Daudi cells) was used as the positive control. We found that the RFB4-NA conjugates were not cytotoxic, whereas the goat anti-IgM reduced [^{3}H]-thymidine incorporation by > 50% (Figure 3.c).

To determine the amount of B-CNTs that could be targeted to Daudi cells, the Daudi cells were precoated with a saturating concentration of RFB4-NA. The excess RFB4-NA was washed off and cells were then incubated with increasing amounts of B-CNTs. It was found that the RFB4-NA, but not the RFT5-NA conjugate, could target an average of 0.237 pg of B-CNTs

per cell. No detectable B-CNT binding was found on uncoated cells or cells precoated with RFT5-NA (negative control) (Figure 3.d).

Overall, the data indicate that the MAb-NA conjugates were pure, non-cytotoxic and that they could bind specifically to cells. Once bound, B-CNTs could be targeted to the cells.

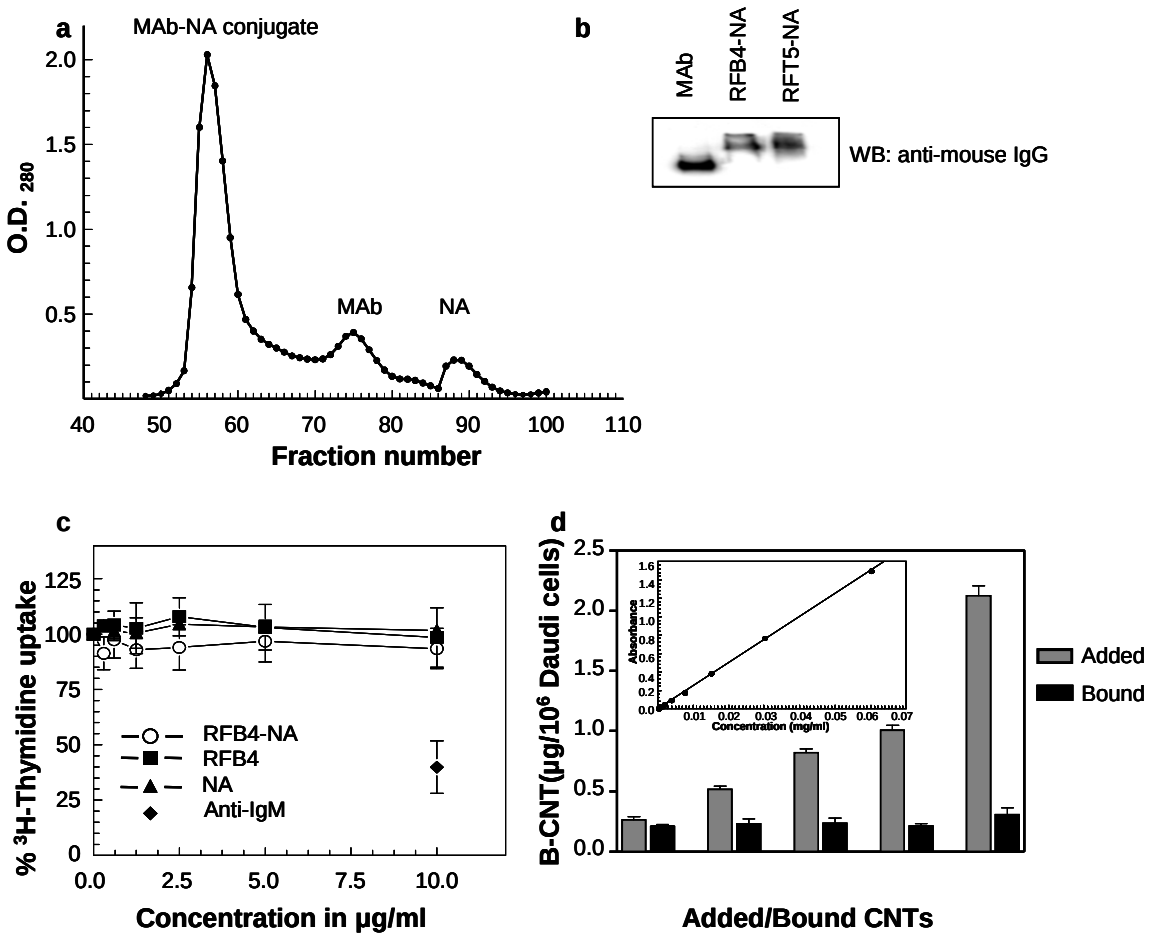

Figure 3. Characterization of a MAb-NA conjugate. (a) A typical chromatographic separation of RFB4-NA from unconjugated RFB4 and NA using a Sephacryl S-300 HR column. Fractions of the first peak containing the RFB4-NA conjugate were pooled and concentrated. (b) Purified RFB4-NA, RFT5-NA or MAb were electrophoresed under non-denaturing conditions on a 7.5% polyacrylamide gel (PAGE) and immunoblotted with HRP-labeled sheep anti-mouse IgG. Data in a and b are representative of at least three independent experiments. (c) $5x10^4$ Daudi cells were incubated for 24 hr with increasing concentrations of the RFB4-NA conjugate and cytotoxicity was detected by [^{3}H]-Thymidine incorporation. Similar concentrations of unconjugated RFB4 or NA were used as negative controls whereas10 µg/mL goat anti-IgM was used as positive control. (d) A million Daudi cells precoated with a saturating concentration of RFB4-NA, were incubated with increasing amounts of B-CNT. Saturating concentration of RFB4-NA can target 0.237 pg of B-CNT per Daudi cell. No detectable B-CNT binding was found on uncoated cells or on cells precoated with RFT5-NA (control). Data in c and d represent mean ± S.D. of three independent experiments

3.3 Preparation and characterization of MAb-CNT conjugates

MAb-CNT conjugates were prepared in two ways: non-covalently and covalently. For the non-covalent conjugates, MAb-NA was coupled to the B-CNTs (to which the biotin had been adsorbed) by the formation of the avidin-biotin bond, one of the strongest non-covalent bonds [261]. A concern with the non-covalent approach was that the targeting ligand might dissociate from the CNTs *in vivo*. To overcome this and achieve linkage stability, a covalent approach to coupling MAbs to CNTs was developed and tested. A concern with the covalent approach however, was that the photothermal efficiency could be compromised by the chemical functionalization of the CNTs by the introduction of carboxyl groups.

3.3.1 Non-covalent approach

The MAb-CNTs were prepared by coupling the B-CNTs to either the RFB4-NA or RFT5-NA for 35 min at room temperature. After the removal of the supernatant containing the unreacted MAb-NA, the optical properties of the freshly prepared MAb-CNTs were tested. The UV-Vis-NIR spectra of the MAb-CNT conjugates displayed the same metallic and semiconducting CNT types as observed for the B-CNTs, indicating that the optical properties of the CNTs were not affected by the coupling (Figure 4.a). The characteristic CNT resonances displayed in the Raman spectra of the MAb-CNTs again confirmed the presence of CNTs in the sample. The Raman spectra of the MAb-CNTs and the B-CNTs were similar indicating that the coupling of the B-CNTs to the MAb-NA did not alter the optical properties of the CNTs. (Figure 4.b).

These data indicate that the properties of the B-CNTs were not affected by the coupling to MAb-NA and the confirmed presence of the CNTs in the MAb-CNT conjugates.

3.3.2 Covalent approach

RFB4-CNTs and RFT5-CNTs were prepared by first activating ~0.5 mg of carboxylated CNTs (c-CNTs) with EDC and NHS. After the excess reagents were removed, the NHS-derivatized CNT suspension was transferred to 0.1 M PBS with 0.2% Tween20 and coupled to

RFB4 or RFT5 for 1 hr at room temperature. In order to rule out non-covalent attachment of IgG to CNTs, the non-activated carboxyl-functionalized CNTs were incubated with MAbs under the same conditions. Finally, the conjugates were transferred to 10 mM PBS by washing to remove the free Tween 20 and unreacted MAbs from the solution. The concentration of the CNTs was calculated from the OD_{808} whereas the bound MAb was detected using a BCA protein assay. The dimensions of the MAb-CNTs were determined using AFM. The MAb-CNT sample showed signs of cross-linking with lengths that ranged from 0.5 – 2.0 μm with an average length of 1.0 ± 0.3 μm. The diameters of the MAb-CNTs ranged from 9.0 – 20.0 nm with an average diameter of 12.3 ± 2.5 nm. There was a 6 nm increase in diameter between the MAb-CNTs and the CNTs, which could be attributed to the presence of the MAb (Figure 5.a). It was important to demonstrate that the MAb-CNTs would be effective in phototherapy. To this end it was determined whether the optical properties of these MAb-CNTs were affected by covalent coupling. The UV-Vis-NIR absorption spectrum of the MAb-CNTs closely matched that of the starting material (carboxylated CNTs dispersed in MES) in that both displayed a large pie-plasmon absorption band (Figure 5.b).

The MAb-CNTs were next analyzed using Raman spectroscopy. The G-band, observed at ~ 1590 cm^{-1} in the Raman spectrum of the MAb-CNT exhibited a G^-/G^+ line shape that was characteristic of single-walled CNTs and that was identical to the starting material. The ratio of the G band to the D band for the MAb-CNTs was at least 2-fold greater than that observed for the original dispersed CNTs indicating that the MAb-CNT coupling additionally purified the conjugate (Figure 5.c).

These data indicate that the binding of MAbs to the CNTs was specific and covalent, that the CNT component was present in the MAb-CNT conjugates, that the optical properties of the MAb-CNTs were identical to CNTs alone, and that the purity of the MAb-CNTs was superior to that of the starting material.

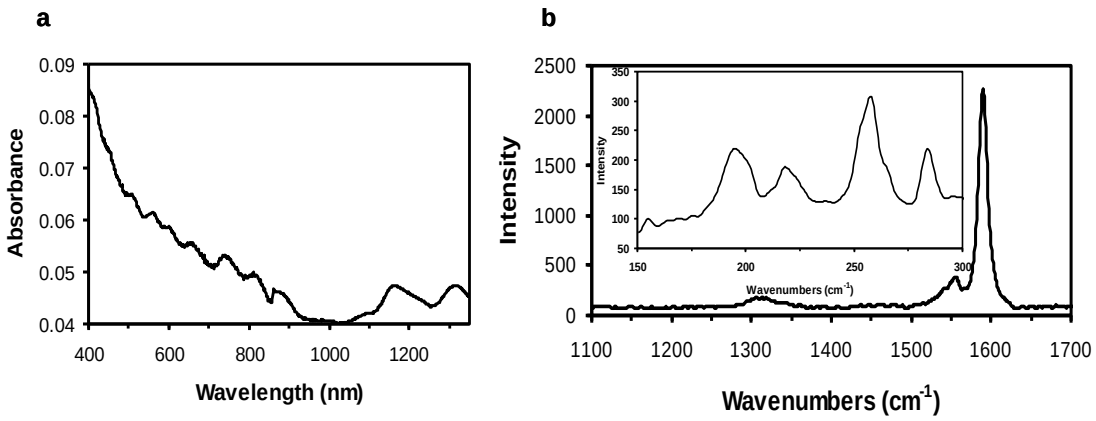

Figure 4. Characterization of CNTs following coupling with MAb-NA (MAb-NA-B-CNTs). (a) UV-Vis-NIR spectrum of MAb-NA-B-CNTs show the same metallic and semiconducting CNT types observed for the B-CNTs, indicating the retention of the optical properties of CNTs after coupling with MAb-NA. (b) Raman spectrum of MAb-NA-B-CNTs show an intense G band (1590 cm^{-1}) as the B-CNTs, indicating the presence of CNTs in the conjugate. The spectra are representative of three independent experiments.

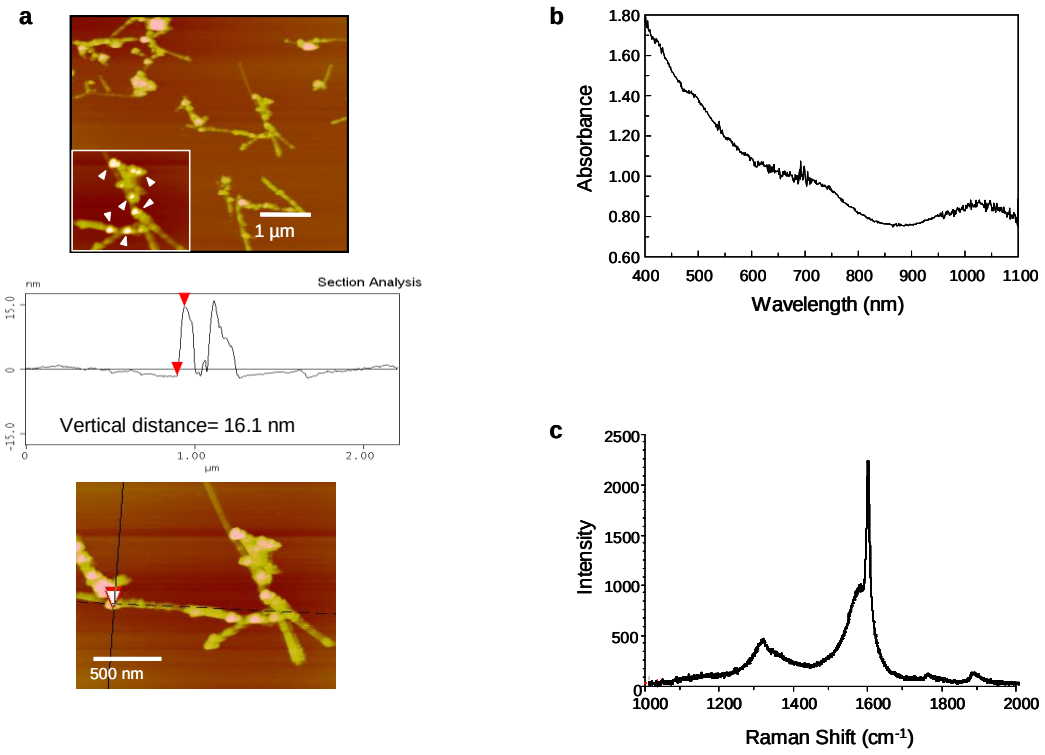

Figure 5. Characterization of CNTs following coupling to MAb (MAb-c-CNTs). (a) AFM image showing CNTs coated with MAbs. The enlarged inset shows where the MAbs are presumably attached to the CNTs (white arrowheads). This AFM image is representative of AFM images acquired from two unique MAb-CNT dispersions. (b) Background corrected UV-Vis-NIR absorption spectrum. (c) Representative Raman spectrum of MAb-c-CNTs showing the D-band at ~1310 cm^{-1} and the G-band at ~1590 cm^{-1}.

3.4 Specific binding of MAb-CNTs to target cells

To demonstrate that the MAb-CNTs could bind specifically to target cells, in the next set of experiments we used both a control ligand and a control cell to show that only the MAb-CNTs bind to cells that express the corresponding ligand. Specificity is critical because non-specific binding to ligand-negative cells could cause major side effects *in vivo*.

3.4.1 Non-covalent approach

The ability of the MAb-CNT conjugates to bind to ligand (antigen)-positive but not antigen-negative target cells was assessed by flow cytometry. Following coupling of MAbs and CNTs, Daudi cells or PHA-activated PBMCs (> 95% $CD25^+$ cells) were incubated with MAb-CNTs (containing 3.6 µg CNTs), the excess MAb-CNTs were washed off and the cells were incubated with FITC-GAMIg (which binds to mouse MAb) or phycoerythrin-streptavidin (PE-SA) (which binds to the biotin on the CNT). The bound fluorescence was analyzed on a FACScan. RFB4-CNT and RFB4 (positive control) bound equally well to Daudi cells, whereas RFT5-CNT (negative control) bound poorly ($P < 0.001$) (Figure 6.a). Conversely, RFT5-CNT and RFT5 bound equally well to $CD22^-CD25^+$ PHA-activated PBMCs whereas the negative control conjugate, RFB4-CNT, did not ($P < 0.002$) (Figure 6.b).

These results demonstrate that the coupling of the MAbs to CNTs did not alter their cell-binding activity and that the MAb-CNTs bind to antigen-expressing cells as specifically as the uncoupled MAbs.

3.4.2 Covalent approach

Following coupling of MAbs and CNTs, Daudi cells or PHA-activated PBMCs (> 95% $CD25^+$ cells) were incubated with MAb-CNTs (containing 1 µg CNTs), the excess MAb-CNTs were washed off and the cells were incubated with FITC-GAMIg. The bound fluorescence was analyzed on a FACScan. RFB4-CNTs bound well to Daudi cells, whereas the RFT5-CNTs (negative control) bound poorly (Figure 7.a). Conversely, RFT5-CNTs bound equally well to PBMCs, whereas the negative control conjugate, RFB4-CNT, did not (Figure 7.a). Additional

experiments using non-activated, carboxyl-functionalized CNTs incubated with targeting antibody (control) indicated no detectable binding to cells. This indicated that the CNTs were free of adsorbed MAb. Taken together, these results demonstrated that the MAb-CNTs bound specifically to antigen-expressing cells. Direct immunofluorescence was also performed to confirm the binding of the MAb-CNTs to the target cells with EGFP-conjugated RFB4-CNTs. Half the cells were analyzed by flow cytometry (Figure 7.a) while the other half were used in fluorescence microscopy (Figure 7.b). Saturation levels of MAb-CNTs on Daudi cells was detected by adding increasing amounts of RFB4-CNTs from 0.25 to 4 μg CNTs, containing an equivalent of 0.75 to 12 μg bound RFB4 (Figure 7.c). The results indicate that saturation was achieved at 0.25 μg CNTs.

These data indicate that the MAb-CNTs contain only covalently-bound MAb and are free of adsorbed MAb, that they bind specifically to antigen-positive but not antigen-negative target cells and that saturation binding is achieved.

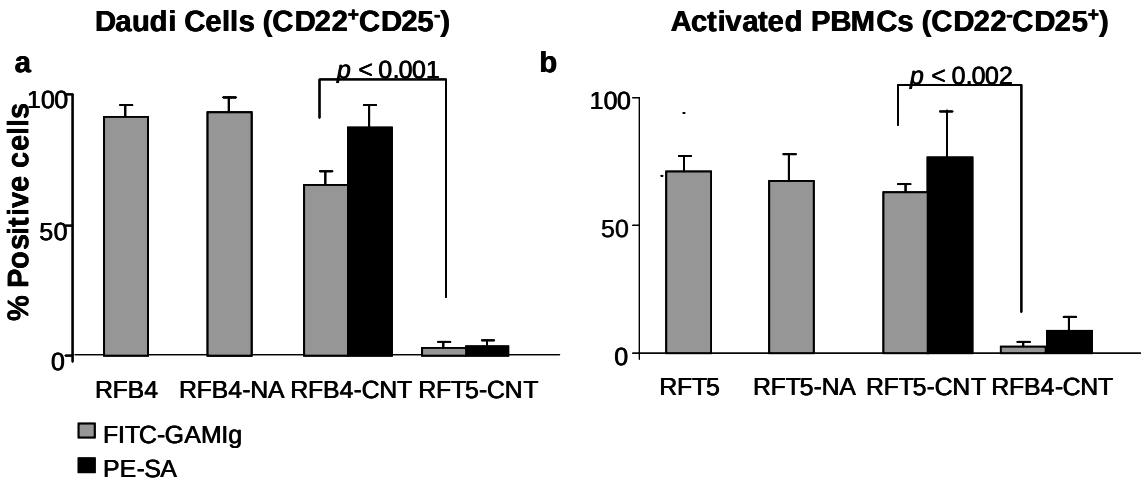

Figure 6. Specific binding of MAb-NA-B-CNTs to target cells. A million cells were incubated with saturating concentrations of RFB4-CNT or RFT5-CNT and then incubated with either FITC-GAMIg to detect the MAb-NA, or with PE-SA to detect the B-CNT and analyzed on a FACScan. (a) The specific binding of RFB4-CNT to Daudi cells using RFT5-CNT as a negative control ($p < 0.001$). (b) The specific binding of RFT5-CNT to activated PBMCs (>95% T cells) using RFB4-CNT as negative control ($p < 0.002$). Data represent mean ± S.D. of at least three independent experiments. *P*-values comparing binding of RFB4-CNT and RFT5-CNT were calculated utilizing paired, two-tail distribution Student's *t*-test.

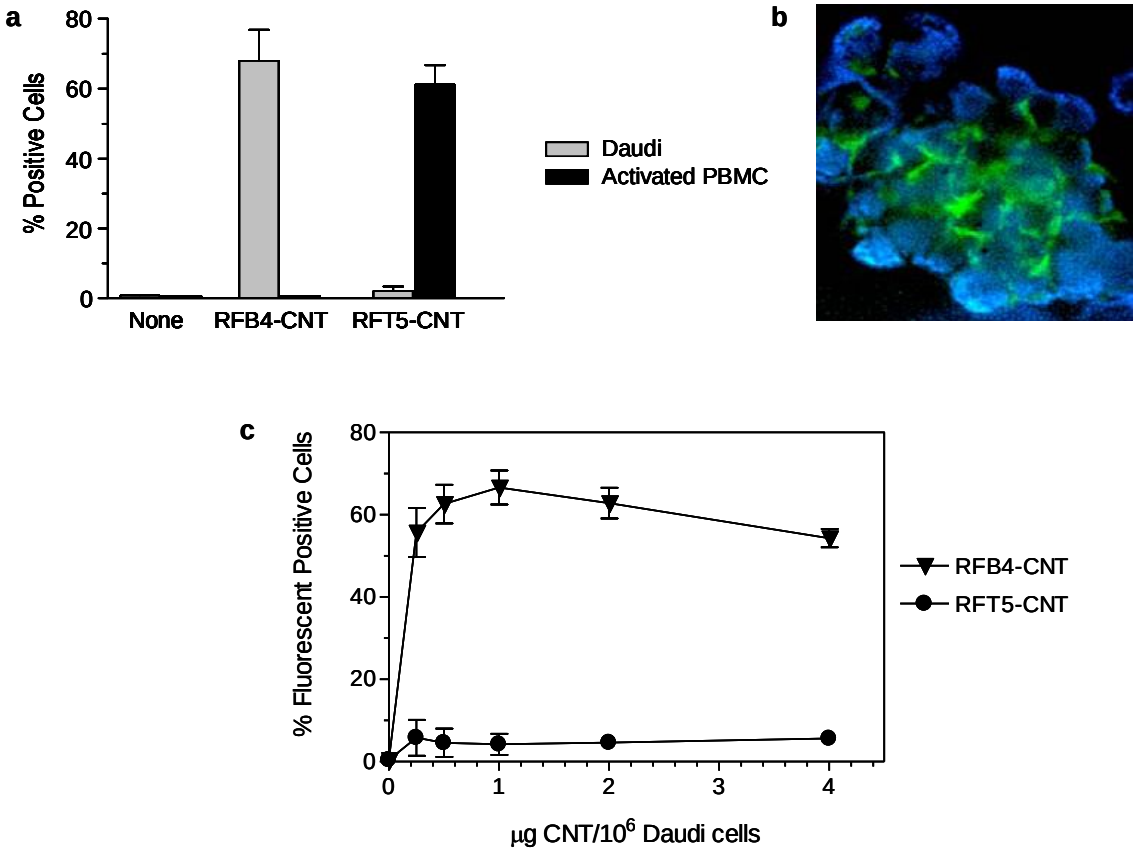

Figure 7. Specific binding of MAb-c-CNTs to target cells. Daudi cells or PHA-activated human PBMCs were stained with either RFB4-CNTs or RFT5-CNTs (1 µg CNT) followed by FITC-GAMIg and cells were analyzed on a FACScan. (a) The binding of MAb-c-CNTs to target *vs.* non-target cells was highly specific ($p<0.01$). The results of three independent binding experiments are presented as means of % positive cells ± SD. (b) The binding of RFB4-CNTs to Daudi cells was confirmed by direct fluorescence using c-CNTs co-conjugated to RFB4 and EGFP and visualized by fluorescence microscopy. (c) The saturation of Daudi cells with RFB4-CNTs was determined by incubating a million cells on ice with RFB4-CNTs or RFT5-CNTs in concentrations ranging from 0.25 to 4 µg in a total volume of 200 µl of PBS. After 3 washes with PBS cells were incubated with FITC-GAMIg, washed and analyzed on a FACScan. The results of three independent binding experiments are presented as the means of % positive cells ± SD.

3.5 Ablation of cells coated with MAb-CNTs by NIR light

One of the concerns of coupling MAbs non-covalently to CNTs is that the targeting ligand might dissociate from the CNTs. To circumvent this, ligands are covalently attached to CNTs to increase chemical stability. However, the concern with that is that chemical stability of covalent linkages can increase at the expense of photothermal efficacy i.e., chemical coupling of the MAb to CNTs could destroy the optical properties of the CNTs such that they could not convert NIR light to heat. For this purpose, it was important to see if there were significant differences in the killing efficiencies between the non-covalent and covalent conjugates.

3.5.1 Non-covalent approach

The ability of the cell-bound non-covalent MAb-CNTs to thermally ablate cells after exposure to NIR light was determined. Cells were incubated with the MAb-CNTs, washed three times with PBS, and then dispensed into 96-well plates in cell culture media. The cells in the plate were exposed to an 808-nm laser (5 W/cm^2) for 7 min and pulsed for the next 12 h with 1 μCi [^{3}H]-thymidine to assess cell viability. The viability of the RFB4-CNT-treated Daudi cells, as compared to treatment with the nonbinding RFT5-CNTs, was significantly reduced after exposure to NIR light (P<0.0001) (Figure 8.a). Conversely, when activated PBMCs were used as target cells, RFT5-CNT, but not RFB4-CNT, killed the cells after exposure to NIR light (P<0.0001) (Figure 8.b).

In conclusion, these experiments demonstrated that the binding of the MAb-CNTs to their respective antigen-positive target cells lead to their specific ablation after exposure to NIR light.

3.5.2 Covalent approach

The ability of the cell-bound covalent MAb-CNTs to thermally ablate target cells, following exposure to NIR light, was also determined. Cells were incubated with the MAb-CNTs in PBS for 15 min, the excess unbound MAb-CNTs were removed, cells were suspended in culture medium and dispensed into 96-well plates. The cells in the plate were exposed to an

808 nm laser (9.5 W/cm^2) for 4 min and pulsed for the next 12 hrs with 1 μCi [^{3}H]-thymidine to assess their proliferative capacity. As compared to the non-binding control RFT5-CNTs, the viability of the RFB4-CNT-treated Daudi cells was significantly reduced following exposure to NIR light (p<0.01) (Figure 9.a). Conversely, when activated PBMCs were used as target cells, RFT5-CNTs, but not the control RFB4-CNTs, killed the cells following exposure to NIR light (Figure 9.b). The proliferation of cells treated with the covalent MAb-CNTs (Daudi treated with RFB4-CNT and PBMCs treated with RFT5-CNTs) in the absence of NIR light was significantly lower (p<0.05) than the proliferation of untreated cells (Figure 9.a and 9.b). This may be due to an extensive cross-linking of the target antigen by the MAb-CNTs and subsequent signaling of growth arrest and/or apoptosis. This possibility is supported by the observation that cells undergo massive clustering. No inhibition of cell proliferation occurred when Daudi cells were treated with control RFT5-CNTs or when PBMCs were treated with the control RFB4-CNTs (Figure 9.a and 9.b).

Since both the non-covalent and covalent constructs thermally ablated target cells with the same specificity and efficiency, we concluded that there were no significant differences in the killing efficiencies of the two constructs following exposure to NIR light.

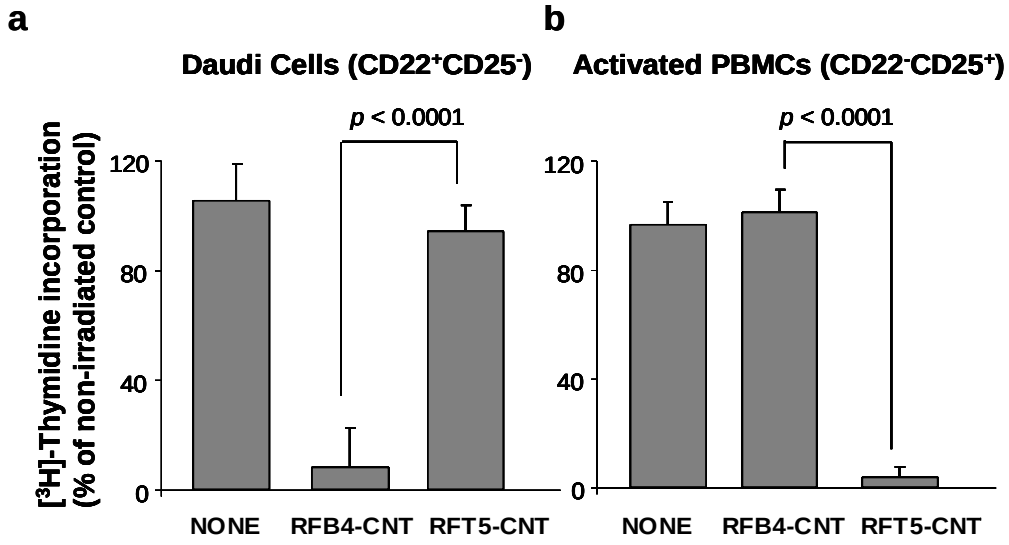

Figure 8. Ablation of cells coated with MAb-NA-B-CNTs by NIR light. A million cells were incubated with saturating concentrations of RFB4-CNT or RFT5-CNT. Cells were exposed for 7 min to 808 nm NIR light (5 W/cm^2), pulsed with 1µCi [^{3}H]-Thymidine and harvested 12 hr later. The percentage of radioactivity incorporated by each sample was calculated relative to corresponding non-irradiated sample. (a) The specific killing by RFB4-CNT of Daudi cells using RFT5-CNT as a negative control ($P < 0.0001$) (b) The specific killing by RFT5-CNT of activated PBMCs (>95% T cells) using RFB4-CNT as a negative control ($P < 0.0001$). Data represent the mean ± SD of at least three independent experiments.

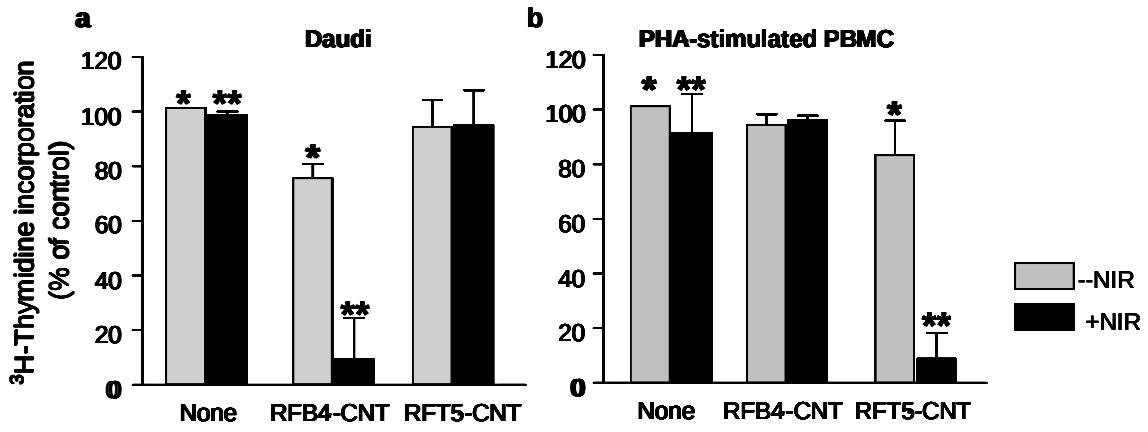

Figure 9. Ablation of cells coated with MAb-c-CNTs by NIR irradiation. A million cells were incubated with MAb-c-CNTs containing 3 µg CNTs in PBS for 15 min at 4°C. The cells were exposed for 4 min to continuous NIR light at 808 nm (9.5 W/cm^2), pulsed with 1µCi [^{3}H]-Thymidine and harvested 12 hr later. The percentage of radioactivity incorporated by each sample was calculated relative to corresponding non-irradiated sample. (a) The specific killing of Daudi cells by RFB4-CNTs using RFT5-CNTs as the negative control. (b) The specific killing of activated PBMCs (> 95% T cells) by RFT5-CNTs using RFB4-CNTs as the negative control (*, p< 0.01; **, p< 0.05). Data represent mean ± S.D. of at least three independent experiments.

3.6 Stability of MAb-CNTs

Since the MAb-CNTs are being developed for *in vivo* use, it was important to establish the stability of the constructs under conditions designed to mimic the *in vivo* environment. Hence, the MAb-CNTs were incubated in mouse serum at 37°C for different durations of time and then tested to determine whether the MAb and CNT components remained stably linked together.

3.6.1 Non-covalent approach

Non-covalent MAb-CNTs were freshly prepared as described in the Methods. They where then incubated in mouse serum at 37°C for 0, 24, 48, and 72 h. At each time point, the MAb-CNTs were washed with PBS, incubated with Daudi cells, and irradiated with NIR light in a procedure similar to the thermal ablation described in Methods. No loss in their ability to thermally ablate Daudi cells was observed, even after 72 h in mouse serum at 37°C (Figure 10).

In conclusion, the data indicated that the MAb was stably coupled to the non-covalently bound DSPE-PEG-biotin and the DSPE-PEG-biotin was being retained on the CNTs under conditions designed to mimic the *in vivo* environment.

3.6.2 Covalent approach

To demonstrate that the coupling of the MAbs to the CNTs was covalent and stable, the covalently coupled MAb-CNTs were heated in SDS. Two covalently coupled RFB4-CNT samples were used, one containing 2 μg CNTs and the other containing 5 μg CNTs. They were electrophoresed on a 7.5% polyacrylamide gel under non-reducing conditions. The IgG was stained for by Simply Blue SafeStain. It was found that the CNTs remained in the loading well. No IgG from the RFB4-CNT samples entered the running gel, demonstrating that the CNT-bound IgG remained in the loading well, firmly attached to the CNTs. In contrast, in a control sample that contained a mixture of equivalent amounts of IgG and carboxylated-CNTs that were not activated with EDC and NHS, an IgG band was detected in the running gel (Figure 11.a).

In summary, the data demonstrate that the linkage between the MAbs and the CNTs was stable and that it did not disassociate even when boiled in SDS.

The stability of the MAb-CNT conjugate was also established by incubating RFB4-CNTs (containing 1 μg CNTs) in 500 μl mouse serum at 37 °C for up to 24 h. At the end of incubation, the RFB4-CNTs were recovered by centrifugation and then tested for their ability to bind to $CD22^{+}$ Daudi cells, using RFT5-CNT as the negative control. The binding to cells was determined by flow cytometry (Figure 11.b). The binding of the MAb-CNTs to the cells was not diminished at the different time points. This indicates that the MAbs remain stably bound to the CNTs under conditions that mimic the *in vivo* environment.

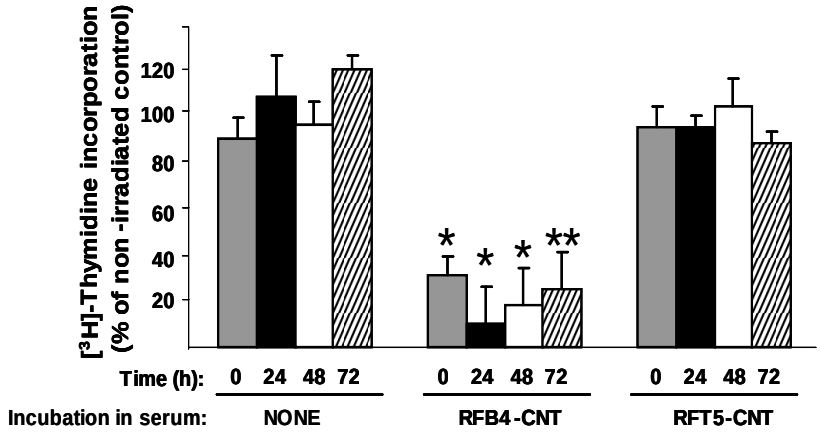

Figure 10. Stability of MAb-NA-B-CNTs. The stability of the MAb-NA-B-CNTs *in vitro* was determined by incubating them in mouse serum at 37°C for 0, 24, 48, and 72 hr. At each time point, the MAb-NA-B-CNTs were washed with PBS, incubated with Daudi cells, and exposed to NIR light for 7 min to 808 nm NIR light (5 W/cm^2), pulsed with 1µCi [^{3}H]-Thymidine and harvested 12 hr later. The percentage of radioactivity incorporated by each sample was calculated relative to corresponding non-irradiated sample. The activity of the RFB4-CNTs at the different time points remained unchanged. *, $P < 0.0001$; **, $P < 0.05$ for the values obtained at the corresponding time points with RFT5-CNTs. Data represent the mean ± SD of three independent experiments.

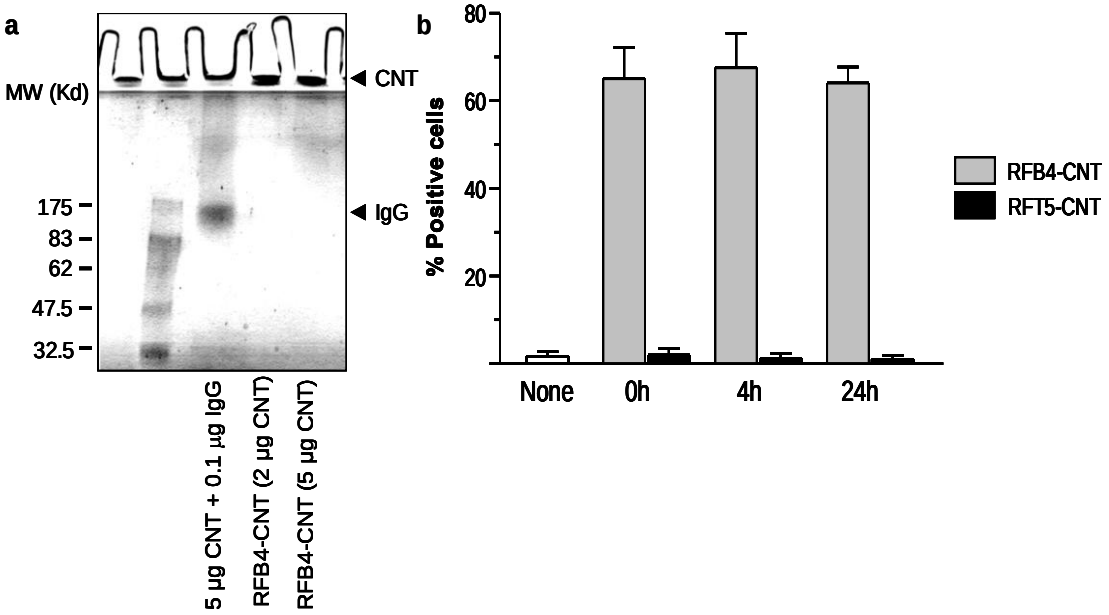

Figure 11. Stability of MAb-c-CNTs. (a) Purified RFB4-CNTs or a mixture of carboxylated CNTs (c-CNTs) and RFB4 (control) were subjected to SDS-PAGE. Samples containing 2 or 5 µg CNTs were loaded on the gel. The stacking gel shows the accumulation of CNTs whereas dissociated IgG migrated into the gel. The presence of dissociated protein was detected by staining with SimplyBlue SafeStain. (b) The stability of the RFB4-CNTs *in vitro* was determined by incubating them (1 µg CNT) in mouse serum at 37^{o}C for 0, 4 and 24 hr. At each time point, the RFB4-CNTs were recovered by centrifugation, washed with PBS and incubated with Daudi cells and the positive binding analyzed on a FACScan. Data represent the mean ± S.D. of at least three independent experiments.

3.7 Morphology of cells coated with MAb-c-CNTs and treated with NIR light

Since selective photothermal damage was determined by the failure of the cells to proliferate, it was important to confirm the inhibition of proliferation by investigating the effect of thermal ablation on the morphological integrity of the cells. For this purpose, the morphology of the cells was visualized by light microscopy.

A million Daudi cells were incubated with MAb-c-CNTs containing 3 µg CNTs for 15 min at 4^{o}C. The cells were exposed for 4 min to continuous NIR light at 808 nm (9.5 W/cm^2). Following NIR light, the selective photothermal damage responsible for the inhibition of proliferation was confirmed under light microscopy as the loss of morphological integrity in Daudi cells pretreated with RFB4-CNT (Figure 12.b) but not in untreated or control cells treated with RFT5-CNT (Figure 12.a and 12.c). Daudi cells pretreated with RFB4-CNTs and not subjected to NIR light formed “tissue-like” structure of aggregates with large contact areas after 12 h of incubation (Figure 12.e). In contrast, no aggregates (Figure 12.d and 12.f) formed when Daudi cells were untreated or when they were treated with non-binding RFT5-CNTs.

In conclusion, these data indicate that the homotypic adhesion and the concurrent inhibitory effect are specific and hence ligand -dependent. CNT-mediated nonspecific adhesion was not observed since untreated cells and cells treated with the control conjugate were not damaged.

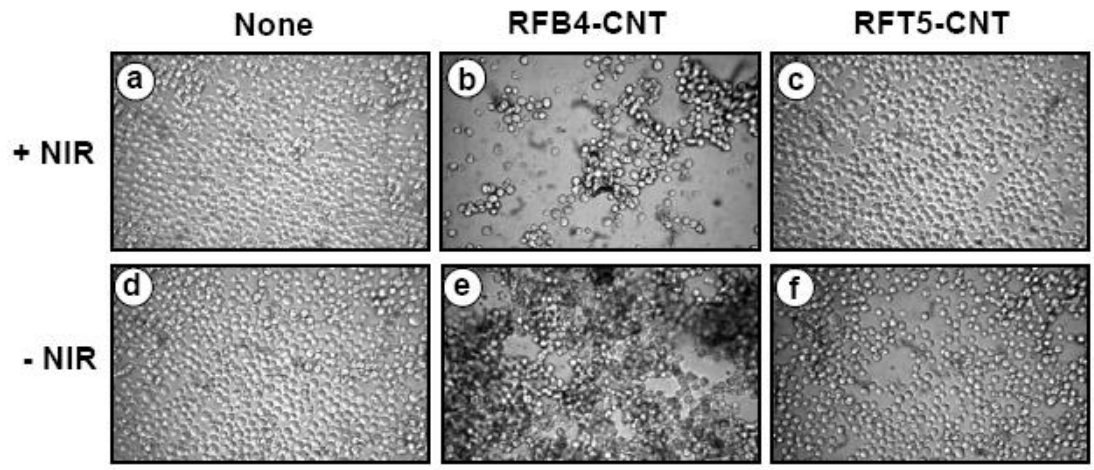

Figure 12. Morphology of cells coated with MAb-c-CNTs following exposure to NIR light. A million cells were incubated with MAb-c-CNTs containing 3 µg CNTs in PBS for 15 min at 4°C. The cells were exposed for 4 min to continuous NIR light at 808 nm (9.5 W/cm^2). Cell morphology was assessed 12 h later by light microscopy (Magnification, x40 in all panels).

3.8 Calibration curves of RFB4-CNT in organ lysates, blood and PBS

Radio labels or fluorescent labels for nanomaterials are useful for *in vivo* tracking over short periods of time (a few hrs to a few days); however, there is always the possibility that they could dissociate or decay over time. It was thus important to detect the nanotubes based on their intrinsic physical properties such as the Raman G band peak of the CNTs at 1590 cm^{-1}. Raman G band intensities of CNT solutions with known concentrations could be plotted against their concentrations to obtain a calibration curve.

Non-covalent RFB4-CNTs, organ lysates and blood were prepared as described in Methods. Raman spectra of RFB4-CNT solutions with known CNT concentrations from 4 – 0.063 µg/ml (4 – 0.25 µg/ml for blood, kidney and PBS) were acquired and the G-band intensities (integrated peak area from 1572 cm^{-1} to 1610 cm^{-1}) were plotted against CNT concentrations (as determined by their NIR absorption) for the calibration curve (Figure 13). This was carried out for each of the organ lysates, blood and PBS. RFB4-CNT dilutions, made up in organ lysate/blood/PBS, were added to glass imaging dishes, placed under the 10X objective and the Raman spectra acquired. Linear dependence was observed from 4 – 0.5 µg/ml (Figure 13). The lower detection limit of 0.5 µg/ml corresponded to ~ 8% ID/g in the liver and tumor, ~ 10 and ~ 13% ID/g in the kidney and lung respectively and ~ 2.7% ID/g in the blood.

Strong correlation coefficients were obtained for all the organ lysates, PBS and blood indicating that the linear dependence would make it possible to do quantitative measurement of CNT concentration in tissue lysates and blood of mice using Raman spectroscopy. It was also observed that RFB4-CNTs exhibited similar Raman intensities in the organ lysates but were slightly different in PBS and blood (Figure 13).

Linear dependence was observed over a relevant concentration range which would enable the use of this technique to quantify the concentration of MAb-CNTs in tissues and blood *in vivo*.

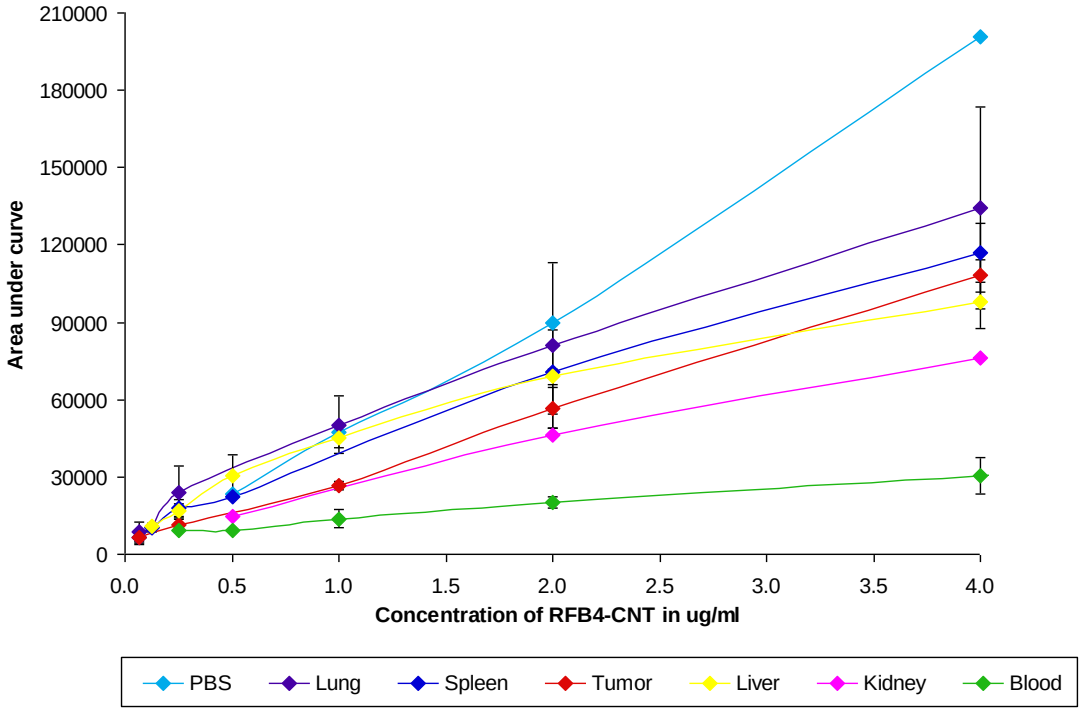

Figure 13. Calibration curves of RFB4-CNT in organ lysates, blood and PBS. RFB4-CNT conjugates were prepared as detailed in the Methods. The organ lysates and blood were collected from untreated mice (n=3) and processed as detailed in the Methods. The concentration of the CNT component of the RFB4-CNT was determined by UV-Vis-NIR at a wavelength of 808 nm. Sixty five µl of RFB4-CNT dilutions ranging from 4 - 0.063 µg/ml (4 – 0.25 µg/ml for blood, kidney and PBS) were placed in imaging dishes, Raman spectra were recorded at two different locations (90-sec acquisition time/spectrum) using a 10X objective and the Raman intensity obtained by averaging the CNT G-band peak area under curve from 1572 cm^{-1} to 1610 cm^{-1}. Correlation coefficients were calculated and were 0.9967 (PBS), 0.9856 (Lung), 0.9923 (Spleen), 0.9981 (Tumor), 0.9514 (Liver), 0.9895 (Kidney) and 0.9937 (Blood). Data represent mean ± S.D. of three independent experiments where, for each concentration, at least two spectra were obtained.

3.9 Clearance of RFB4-CNT from the blood of SCID/NOD mice

Prior to carrying out tumor ablation studies *in vivo* it was important to determine the blood circulation time of MAb-CNTs. Longer blood circulation times should provide more time for the MAb-CNT constructs to accumulate at the target site or penetrate large tumors. The intrinsic Raman signature of the CNTs was used to quantify the MAb-CNT constructs *in vivo*. 160 µl of RFB4-CNTs in PBS at a concentration of 116 µg/ml (18.6 µg of CNTs) were injected i.v. into mice with s.c. BL tumor, as described in Methods. Blood was drawn from the mice at < 1 min, 8 and 24 hrs p.i. and processed as described in Methods. This experiment was carried out three times with 5 mice per experiment (total number of mice = 15); however, data was only collected from four mice in total because the other eleven mice did not appear to have received the correct dose of the RFB4-CNTs due to technical problems. The blood from the four mice was stored at 4^{o}C for about six months resulting in some samples that had lost their liquid content. Hence, those blood samples had to be resuspended in a fixed volume of DI water. Unfortunately, this was not accurate because the initial volume of blood collected for those samples was unknown.

According to the results obtained here, the RFB4-CNTs rapidly clear the blood, with 2 animals having 0% ID and 2 animals having ~ 8% ID at 24 hrs p.i. (Figure 14). It is difficult to make a prediction of the half-life in blood because the time-points were so far apart, i.e. 1 min vs 8 hrs. It will therefore be important to investigate time points between 10 min and 1 hr.

Due to sample storage issues in addition to the small number of animals for data collection, the blood circulation data may not provide statistical power; however, the overall profile is unlikely to change very much even if repeated with a larger number of animals and better storage methods.

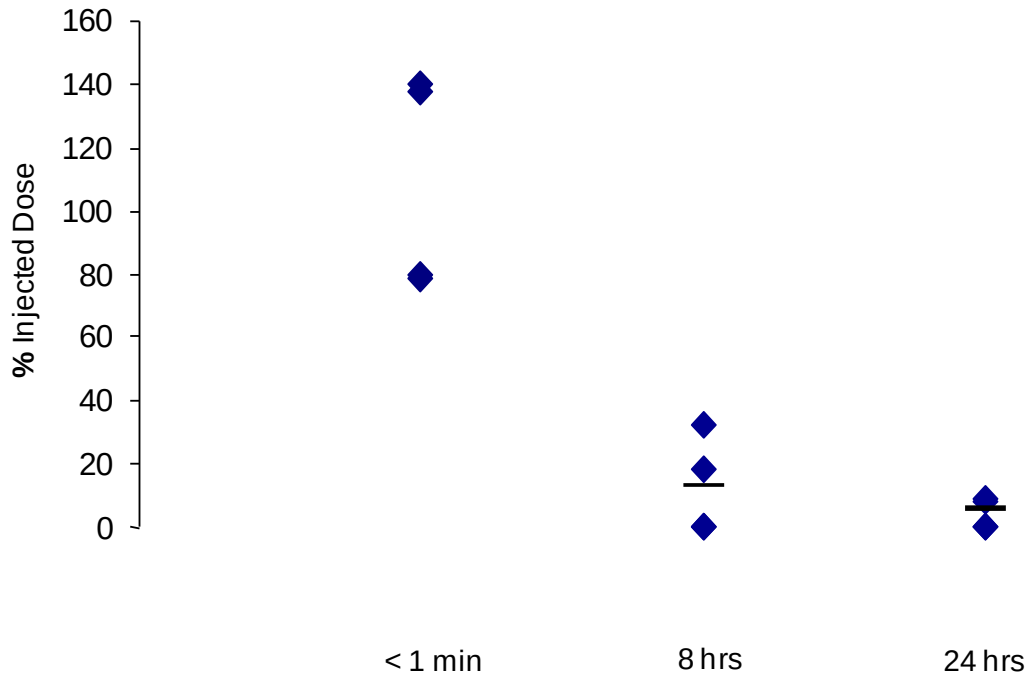

Figure 14. Clearance of RFB4-CNT from the blood of SCID/NOD mice. Blood was collected at < 1 min, 8 and 24 hrs following injection of 18.6 µg of RFB4-CNT as detailed in the Methods. The blood was mixed thoroughly 1:1 with lysis buffer (1% SDS, 1% Triton X-100, 40 mM Tris Acetate, 10 mM EDTA, 10 mM DTT) and incubated at 4^{o}C for 72 hrs prior to use. Sixty five µl of blood was placed in imaging dishes, Raman spectra recorded (90-sec acquisition time/spectrum) at two different locations using a 10X objective and the Raman intensity obtained by averaging the CNT G-band peak area under curve from 1572 cm^{-1} to 1610 cm^{-1}. The percent injected dose (%ID) was calculated by the following equation:

$$\%ID = \frac{[RFB4\text{-}CNT]_{blood\ lysate} \times V_{blood\ lysate}}{[RFB4\text{-}CNT]_{injected} \times V_{injected}} \times 100\%$$

The concentration of RFB4-CNT in the blood of the injected animal ($[RFB4\text{-}CNT]_{blood\ lysate}$) was determined from the Raman intensity of the blood lysate and the corresponding calibration curve. The volume of the blood lysate ($V_{blood\ lysate}$) was 6% of the mouse body weight [260]. This experiment was repeated three times with five mice per experiment. We have data from only four mice as we could not measure a Raman signal of sufficient intensity from the remaining eleven mice. %ID from animals were compiled and then grouped; each dot represents one animal, the average of all animals in a group is represented by a horizontal line.

3.10 Biodistribution of RFB4-CNT in SCID/NOD mice

The use of Raman spectroscopy to quantify CNTs provides the ability to determine the biodistribution of the conjugates in various organs over a period of time. Organs can be frozen down, lyophilized and stored until Raman spectroscopy can be done to determine the level of RES uptake and the excretion profile.

160 µl of RFB4-CNTs in PBS at a concentration of 116 µg/ml (18.6 µg of CNTs) were injected i.v. into mice with s.c. BL tumor, as described in Methods. To investigate the biodistribution of the RFB4-CNTs in several major organs 24 hr after injection, mice were sacrificed, their organs lyophilized and then homogenized in lysis buffer as described in Methods. This experiment was carried out three times with 5 mice per experiment (total number of mice = 15). However, data were only collected from six mice because the other nine mice did not appear to have received the correct dose of the RFB4-CNTs. Most of the RFB4-CNTs accumulated in the liver, lung and spleen as would be predicted (Figure 15). When the injected dose was 18.6 µg of CNTs, no obvious CNT signals were detected in the kidney. The detection limit of 0.5 µg/ml corresponded to ~ 8% ID/g in the liver and tumor, ~ 10 and ~ 13% ID/g in the kidney and lung. Therefore, with the injected dose, the lack of appreciable CNT signals in organs other than the RES did not mean that there was no CNT uptake; however, it suggested that the level of uptake was lower than what could be detected by Raman spectroscopy for that organ (Figure 15). It was not possible to predict whether the DSPE-PEG-biotin coating with the attached RFB4, was still present on the CNTs as suggested by the *in vitro* experiments.

Since this was a pilot experiment, the goal was to determine if the RFB4-CNTs would reach the tumor and if so, what percentage of injected dose would be present.

In conclusion, the data indicate that there was predominantly RES uptake of the MAb-CNTs, little to no tumor uptake, possible long-term presence of the CNTs in organs *in vivo* and no consensus on the presence of MAb on the surface of the CNTs. More experiments must be

carried out to increase the sensitivity of detection in order to determine the uptake of the conjugates in the various tissues.

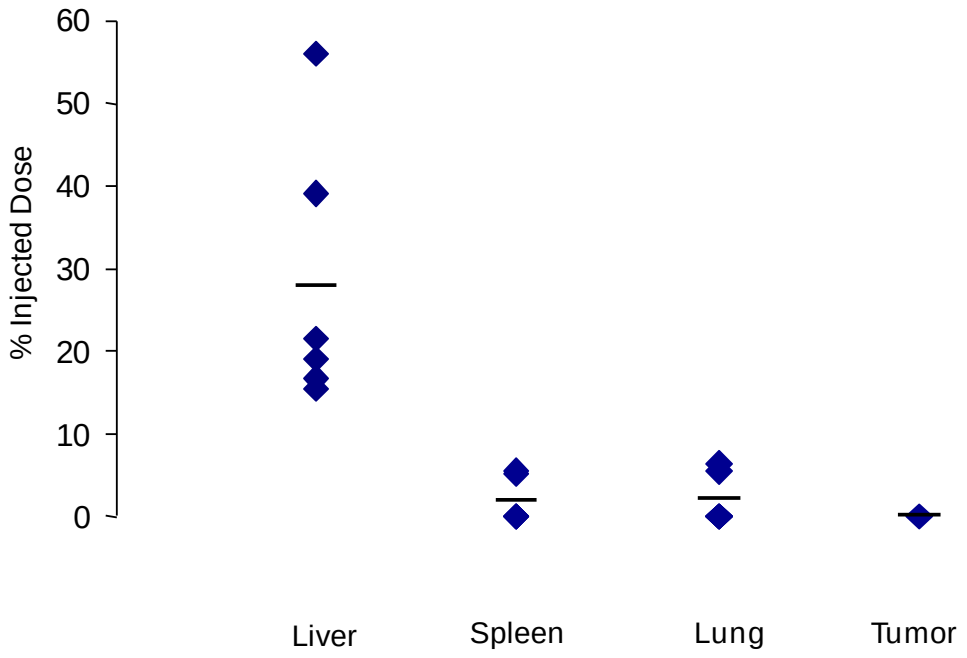

Figure 15. Biodistribution of RFB4-CNT in SCID/NOD mice. Organs were collected from the mouse after perfusion, 24 hrs p.i.of 18.6 µg of RFB4-CNT as detailed in the Methods. The organs were cut into pieces, frozen, lypohilized and processed as detailed in the Methods. Briefly, they were ground into a fine powder, suspended in 10 mg/ml of Collagenase Type I in HBSS and placed in the incubator at 37^{o}C for 2 hrs 45 min. They were then mixed 1:1 with lysis buffer (1% SDS, 1% Triton X-100, 40 mM Tris Acetate, 10 mM EDTA, 10 mM DTT), sonicated by 3 pulses of 15 sec at a power level of 10 W and passed though a 23G needle five times. Sixty five µl of blood was placed in imaging dishes, Raman spectra were recorded (90-sec acquisition time/spectrum) at two different locations using a 10X objective and the Raman intensity was obtained by averaging the CNT G-band peak area under the curve from 1572 cm^{-1} to 1610 cm^{-1}. The percent injected dose (%ID) was:

$$\%ID = \frac{[RFB4\text{-}CNT]_{tissue\ lysate} \times V_{tissue\ lysate}}{[RFB4\text{-}CNT]_{injected} \times V_{injected}} \times 100\%$$

The concentration of RFB4-CNT in the organ of the injected animal ([RFB4-CNT] $_{tissue\ lysate}$) was determined from the Raman intensity of the tissue lysate and the corresponding organ calibration curve. The volume of the tissue lysate ($V_{tissue\ lysate}$) was the volume of buffer in which the organ had been suspended. This experiment was repeated three times with five mice per experiment. We have data from only six mice as we could not measure a Raman signal of sufficient intensity from the remaining nine mice. %ID from animals were compiled and then grouped; each dot represents one animal, the average of all animals in a group is represented by a horizontal line.

CHAPTER 4

DISCUSSION

4.1 Study objectives and major findings

The use of NIR-resonant nanostructures, including gold nanoshells and CNTs, to thermally ablate cancer is being explored by several groups [121, 125, 132-133, 135-136, 139, 141, 151-152, 179, 262]. The use of NIR light in the 700 – 1100 nm range for the induction of hyperthermia is particularly attractive because living tissues do not strongly absorb in this range [263]. Hence an external NIR light source should safely and effectively penetrate normal tissue and ablate any cells to which the CNTs are attached. The critical aspect for selective CNT-mediated thermal ablation of cells is to stably attach targeting moieties that will not interfere with the optical properties of the CNTs and yet retain specificity. The targeting of CNTs to tumor cells can be accomplished by coating them with cell-binding ligands such as peptides or MAbs [150, 155, 189, 243, 264-265]. Several studies have reported that the targeting of such CNTs is ‘‘specific’’ [150, 155, 189, 264], but no study has used both a control ligand and a control cell to convincingly demonstrate ligand-specific binding and thermal ablation of tumors cells with CNTs. Specificity is critical because nonspecific binding to antigen-negative cells *in vivo* could cause major side effects, which has been a confounding issue in the cancer targeting field for > 25 years.

We were interested in “assembling” our targeted CNTs using any targeting MAb that could be bound to the CNT. For this reason, we generated targeted CNTs consisting of NA-conjugated MAbs attached to a biotinylated polymer that non-covalently coated the CNTs. However, the potential limiting factor in this design *in vivo* was that the non-covalently attached

molecules could be displaced by macromolecules in biological fluids, resulting in the disassociation of the targeting moiety from the CNTs. We therefore also tried an alternative strategy where the targeting molecule was covalently coupled to the CNTs. The potential drawback to this strategy was that covalent modification of CNTs might interfere with the NIR-absorption properties of the CNTs. However, there do exist ways to modulate electromagnetic signals that might be transferred to NIR technology ("stealth" coatings for magnetically suscpetible devices in patients undergoing magnetic resonance imaging (MRI), "stealth" aircraft that can defeat radar interception [29]).

One of the goals of this study was to characterize the binding and killing properties of the non-covalent and covalent constructs *in vitro.* Both a control CNT construct and a control cell were used to definitely prove specificity. Another goal was to determine the behavior of the non-covalent and covalent constructs *in vivo*. However, there were major technical issues with trying to quantify the levels of the covalently targeted CNTs in organs and blood, and hence the *in vivo* data for only the non-covalently targeted CNTs are presented. However, results to date do not rule out the covalent conjugation approach.

The objectives of this study were: 1) to design and characterize non-covalent and covalent anti-CD22 and anti-CD25-targeted CNT constructs, 2) to determine the binding of the non-covalent and covalent CNT constructs *in vitro,* 3) to investigate the killing properties of the non-covalent and covalent CNT constructs *in vitro,* 4) to determine the behavior of the non-covalent CNT constructs *in vivo.*

The major findings to emerge from this study were that the non-covalent and covalent MAb-CNT conjugates were well-dispersed, optically active, stable and biocompatible, demonstrated excellent specificity in targeting and thermal ablation of target cells *in vitro* and the non-covalent MAb-CNT conjugate rapidly cleared the bloodstream and accumulated in the RES *in vivo*.

4.2 MAb-CNT conjugates were well-dispersed, optically active, stable and biocompatible

The technical challenges facing the application of CNTs in biomedicine are that CNTs are extremely hydrophobic with a tendency to bundle together, are chemically inert and have a biocompatibility profile that is conflicting.

To modify the hydrophobic surface of the CNTs and make them water-soluble and to optimize biocompatibility and reduce toxicity, the CNTs have been functionalized non-covalently and covalently with water-soluble materials [144, 166, 266-270]. Chemical reactions that form carboxyl groups on the sidewalls and the ends of the tube are carried out in covalent functionalization, while the noncovalent functionalization results in interactions between the hydrophobic domain of an amphiphilic molecule and the surface of the CNT with the amphiphilic molecule wrapping itself around the CNT. Functionalized CNTs have been shown to shuttle various biological molecular cargoes into cells [190, 208, 222-223, 225, 238, 271].

In this study we chose to try both the covalent and non-covalent methods of coupling MAbs to CNTs. The covalent approach dispersed the CNTs in MES buffer to which Tween-20 surfactant was added. This helped to coat the CNTs and disperse them following sonication. The carboxyl groups present on the sidewalls and the ends of the CNTs were used for the conjugation of MAbs that would target the CNTs to cells. While this approach resulted in MAbs being robustly bonded to the CNTs, there are accounts that the intrinsic physical properties of the CNTs such as photoluminescence and Raman scattering are reduced to a large extent [175].

In the noncovalent approach to functionalizing the CNTs, the surface of the CNTs was coated with an amphiphilic polymer that would not disrupt the carbon-carbon bonds. It was important to choose an amphiphilic polymer that would impart solubility, was biocompatible, nontoxic, stable and had functional groups that would be available for bioconjugation with antibodies. PEGylated phospholipids (PL-PEG) with attached biotin was the polymer of choice as it met the above requirements. PEG forms the corona, which provides steric stabilization and

confers “stealth” properties to prevent protein adsorption. Protein adsorption leads to aggregation and rapid clearance from the bloodstream *in vivo* [209, 272]. C16 alkylation is another option to prevent protein adsorption. Enhanced albumin adsorption on alkylated surfaces has been observed [273]. The albumin can buttress the targeting sites. This has been shown to occur in 2-protein adsorption-desorption studies [274].

The non-covalent approach also used the biotin-avidin interaction as a general “bridge” system to generate targeting moieties (avidin coupled to MAb) attached to CNTs (biotin coupled to CNTs). This provided the flexibility to assemble the targeted CNT using any cell-binding MAb. The unique characteristics of the biotin-avidin interaction that make it ideal as a bridge system are the high affinity and specificity of biotin for avidin, the four binding sites in avidin for biotin, making it possible to multiply biotinylated moieties, the small size of biotin that enables biotinylation of molecules without altering their properties and the stability of the biotin and avidin proteins that can survive harsh reaction conditions and extensive derivatization [261] .

AFM analyses revealed well dispersed CNTs existing in small bundles. UV-Vis and Raman spectroscopy revealed that the spectra of the MAb-CNT conjugates were similar to what was observed with the CNT dispersion alone, thus indicating that the optical properties of the CNTs were undisturbed following conjugation to MAbs. The covalent MAb-CNT conjugates did show an increase in the disorder mode (D-band at ~ 1300 cm^{-1}) in the Raman spectrum and loss of interband transitions between van Hove singularities in the absorption spectrum relative to the noncovalent conjugate; however this was also observed with the carboxylated CNT dispersion alone (prior to MAb conjugation).

Testing for stability of targeted CNT constructs *in vitro* is a critical step in designing MAb-CNT conjugates because it provides proof of the *in vivo* stability. If the constructs are found to be stable in conditions designed to mimic the *in vivo* environment, it might indicate that they could be used *in vivo*. However, most studies do not address this issue and it is very critical that it be done. Indeed Cherukuri et al. have observed displacement of polyethylene

oxide CNT coatings by proteins *in vivo* [158]. Studies have shown the stability by incubating radioactively- labeled constructs in human plasma at 37^{o}C for 96 hrs [243] or in mouse serum at 37^{o}C for up to 24 hrs [194] and then determining the intact radioactivity on the CNTs. In this study, it was found that the MAb-CNT conjugates had excellent aqueous stability as determined visually and by optical means such as UV-Vis-NIR absorption spectra and AFM analyses. Some decanting of the CNTs was observed over time; however, this was easily resolved by a quick sonication. Following incubation at 37^{o}C in mouse serum, it was observed that the MAb-CNT constructs did not exhibit any change in their ability to ablate (non-covalent) or to bind to (covalent) target cells relative to MAb-CNT constructs that had not been incubated in mouse serum. Boiling the MAb-CNT constructs (covalent) in SDS did not result in the MAbs being dissociated from the CNTs.

It was important to determine the potential inherent toxicity of the CNTs before determining their efficacy as photothermal agents in the treatment of cancer. *In vitro* studies highlight that CNTs can be toxic to macrophages [275-276], lymphocytes [277], keratinocytes [278-279], mesothelial cells [280], aortic smooth muscle cells [281], skin fibroblasts [282-284] and embryo kidney cells [211]. The toxicity of CNTs depends on their physicochemical properties which are influenced by the synthesis method, the presence of bundles in the dispersion, number of walls in the CNTs (single or multi-walled), amount of metal catalyst and carbon impurities present, size and surface modification (acid treatment or functionalization). Sayes et al. showed that the toxicity of CNTs was decreased as the degree of functionalization with COOH or SO_3H groups was increased [283]. However, Magrez et al. showed that cellular toxicity increased with the grafting of putatively “toxic” chemical groups on the surface of the CNTs [285]. Dumortier et al. showed that NH_3-functionalized CNTs did not induce toxicity *in vitro* [207]. The presence of surfactants and metal catalysts are highly toxic to cells [217-218, 286]. Other groups have shown that well functionalized, and serum stable CNT dispersions have not caused toxicity *in vitro* [154, 157, 179, 189-191, 199-200, 203-205, 243, 287-289]. The

CNTs that we used had relatively low levels of amorphous carbon (HiPCO CNTs, [290]), existed in small bundles of cell-culture compatible length and diameter, had low levels of metal contaminants relative to the raw powder, were well-functionalized and serum-stable without dangling “toxic” chemical groups and were suspended in surfactant at levels that was shown to be non-toxic to cells.

One of the issues also to consider is the potential interaction of CNTs with currently used viability assays. Wörle-Knirsch et al. showed that CNTs can interact with the tetrazolium salt (3-(4,5-dimethylthiazol-2-yl)-2,5-diphenyltetrazolium bromide [MTT]) leading to the false conclusion that CNTs are cytotoxic to human lung alveolar cells [220]. Pulskamp et al. also reported differences in toxicity results using 2 different assays, the MTT and 4-[3-(4-iodophenyl)-2-(4-nitrophenyl)-2H-5-tetrazolio]-1,3-benzene disulfonate (WST-1) assays [276]. CNTs have also been reported to interfere with other assays such as neutral red incorporation, lactate dehydrogenase, adenylate kinase release and ELISA [219, 291-292]. With all this in mind, we chose to use the [^{3}H]-Thymidine incorporation assay to determine the viability of cells following incubation with the CNTs. This assay had been validated before both by us and other groups [293-294] to ensure that it was compatible with nanotubes and that there was no false readout of cytotoxicity. In this project, the viability of cells cultured with nonbinding MAb-CNTs was indistinguishable from that of cells grown in the absence of CNTs. By contrast, cells cultured with targeted-CNTs did not proliferate as well due to receptor-mediated signaling of cell cycle arrest and/or cell death. This has been observed previously using cross-linking MAbs specific for different B cell surface markers and is therefore not surprising [295-296]. It is possible that there is extensive cross-linking of the target antigen by the CNT-bound MAbs and subsequent signaling of growth arrest and/or apoptosis. In support of this, we observed that after 12 hrs of incubation at 37^{o}C, there was massive clustering of Daudi cells treated with the RFB4-CNT (targeting CNT) and no NIR light. “Tissue-like” structures of cell aggregates were formed with large contact areas. In contrast, no aggregates and no inhibition of cell proliferation

occurred when cells were treated with the control RFT5-CNT (non-targeting CNT). This suggests that the homotypic cell adhesion and the concurrent inhibitory effect are receptor-dependent and MAb-related and do not involve any CNT-mediated non-specific adhesion or CNT-mediated toxicity. This demonstrates that the CNT conjugates described in this study are biocompatible with cells *in vitro*.

4.3 MAb-CNT conjugates displayed excellent specificity in targeting and thermal ablation of target cells *in vitro*

CNTs are thought by many to represent excellent therapeutic platforms in the biomedical field, due to their quasi-one-dimensional cylindrical structure, unique optical, electronic and mechanical properties, large aspect ratio, good cell penetration and the ability to be functionalized in a variety of ways. However, there are some concerns regarding their biocompatibility. The aggregation of hydrophobic CNTs and their metal contamination from the catalysts clearly contributes to their toxicity. These issues need to be resolved before CNTs can be used for the development of cancer therapeutics. CNTs also release substantial vibrational energy after being exposed to NIR light. This release of energy within a tissue produces localized heating that is sufficient to cause cell death.

Most modern cancer treatments require the cancer cell to affect its own death [297-298]. However, this drives the evolution of treatment-resistant cancer cell clones. In contrast, treatments that work regardless of the phenotypic diversity of the cancer cell, offer a means to kill off all or most of the cancer cells. Hyperthermia, or the use of selective heat for tumor ablation, represents one such therapy. It is a relatively noninvasive treatment for cancer. The critical temperature threshold in hyperthermic damage of 43^{o}C should be borne in mind as far as the clarification of the hyperthermic effect is concerned [22]. Malignant cells heated within the range of 41-43^{o}C are selectively destroyed by hyperthermia. At temperatures above 43^{o}C, selective heat destruction of malignant cells is more doubtful. Hyperthermic treatment between 41-43^{o}C leads to an increased lysosomal activity in the cytoplasm. Also, there is an inhibition of

respiratory metabolism without a similar depression of anaerobic glycolysis. This leads to a higher amount of lactic acid in the cytoplasm which leads to greater acidity. In the center of the tumor, where the exchange between intracellular fluid and blood is slow, this leads to increased lysosomal activity. There is also inhibition of RNA synthesis and later DNA synthesis and proliferation [22, 126, 299-300]. Membrane lipids also begin to melt at 43^{o}C affecting membrane integrity, integrin mobility, signaling, etc [29].

CNTs have the property of being able to release energy after being exposed to NIR light. This energy causes localized heating which can cause cell death. The use of NIR light in the 700- to 1100-nm range for the induction of hyperthermia is an attractive option because living tissues do not strongly absorb in this range [263]. Hemaglobin and water, the major absorbers of visible and infrared light respectively, have their lowest absorption coefficient in the NIR region [263]. Hence, an external NIR light source should effectively and safely penetrate normal tissue and ablate any cells to which the CNTs are attached. NIR light has been shown to travel at least 10 cm through breast tissue and 4 cm of skull/brain tissue or deep muscle using microwatt laser sources. With higher power levels, light has been shown to penetrate through 7 cm of muscle and neonatal skull/brain [263].

However, heat affects both healthy and cancerous tissue. To be successful as a therapeutic option, hyperthermia must be specifically targeted to tumor tissue and the nonspecific injury to the surrounding healthy tissue must be at a minimum. However, it is important to understand the thermoregulatory system in estimating heat exchange in hypo- and hyperthermic applications. For the most part, convective heat exchange dominates the heat balance in a tissue or organ. As determined by studies of the heart, following exercise and a subsequent increase in myocardial blood flow, a greater proportion of heat removal was carried out by the coronary venous system [15]. This heat transport should be considered when we consider the tumor tissue temperature following hyperthermic therapy. One could also consider different modes of laser exposure that might influence this heat exchange; short (nanosecond)

laser pulses that cause a local temperature of 150^{o}-300^{o}C with negligible heat disspiation, long continuous laser exposure with lower temperature increases (temperature of 43^{o}-65^{o}C) which is more effective for primary tumors with relatively large sizes due to greater heat distribution and the intermediate mode which accomplishes moderate temperature increases (temperature of 80^{o}-95^{o}C) with short exposure time to limit heat dissipation [301].

A great deal of research has been done on the delivery of macromolecules and small particles through tumor vasculature. Tumor vasculature shows enhanced vascular permeability with fenestrae sizes of 100 to 1200 nm [302]. Their structural irregularity, heterogeneity and leakiness are all very different from the structure of normal blood vessels [303]. This tumor architecture should facilitate extravasation, accumulation and retention of macromolecules in an effect known as the 'enhanced permeability and retention' (EPR) effect. However, we have chosen to also specifically target the CNTs to the tumor and that way use both the advantage of EPR and specific targeting on the CNTs. Furthermore, every cancer cell need not bind the targeting moiety due to the heat in the tumor mass generated by external exposure to NIR light.

To make the CNTs specific targeting agents, targeting moieties need to be linked to them. Specificity is critical because non-specific binding to antigen-negative cells *in vivo* could cause major side effects, a confounding issue in the cancer targeting field for > 25 years. The linker between the ligand and the CNTs is important for the overall performance of the conjugates. Previously, targeted CNTs that were used *in vitro* have been prepared using both covalent [243, 245, 304-306] and non-covalent [155, 179, 189, 264, 287-288, 307-309] methods. The concern of using noncovalently attached targeting ligands is that the targeting ligand might dissociate from the CNTs *in vivo*. Linkage stability and specific targeting can be achieved by covalent attachment of the targeting moiety to CNTs and that is why the project also attempted to generate covalently coupled MAb-CNT constructs.

The targeting agents used have been small molecules such as folate [179, 288, 309], cyclic peptides such as RGD [189], MAbs [155, 243, 264, 287, 304-305, 308] and

oligonucleotides [245]. The issue with small molecules, oligonucleotides and peptides is that many do not have the same specificity as MAbs. In this project, MAbs have been used as the targeting agent. MAb half-lives are much longer than those of small molecules. The $T_{1/2}$ of murine MAbs in normal mice ranges from 121 hr (IgG_{2b}) to 228 hr (IgG_3), in particular, 197 hr for the targeting MAbs used in this work (IgG_1), although the presence of the tumor could act as a sink for the injected MAbs and decrease their $T_{1/2}$ [310]. The idea is that the attachment of MAbs to CNTs might improve the $T_{1/2}$ of the CNTs and increase the chance to target the tumor. MAbs however, are less efficient for tumor penetration, tumor retention and blood clearance. [32, 311]. Also, the epitopes they target might be downregulated or shed and even when MAbs are humanized, they can cause immune reactions [312]. Directly adsorbing MAbs to CNTs as done by Shao et al. [264], while easy to execute, could be problematic because the weak interaction between the MAb and CNTs could result in the loss of the targeting MAbs. We observed that 50% collateral damage was mediated by the irrelevant MAb-CNT control after exposure to NIR light, possibly because of the loss of the MAb and non-specific binding by the CNTs. While Scheinberg et al. [243] have demonstrated specific targeting of their MAb-CNT constructs with both a control cell line and a control isotype-matched irrelevant MAb-CNT conjugate, their final goal was not thermal ablation of cells, so it is hard to determine if the covalent conjugation of the MAb to CNTs disturbed the NIR-absorption capabilities of the CNTs. Xiao et al. [304] have shown that CNTs with covalently conjugated MAbs are able to effectively ablate cells, thus showing that it is possible to covalently couple the MAbs to the CNTs, while still retaining the NIR absorption capabilities of the CNTs. However, both Xiao et al. and Zhou et al. [288] failed to use a control MAb-CNT conjugate with an irrelevant isotype-matched MAb to show the specificity of their targeted construct.

In this work, we showed that the RFB4-CNTs bound to the $CD22^+CD25^-$ Daudi cells and RFT5-CNTs bound to $CD22^-CD25^+$ PBMCs and induced cell death after NIR irradiation. RFB4-CNTs (anti-CD22-CNTs) did not bind to PBMCs, which do not express CD22 and RFT5-CNTs

(anti-CD25-CNTs) did not bind to Daudi cells which do not express high levels of CD25. Cell death required the simultaneous exposure of cells to both specifically targeted CNTs and NIR light.

Nonspecifically targeted MAb-CNTs, not bound to the cell surface, were rinsed away during washing thus preventing cell death after NIR irradiation. The *in vitro* studies demonstrate the ability of the targeted CNTs to bind specifically to and to induce thermal ablation of targeted cells following exposure to NIR light. This should prove to be an advantage *in vivo* since the specific binding of the MAb-CNTs to their target should facilitate increased uptake into the tumor. Though we have not determined if the MAb-CNTs can be internalized by their target cells, this factor will be relevant during thermal ablation. Recent studies have demonstrated that targeted nanoparticles may not mediate an increase in tumor accumulation when compared to non-targeted nanoparticles. However, targeted nanoparticles have better anti-tumor activity compared to non-targeted nanoparticles, due to enhanced internalization [46-50, 313]. This should also increase the specificity of the therapy *in vivo* as indicated by the ablation results *in vitro*, where only the cells bound by the targeted CNTs were killed, leaving the normal cells unharmed. This study found that there were no significant differences in the selectivity and killing efficiencies between the noncovalently and covalently coupled MAb-CNT conjugates *in vitro*.

4.4 Non-covalent MAb-CNT conjugates rapidly cleared the bloodstream and accumulated in the RES *in vivo*

The biggest challenge for targeting therapy is to translate specificity from *in vitro* to *in vivo* settings. In the latter, biodistribution and pharmacokinetics are major issues. Many targeted agents are taken up by the RES or fail to penetrate tumors. While they might be highly specific *in vitro*, unexpected cross reactions can occur *in vivo*. Furthermore, with a thermal ablation strategy such as that used here, penetration of NIR light into deep tumors is clearly an issue. Indeed these agents might find utility in the ablation of primary tumors that are not in the body

cavity, e.g. breast, melanoma and lymphoma. In addition CNTs are unlikely to be useful in metastatic sites.

CNTs exhibit unique size, shape and physical properties [145, 314]. Three categories of CNTs have been used in *in vivo* applications. First, are the pristine CNTs (produced materials that are so difficult to handle biologically because they are not dispersed in anything and they tend to aggregate because of their hydrophobic interactions) [253]. Second, are the CNTs coated with amphiphilic macromolecules (pristine CNTs coated with lipid-PEG conjugates, copolymers or surfactants) to improve water dispersability and solubility [251-252]. Third, are the covalently functionalized CNTs (pristine CNTs modified using cycloaddition reactions to attach ammonium groups or acid treatments to generate carboxylic groups) to reduce the degree of aggregation and improve debundling of the nanotube materials [251-252]. Comparing and contrasting reports involving the *in vivo* behavior of CNTs, has been confounded by the differences in experimental approaches. The CNTs used were of different dimensions and surface charges, were either SWNTs or MWNTs and had different kinds of functionalization resulting in large variations in the quality of dispersions. In addition they were administered by different routes, were quantified differently and they were monitored for different durations of time. However, some common themes emerged. For example, better covalent functionalization of CNTs of short lengths in dispersions of individual tubes resulted in urinary excretion and low organ accumulation, whereas CNTs that had been non-covalently coated were more likely to accumulate in the RES for long durations with slow excretion of non-degraded CNTs through the bile and fecal pathways.

Highly covalently surface-functionalized water dispersable SWNTs (diameter 1 – 10 nm; length 0.2 – 1 um) coupled to either DOTA [243, 245-246] or DTPA [247] were capable of rapid renal clearance and urinary excretion with a blood circulation half-life of a few hrs. This was also seen for surface-functionalized MWNTs (diameter 20 – 30 nm; length 0.5 – 2 um) coupled to DTPA [247] or DOTA [248] or glucosamine [249] or to no group [250]. This was observed by

Wang et al. using hydroxylated SWNTs (length < 0.6 um) [251-252]. There were varying levels of accumulation in all the above cases in the liver, lung and spleen where the whole body clearance was slow. However, the predominant excretion route was through the kidneys. Lacerda et al. emphasize the importance of nanotube shape in its excretion [250]. Using TEM they showed that CNTs translocated through the glomerular filter. Even though the length of the MWNTs was larger than the dimensions of the glomerular capillary wall (diameter of MWNTs 20 – 30 nm and length 0.5 – 2 um; glomerular capillary wall: diameter of fenestrae 30 nm, thickness of glomerular basement membrane 200-400 nm, epithelial podocyte slit 40 nm), it was believed that they acquired a spatial conformation in which the longitudinal CNT dimension was perpendicular to the endothelial fenestrations. Choi et al. [42] address the importance of nanoparticle size on renal excretion by considering different hydrodynamic diameters. They reported that renal filtration threshold for metal-based nanometer-sized objects was 5.5 nm and that zwitterionic coatings were most compatible with renal clearance.

In our own studies where we used non-covalently coupled MAb-CNT conjugates (length 0.2 - 1.4 μm), we found that the MAb-CNTs cleared the blood rapidly and accumulated predominantly in the RES. It is possible that the MAb-CNTs could have also distributed in other organs; however, the lower detection limit of our technique was 0.5 μg/ml and it is possible that the levels of accumulation in the other organs was below this limit. Indeed, in studies where SWNTs were non-covalently coated with surfactants, Pluronic F108 (diameter 1 nm; length 0.3 um) [158] or 1 wt% Tween 80 (diameter 10 – 30 nm; length 2 – 3 um) [201, 253], the liver [158] and the lungs [201, 253] were the predominant organs where the CNTs accumulated with uptake in other RES organs. SWNTs, non-covalently functionalized with phospholipid-PEG (PL-PEG) (diameter 1 – 5 nm, length 0.1 – 0.3 um), [193-194, 206] cleared the bloodstream rapidly and were taken up by the liver and spleen. However, it was also found that increasing the molecular weight of linear PEG from 2000 to 5000 or using branched PEG (MW 7000) increased the blood circulation time of the CNTs, decreased the levels of RES uptake and also

resulted in more rapid clearance of the CNTs from mouse organs [193-194] . We found that non-covalent PEGylation of our MAb-CNT constructs by PL-PEG (PEG MW 2000) was insufficient in prolonging the blood circulation time or preventing RES uptake. While we, Liu et al. and Schipper et al. used non-covalently PEGylated CNTs, Yang et al. [209] found that covalent PEGylation was a considerably more effective approach to improving the *in vivo* behavior of CNTs. They had the longest $T_{1/2}$ of 15.3 hrs of their covalently coupled PEG-CNTs *in vivo* and lower levels of uptake by the RES. Owens et al. [315] showed that covalently bound PEG chains achieve longer half-lives than similar particles with only surface adsorbed PEG. Sayes et al. [283] demonstrated that covalent functionalization could reduce the toxicity of CNTs. Cherukuri et al. [158] reported the detachment of non-covalently adsorbed molecules from the sidewall of CNTs *in vivo*. Hence, it appears that covalently PEGylating our constructs with either a larger MW or branched PEG polymer would have improved the performance of the CNTs *in vivo*.

While our study did not look into the long-term accumulation of CNTs *in vivo*, Yang et al. [201, 253] found that the levels of SWNTs in the lungs remained high at 90 days p.i. Deng et al. (length 10 nm – 0.6 um) [254-255] found that 80% of the ID of taurine-MWNTs accumulated in the liver 5 min after injection, and remained at that level for 28 days. 90 days following injection, the levels in the liver were still high at 20% ID. Georgin et al. [256] found that pristine MWNTs (diameter 20 – 70 nm, length 10 um) cleared the blood quickly and accumulated in the liver, lung and spleen where they remained for 14 days and at which point the study was terminated. Schipper et al. [206] showed Kupffer cell localization of their PL-PEG-CNT constructs and long-term (4 months) persistence of the CNTs in liver macrophages. Liu et al. [193] found appreciable levels of PL-PEG(2000)-CNTs in the liver and spleen at 7% ID/g even after 90 days following injection.

To determine the means of clearance of the CNTs, Liu et al. [193] found appreciable levels of PL-PEG-CNTs in the dry feces sample and in the intestine at 24 hrs p.i., revealing CNT

excretion through the biliary pathway. The CNTs were thought to be stable against biotransformation [254]. CNTs were also observed in the kidneys and bladder of the mice showing that some were also excreted through the renal pathway. Since the majority of the CNTs accumulated in the liver, the renal excretion accounted for a very small percentage of CNTs of very short lengths which were not aggregated. Liu et al. [193] suggest that CNTs with a very short length of less than 50 nm and diameter of 1-2 nm can be cleared by urinary excretion. We did not collect samples of urine and feces from our mice although our PL-PEG-CNTs were prepared in a manner similar to that of Liu et al. and probably behave similarly. Our results and those of Liu et al. differ from previous findings where the CNTs were reported to behave like small molecules and clear the body through the renal pathway without RES uptake [247, 252]. The dimensions of our CNTs (diameter 1 – 5 nm length 0.2 – 1.4 µm) were smaller than the CNT bundles (diameter 10 – 40 nm length 1 µm) used by Wang et al. and Singh et al. and it is known that RES uptake is size-dependent and is higher for larger sizes [316]. Hence, we disagree with Wang et al. and Singh et al. who reported that their CNT bundles behaved like small molecules.

In conclusion, this study showed that MAb-CNTs injected i.v. into mice were rapidly cleared by the RES. It is unknown if the PL-PEG coating still remained adsorbed on the CNTs *in vivo*, even though the results *in vitro* indicated its stability for up to 72 hrs in mouse serum.

4.5 The future of CNT therapy *in vivo*

Based on the results observed here, systemic administration of CNTs could result in a very low concentration at the tumor, in addition to increased toxicity to normal tissues due to the accumulation in the RES. We do not know whether the CNTs that accumulated in the tumor were there due to specific targeting. We also do not know if the MAb remained coupled to the CNTs *in vivo*. We did not determine how deeply into the tumor the targeted CNT construct had penetrated and if the MAb-CNTs had been internalized by the cancer cells. If systemic delivery of CNTs is required, this *in vivo* biodistribution must be improved by systematically optimizing the size and surface chemistry of the CNTs to minimize uptake by the RES.

Another way to deliver CNTs to the tumor is by direct i.t. injection. I.t. administration of CNTs does offer a way to achieve high levels of CNT in accessible local tumors without having to surgically remove the tumor and risk releasing tumor cells into the circulation. There have been significant advances in image-guided techniques that would allow more accurate and effective administration into tumors. Direct i.t. injection would ensure that there is minimized non-specific toxicity during thermal ablation due to reduced non-specific uptake by the RES.

APPENDIX A

OPTIMIZATION OF CNTs

In this appendix, we discuss the influence of shape, size and surface coating of CNTs on their clearance from the body. Without this clearance or their biodegradation into biologically non-toxic components within a reasonable timescale, toxicity is potentially amplified. To render CNTs viable for clinical translation, key design considerations that govern their behaviour *in vivo* need to be understood. Work done in the quantum dot field has defined the hydrodynamic diameter (HD) (with targeting ligands) and the surface charge of the quantum dots that enable their elimination through the kidneys [42, 317]. A similar strategy needs to be adopted for CNTs where a precise size-series of CNTs are designed whose ligand properties, ligand conjugation ratio, HD, stability and surface coatings are optimized such that we have tumor-specific targeting and the unbound CNTs are eliminated completely from the body.

It is important to keep in mind that renal excretion is a function of HD [42]. If there is no biodegradation *in vivo*, the other route of elimination is through the liver. This is an extremely slow and inefficient process which leads to large surface areas of tissue being exposed to the CNTs for long durations which could lead to toxicity. A recent study describes that CNTs can be degraded by neutrophil myeloperoxidase into short-chain carboxylated alkanes and alkenes *in vitro* [318]. While this degradation has not been demonstrated *in vivo*, it was shown that the biodegraded CNTs induce less pulmonary inflammation relative to non-degraded CNTs. This indicates that CNTs might undergo degradation *in vivo* into non-toxic compounds.

The aspect of the shape of the CNTs also has to be considered. Quantum dots are spherical structures and hence CNTs as cylindrical structures will need separate and comprehensive *in vivo* analysis.

REFERENCES

1. Jemal, A., et al., *Cancer statistics, 2009.* CA Cancer J Clin, 2009. **59**(4): p. 225-49.
2. Chabner, B.A. and T.G. Roberts, Jr., *Timeline: Chemotherapy and the war on cancer.* Nat Rev Cancer, 2005. **5**(1): p. 65-72.
3. *http://www.everydayhealth.com*.
4. ; Available from: www.cancer.gov/cancertopics/factsheet/Therapy/radiation
5. Brooks, K.J., *The anti-tumor activity of UV3, an anti-CD54 antibody, in SCID mice xenografted with a variety of human tumor cell lines*, in *Department of Immunology*. 2008, The University of Texas Southwestern Medical Center at Dallas: Dallas.
6. Gilman, A., *The initial clinical trial of nitrogen mustard.* Am J Surg, 1963. **105**: p. 574-8.
7. *http://training.seer.cancer.gov/treatment/*.
8. Henderson, A.R., *Temple Fay, M.D., Unconformable Crusader and Harbinger of Human Refrigeration 1895–1963.* Journal of Neurosurgery, 1963. **20**(7).
9. LAWRENCE W. SMITH, T.F., *TEMPERATURE FACTORS IN CANCER AND EMBRYONAL CELL GROWTH.* Journal of the American Medical Association, 1939. **113**(8): p. 653-660.
10. Fay, T., *Early Experiences with Local and Generalized Refrigeration of the Human Brain.* Journal of Neurosurgery, 1959. **16**(3).
11. Richard L. Lawton, N.L.L.a.W.S., *General hypothermia and survival following use of alkylating agent* Journal of Surgical Research, 1963. **3**(3): p. 159-161.
12. Masironi, V.P.P.a.R., *Effect of generalized hypothermia on normothermic tumors.* Am J Physiol, 1966. **211**(2): p. 462.
13. Masironi, V.P.P.a.R., *Disappearance of Normothermic Tumors in Shallow (30°C) Hypothermia.* Cancer Research, 1966. **26**: p. 863-864.
14. I. Yu. Chen, C.T.H., John Shun, Chien Chun Huang and Tak Wah Wong, *Hyperthermia hypothermia integration therapy (HIT): a potential new anti-cancer therapy.* Cell Biology International, 2008. **32**(3): p. S29-S30.
15. A.Shitzer, R.C.E.a., *Heat transfer in medicine and biology*. 1985: Springer.
16. Yot Navalitloha, E.S.S., Elizabeth N. Groothuis, Cathleen V. Allen, Robert M. Levy and Dennis R. Groothuis, *Therapeutic implications of tumor interstitial fluid pressure in subcutaneous RG-2 tumors.* Neuro-Oncology 2006. **8**(3): p. 227-233.
17. JOAN M. BULL, D.L., WILLIAM SCHUETTE, JACQUELINE WHANG-PENG, ROSALIE SMITH, GAITHER BYNUM, E. RONALD ATKINSON, JOHN S. GOTTDIENER, HARVEY R. GRALNICK, THOMAS H. SHAWKER, and VINCENT T. DeVITA, Jr, *Whole Body Hyperthermia: A Phase-I Trial of a Potential Adjuvant to Chemotherapy* Ann Intern Med, 1979. **90**: p. 7.
18. Bull, J.M., *An update on the anticancer effects of a combination of chemotherapy and hyperthermia.* Cancer Res, 1984. **44**(10 Suppl): p. 4853s-4856s.
19. Dahl, O., *Interaction of hyperthermia and chemotherapy.* Recent Results Cancer Res, 1988. **107**: p. 157-69.
20. Kim, J.H. and E.W. Hahn, *Clinical and biological studies of localized hyperthermia.* Cancer Res, 1979. **39**(6 Pt 2): p. 2258-61.
21. Wust, P., et al., *Hyperthermia in combined treatment of cancer.* Lancet Oncol, 2002. **3**(8): p. 487-97.
22. Overgaard, J., *Effect of hyperthermia on malignant cells in vivo. A review and a hypothesis.* Cancer, 1977. **39**(6): p. 2637-46.

23. Dewey, W.C., et al., *Cellular responses to combinations of hyperthermia and radiation.* Radiology, 1977. **123**(2): p. 463-74.
24. Overgaard, K. and J. Overgaard, *Radiation sensitizing effect of heat.* Acta Radiol Ther Phys Biol, 1974. **13**(6): p. 501-11.
25. Overgaard, K., and Overgaard, J. *Pathology of heat damage*. in *Proceedings International Symposium on Cancer Therapy by Hyperthermia and Radiation*.
26. Overgaard, J. and H.S. Poulsen, *Effect of hyperthermia and environmental acidity on the proteolytic activity in murine ascites tumor cells.* J Natl Cancer Inst, 1977. **58**(4): p. 1159-61.
27. Emami, B., et al., *Histopathological study on the effects of hyperthermia on microvasculature.* Int J Radiat Oncol Biol Phys, 1981. **7**(3): p. 343-8.
28. Emami, B. and C.W. Song, *Physiological mechanisms in hyperthermia: a review.* Int J Radiat Oncol Biol Phys, 1984. **10**(2): p. 289-95.
29. Eberhart, R.C., P. Chakravarty, Editor.
30. *http://www.pelvicdiseasesatoz.org/Resource-Center/Glossary.aspx*.
31. Zhang, J., P.L. Yang, and N.S. Gray, *Targeting cancer with small molecule kinase inhibitors.* Nat Rev Cancer, 2009. **9**(1): p. 28-39.
32. Imai, K. and A. Takaoka, *Comparing antibody and small-molecule therapies for cancer.* Nat Rev Cancer, 2006. **6**(9): p. 714-27.
33. Sharkey, R.M. and D.M. Goldenberg, *Targeted therapy of cancer: new prospects for antibodies and immunoconjugates.* CA Cancer J Clin, 2006. **56**(4): p. 226-43.
34. Weiner, L.M., *Building better magic bullets--improving unconjugated monoclonal antibody therapy for cancer.* Nat Rev Cancer, 2007. **7**(9): p. 701-6.
35. Allen, T.M., *Ligand-targeted therapeutics in anticancer therapy.* Nat Rev Cancer, 2002. **2**(10): p. 750-63.
36. Pastan, I., et al., *Immunotoxin therapy of cancer.* Nat Rev Cancer, 2006. **6**(7): p. 559-65.
37. Clynes, R.A., et al., *Inhibitory Fc receptors modulate in vivo cytoxicity against tumor targets.* Nat Med, 2000. **6**(4): p. 443-6.
38. Carter, P., *Improving the efficacy of antibody-based cancer therapies.* Nat Rev Cancer, 2001. **1**(2): p. 118-29.
39. Froidevaux, S. and A.N. Eberle, *Somatostatin analogs and radiopeptides in cancer therapy.* Biopolymers, 2002. **66**(3): p. 161-83.
40. Bawa, R., *Nanoparticle-based therapeutics in humans: a survey.* Nanotechnology Law and Business, 2008. **5**(2): p. 20.
41. Venturoli, D. and B. Rippe, *Ficoll and dextran vs. globular proteins as probes for testing glomerular permselectivity: effects of molecular size, shape, charge, and deformability.* Am J Physiol Renal Physiol, 2005. **288**(4): p. F605-13.
42. Choi, H.S., et al., *Renal clearance of quantum dots.* Nat Biotechnol, 2007. **25**(10): p. 1165-70.
43. Matsumura, Y. and H. Maeda, *A new concept for macromolecular therapeutics in cancer chemotherapy: mechanism of tumoritropic accumulation of proteins and the antitumor agent smancs.* Cancer Res, 1986. **46**(12 Pt 1): p. 6387-92.
44. Davis, M.E., Z.G. Chen, and D.M. Shin, *Nanoparticle therapeutics: an emerging treatment modality for cancer.* Nat Rev Drug Discov, 2008. **7**(9): p. 771-82.
45. Gatter, K.C., et al., *Transferrin receptors in human tissues: their distribution and possible clinical relevance.* J Clin Pathol, 1983. **36**(5): p. 539-45.
46. Bartlett, D.W., et al., *Impact of tumor-specific targeting on the biodistribution and efficacy of siRNA nanoparticles measured by multimodality in vivo imaging.* Proc Natl Acad Sci U S A, 2007. **104**(39): p. 15549-54.
47. Choi, C.H., et al., *Mechanism of active targeting in solid tumors with transferrin-containing gold nanoparticles.* Proc Natl Acad Sci U S A. **107**(3): p. 1235-40.

48. Farokhzad, O.C., et al., *Targeted nanoparticle-aptamer bioconjugates for cancer chemotherapy in vivo.* Proc Natl Acad Sci U S A, 2006. **103**(16): p. 6315-20.
49. Kirpotin, D.B., et al., *Antibody targeting of long-circulating lipidic nanoparticles does not increase tumor localization but does increase internalization in animal models.* Cancer Res, 2006. **66**(13): p. 6732-40.
50. Park, J.W., et al., *Anti-HER2 immunoliposomes: enhanced efficacy attributable to targeted delivery.* Clin Cancer Res, 2002. **8**(4): p. 1172-81.
51. Sapra, P. and T.M. Allen, *Internalizing antibodies are necessary for improved therapeutic efficacy of antibody-targeted liposomal drugs.* Cancer Res, 2002. **62**(24): p. 7190-4.
52. Ferrari, M., *Cancer nanotechnology: opportunities and challenges.* Nature Reviews Cancer, 2005. **5**(3): p. 161-171.
53. Cho, K., et al., *Therapeutic nanoparticles for drug delivery in cancer.* Clin Cancer Res, 2008. **14**(5): p. 1310-6.
54. Wang, X., et al., *Advances of cancer therapy by nanotechnology.* Cancer Res Treat, 2009. **41**(1): p. 1-11.
55. Wagner, V., et al., *The emerging nanomedicine landscape.* Nat Biotechnol, 2006. **24**(10): p. 1211-7.
56. Gabizon, A.A., *Stealth liposomes and tumor targeting: one step further in the quest for the magic bullet.* Clin Cancer Res, 2001. **7**(2): p. 223-5.
57. Matsumura, Y., et al., *Phase I and pharmacokinetic study of MCC-465, a doxorubicin (DXR) encapsulated in PEG immunoliposome, in patients with metastatic stomach cancer.* Ann Oncol, 2004. **15**(3): p. 517-25.
58. Laverman, P., et al., *Recognition and clearance of methoxypoly(ethyleneglycol)2000-grafted liposomes by macrophages with enhanced phagocytic capacity. Implications in experimental and clinical oncology.* Biochim Biophys Acta, 2001. **1526**(3): p. 227-9.
59. Gref, R., et al., *Biodegradable long-circulating polymeric nanospheres.* Science, 1994. **263**(5153): p. 1600-3.
60. Duncan, R., *Polymer conjugates as anticancer nanomedicines.* Nat Rev Cancer, 2006. **6**(9): p. 688-701.
61. Gradishar, W.J., *Albumin-bound nanoparticle paclitaxel.* Clin Adv Hematol Oncol, 2005. **3**(5): p. 348-9.
62. Gradishar, W.J., et al., *Phase III trial of nanoparticle albumin-bound paclitaxel compared with polyethylated castor oil-based paclitaxel in women with breast cancer.* J Clin Oncol, 2005. **23**(31): p. 7794-803.
63. Harris, J.M. and R.B. Chess, *Effect of pegylation on pharmaceuticals.* Nat Rev Drug Discov, 2003. **2**(3): p. 214-21.
64. Graham, M.L., *Pegaspargase: a review of clinical studies.* Adv Drug Deliv Rev, 2003. **55**(10): p. 1293-302.
65. Molineux, G., *The design and development of pegfilgrastim (PEG-rmetHuG-CSF, Neulasta).* Curr Pharm Des, 2004. **10**(11): p. 1235-44.
66. Iwai, K., H. Maeda, and T. Konno, *Use of oily contrast medium for selective drug targeting to tumor: enhanced therapeutic effect and X-ray image.* Cancer Res, 1984. **44**(5): p. 2115-21.
67. K. A. Delman, T.D.B., M. Thomas, C. M. Ensor, F. W. Holtsberg, J. S. Bomalaski, M. A. Clark and S. A. Curley, *Phase I/II trial of pegylated arginine deiminase (ADI-PEG20) in unresectable hepatocellular carcinoma.* Journal of Clinical Oncology, 2005. **23**(16S): p. 4139.
68. Wang, Y.S., et al., *Structural and biological characterization of pegylated recombinant interferon alpha-2b and its therapeutic implications.* Adv Drug Deliv Rev, 2002. **54**(4): p. 547-70.

69. Posey, J.A., 3rd, et al., *Phase 1 study of weekly polyethylene glycol-camptothecin in patients with advanced solid tumors and lymphomas.* Clin Cancer Res, 2005. **11**(21): p. 7866-71.
70. Homsi, J., et al., *Phase I trial of poly-L-glutamate camptothecin (CT-2106) administered weekly in patients with advanced solid malignancies.* Clin Cancer Res, 2007. **13**(19): p. 5855-61.
71. Singer, J.W., et al., *Poly-(L)-glutamic acid-paclitaxel (CT-2103) [XYOTAX], a biodegradable polymeric drug conjugate: characterization, preclinical pharmacology, and preliminary clinical data.* Adv Exp Med Biol, 2003. **519**: p. 81-99.
72. Duncan, R., *Designing polymer conjugates as lysosomotropic nanomedicines.* Biochem Soc Trans, 2007. **35**(Pt 1): p. 56-60.
73. Seymour, L.W., et al., *Hepatic drug targeting: phase I evaluation of polymer-bound doxorubicin.* J Clin Oncol, 2002. **20**(6): p. 1668-76.
74. Julyan, P.J., et al., *Preliminary clinical study of the distribution of HPMA copolymers bearing doxorubicin and galactosamine.* J Control Release, 1999. **57**(3): p. 281-90.
75. Heidel, J.D., et al., *Administration in non-human primates of escalating intravenous doses of targeted nanoparticles containing ribonucleotide reductase subunit M2 siRNA.* Proc Natl Acad Sci U S A, 2007. **104**(14): p. 5715-21.
76. Kabanov, V.A.a.A., *Block Copolymer-Based Formulations of Doxorubicin Effective Against Drug Resistant Tumours*, in *Biomedical Polymers and Polymer Therapeutics*. 2007, Springer US. p. 121-137.
77. Nakanishi, T., et al., *Development of the polymer micelle carrier system for doxorubicin.* J Control Release, 2001. **74**(1-3): p. 295-302.
78. Danson, S., et al., *Phase I dose escalation and pharmacokinetic study of pluronic polymer-bound doxorubicin (SP1049C) in patients with advanced cancer.* Br J Cancer, 2004. **90**(11): p. 2085-91.
79. Lee, K.S., et al., *Multicenter phase II trial of Genexol-PM, a Cremophor-free, polymeric micelle formulation of paclitaxel, in patients with metastatic breast cancer.* Breast Cancer Res Treat, 2008. **108**(2): p. 241-50.
80. Y. Yen, T.S., T. Schluep, J. Hwang, J. Oliver and M. E. Davis, *First-in-human phase I trial of a cyclodextrin-containing polymer-camptothecin nanoparticle in patients with solid tumors.* Journal of Clinical Oncology, 2007. **25**(18S).
81. Schluep, T., et al., *Preclinical efficacy of the camptothecin-polymer conjugate IT-101 in multiple cancer models.* Clin Cancer Res, 2006. **12**(5): p. 1606-14.
82. Dr. Donald A. Tomalia, D.A.M.N., Prof. William A. Goddard III, *Starburst Dendrimers: Molecular-Level Control of Size, Shape, Surface Chemistry, Topology, and Flexibility from Atoms to Macroscopic Matter.* Angewandte Chemie International Edition in English, 2003. **29**(2): p. 138-175.
83. Lai, P.S., et al., *Doxorubicin delivery by polyamidoamine dendrimer conjugation and photochemical internalization for cancer therapy.* J Control Release, 2007. **122**(1): p. 39-46.
84. Malik, N., E.G. Evagorou, and R. Duncan, *Dendrimer-platinate: a novel approach to cancer chemotherapy.* Anticancer Drugs, 1999. **10**(8): p. 767-76.
85. Ren Xi Zhuo, B.D.a.Z.R.L., *In vitro release of 5-fluorouracil with cyclic core dendritic polymer.* Journal of Controlled Release, 1999. **57**(3): p. 249-257.
86. Lee, C.C., et al., *A single dose of doxorubicin-functionalized bow-tie dendrimer cures mice bearing C-26 colon carcinomas.* Proc Natl Acad Sci U S A, 2006. **103**(45): p. 16649-54.
87. Bhadra D, B.S., Jain S, Jain NK, *A PEGylated dendritic nanoparticulate carrier of fluorouracil.* Int J Pharm., 2003. **257**(1-2): p. 111-124.
88. Quintana, A., et al., *Design and function of a dendrimer-based therapeutic nanodevice targeted to tumor cells through the folate receptor.* Pharm Res, 2002. **19**(9): p. 1310-6.

89. Kukowska-Latallo, J.F., et al., *Nanoparticle targeting of anticancer drug improves therapeutic response in animal model of human epithelial cancer.* Cancer Res, 2005. **65**(12): p. 5317-24.
90. Kobayashi, H. and M.W. Brechbiel, *Dendrimer-based macromolecular MRI contrast agents: characteristics and application.* Mol Imaging, 2003. **2**(1): p. 1-10.
91. Bruchez, M., Jr., et al., *Semiconductor nanocrystals as fluorescent biological labels.* Science, 1998. **281**(5385): p. 2013-6.
92. Alivisatos, P., *The use of nanocrystals in biological detection.* Nat Biotechnol, 2004. **22**(1): p. 47-52.
93. Jain, R.K. and M. Stroh, *Zooming in and out with quantum dots.* Nat Biotechnol, 2004. **22**(8): p. 959-60.
94. Howarth, M., et al., *Targeting quantum dots to surface proteins in living cells with biotin ligase.* Proc Natl Acad Sci U S A, 2005. **102**(21): p. 7583-8.
95. Alivisatos, A.P., W. Gu, and C. Larabell, *Quantum dots as cellular probes.* Annu Rev Biomed Eng, 2005. **7**: p. 55-76.
96. Bharali, D.J., et al., *Folate-receptor-mediated delivery of InP quantum dots for bioimaging using confocal and two-photon microscopy.* J Am Chem Soc, 2005. **127**(32): p. 11364-71.
97. Goldberg, M., R. Langer, and X. Jia, *Nanostructured materials for applications in drug delivery and tissue engineering.* J Biomater Sci Polym Ed, 2007. **18**(3): p. 241-68.
98. Kim, S.W., et al., *Engineering InAs(x)P(1-x)/InP/ZnSe III-V alloyed core/shell quantum dots for the near-infrared.* J Am Chem Soc, 2005. **127**(30): p. 10526-32.
99. Gu, H., et al., *Facile one-pot synthesis of bifunctional heterodimers of nanoparticles: a conjugate of quantum dot and magnetic nanoparticles.* J Am Chem Soc, 2004. **126**(18): p. 5664-5.
100. Zeev;, W.D.J.H.R.N.R., *Superparamagnetic Fe_2O_3 beads-CdSe/ZnS quantum dots core-shell nanocomposite particles for cell separation.* Nano Letters, 2004. **4**(3): p. 409-413.
101. Ballou, B., et al., *Noninvasive imaging of quantum dots in mice.* Bioconjug Chem, 2004. **15**(1): p. 79-86.
102. Larson, D.R., et al., *Water-soluble quantum dots for multiphoton fluorescence imaging in vivo.* Science, 2003. **300**(5624): p. 1434-6.
103. Stroh, M., et al., *Quantum dots spectrally distinguish multiple species within the tumor milieu in vivo.* Nat Med, 2005. **11**(6): p. 678-82.
104. Ballou, B., et al., *Sentinel lymph node imaging using quantum dots in mouse tumor models.* Bioconjug Chem, 2007. **18**(2): p. 389-96.
105. Gao, X., et al., *In vivo cancer targeting and imaging with semiconductor quantum dots.* Nat Biotechnol, 2004. **22**(8): p. 969-76.
106. Bagalkot, V., et al., *Quantum dot-aptamer conjugates for synchronous cancer imaging, therapy, and sensing of drug delivery based on bi-fluorescence resonance energy transfer.* Nano Lett, 2007. **7**(10): p. 3065-70.
107. Lovric, J., et al., *Unmodified cadmium telluride quantum dots induce reactive oxygen species formation leading to multiple organelle damage and cell death.* Chem Biol, 2005. **12**(11): p. 1227-34.
108. Cho, S.J., et al., *Long-term exposure to CdTe quantum dots causes functional impairments in live cells.* Langmuir, 2007. **23**(4): p. 1974-80.
109. Green, M., *Semiconductor quantum dots as biological imaging agents.* Angew Chem Int Ed Engl, 2004. **43**(32): p. 4129-31.
110. Choi, A.O., et al., *Quantum dot-induced cell death involves Fas upregulation and lipid peroxidation in human neuroblastoma cells.* J Nanobiotechnology, 2007. **5**: p. 1.
111. Craig F. Bohren, D.R.H., *Absorption and Scattering of Light by Small Particles*. 2004.

112. Halas, N. *Playing with Plasmons: Tuning the Optical Resonant Properties of Metallic Nanoshells*. in *Materials Research Society*. 2005.
113. Jain, P.K., et al., *Calculated absorption and scattering properties of gold nanoparticles of different size, shape, and composition: applications in biological imaging and biomedicine.* J Phys Chem B, 2006. **110**(14): p. 7238-48.
114. Jacques, S.L. and S.A. Prahl, *Modeling optical and thermal distributions in tissue during laser irradiation.* Lasers Surg Med, 1987. **6**(6): p. 494-503.
115. Sturesson, C. and S. Andersson-Engels, *A mathematical model for predicting the temperature distribution in laser-induced hyperthermia. Experimental evaluation and applications.* Phys Med Biol, 1995. **40**(12): p. 2037-52.
116. Welch, A.J., *The thermal response of laser irradiated tissue.* IEEE Journal of Quantum Electronics, 1984. **QE-20**(12): p. 1471-1481.
117. Ara, e.a., *Absorption of ns photoradiation of melanosomes generates acoustic waves and induces pigmented melanoma cell toxicity.* Photochem. Photobiol., 1988. **47**: p. 37s.
118. Chen, W.R., et al., *Chromophore-enhanced in vivo tumor cell destruction using an 808-nm diode laser.* Cancer Lett, 1995. **94**(2): p. 125-31.
119. Chen, W.R., et al., *Chromophore-enhanced laser-tumor tissue photothermal interaction using an 808-nm diode laser.* Cancer Lett, 1995. **88**(1): p. 15-9.
120. Pitsillides, C.M., et al., *Selective cell targeting with light-absorbing microparticles and nanoparticles.* Biophys. J., 2003. **84**(6): p. 4023-4032.
121. Zharov, V.P., et al., *Synergistic enhancement of selective nanophotothermolysis with gold nanoclusters: potential for cancer therapy.* Lasers Surg Med, 2005. **37**(3): p. 219-26.
122. Vladimir P. Zharov, V.G., and Mark Viegas, *Photothermal detection of local thermal effects during selective nanophotothermolysis.* Applied Physics Letters, 2003. **83**(4897).
123. Galitovskaya, V.P.Z.a.E., *Photothermal guidance for selective photothermolysis with nanoparticles.* Proc. SPIE, 2004. **5319**(291).
124. Boris Khlebtsov, V.Z., Andrei Melnikov, Valery Tuchin and Nikolai Khlebtsov, *Optical amplification of photothermal therapy with gold nanoparticles and nanoclusters.* Nanotechnology, 2006. **17**: p. 5167-5179.
125. El-Sayed, I.H., X. Huang, and M.A. El-Sayed, *Selective laser photo-thermal therapy of epithelial carcinoma using anti-EGFR antibody conjugated gold nanoparticles.* Cancer Lett, 2006. **239**(1): p. 129-35.
126. Huang, X., et al., *Determination of the minimum temperature required for selective photothermal destruction of cancer cells with the use of immunotargeted gold nanoparticles.* Photochem Photobiol, 2006. **82**(2): p. 412-7.
127. Sokolov, K., et al., *Real-time vital optical imaging of precancer using anti-epidermal growth factor receptor antibodies conjugated to gold nanoparticles.* Cancer Res, 2003. **63**(9): p. 1999-2004.
128. Sokolov, K., et al., *Optical systems for in vivo molecular imaging of cancer.* Technol Cancer Res Treat, 2003. **2**(6): p. 491-504.
129. El-Sayed, I.H., X. Huang, and M.A. El-Sayed, *Surface plasmon resonance scattering and absorption of anti-EGFR antibody conjugated gold nanoparticles in cancer diagnostics: applications in oral cancer.* Nano Lett, 2005. **5**(5): p. 829-34.
130. Hirsch, L.R., et al., *Nanoshell-mediated near-infrared thermal therapy of tumors under magnetic resonance guidance.* Proc Natl Acad Sci U S A, 2003. **100**(23): p. 13549-54.
131. Choi, M.R., et al., *A cellular Trojan Horse for delivery of therapeutic nanoparticles into tumors.* Nano Lett, 2007. **7**(12): p. 3759-65.
132. Loo, C., et al., *Immunotargeted Nanoshells for Integrated Cancer Imaging and Therapy.* Nano Letters, 2005. **5**(4): p. 709-711.

133. Lowery, A.R., et al., *Immunonanoshells for targeted photothermal ablation of tumor cells.* Int J Nanomedicine, 2006. **1**(2): p. 149-54.
134. Gobin, A.M., et al., *Near-infrared resonant nanoshells for combined optical imaging and photothermal cancer therapy.* Nano Lett, 2007. **7**(7): p. 1929-34.
135. Hirsch, L.R., et al., *Nanoshell-mediated near-infrared thermal therapy of tumors under magnetic resonance guidance.* Proceedings of the National Academy of Science U.S.A., 2003. **100**(23): p. 13549-13554.
136. O'Neal, D.P., et al., *Photo-thermal tumor ablation in mice using near infrared-absorbing nanoparticles.* Cancer Lett, 2004. **209**(2): p. 171-6.
137. Hao, E., G.C. Schatz, and J.T. Hupp, *Synthesis and optical properties of anisotropic metal nanoparticles.* J Fluoresc, 2004. **14**(4): p. 331-41.
138. Hao, E. and G.C. Schatz, *Electromagnetic fields around silver nanoparticles and dimers.* J Chem Phys, 2004. **120**(1): p. 357-66.
139. Huang, X., et al., *Cancer cell imaging and photothermal therapy in the near-infrared region by using gold nanorods.* J Am Chem Soc, 2006. **128**(6): p. 2115-20.
140. Kim, E., et al., *Synthesis of gold nanorod-embedded polymeric nanoparticles by a nanoprecipitation method for use as photothermal agents.* Nanotechnology, 2009. **20**(36): p. 365602.
141. Tong, L., et al., *Gold Nanorods Mediate Tumor Cell Death by Compromising Membrane Integrity.* Adv Mater Deerfield, 2007. **19**: p. 3136-3141.
142. Geoffrey von Maltzahn, J.-H.P., Amit Agrawal, Nanda Kishor Bandaru, Sarit K. Das, Michael J. Sailor and Sangeeta N. Bhatia, *Computationally Guided Photothermal Tumor Therapy Using Long-Circulating Gold Nanorod Antennas.* Cancer Research, 2009. **69**: p. 3982.
143. Park, J.H., et al., *Cooperative nanomaterial system to sensitize, target, and treat tumors.* Proc Natl Acad Sci U S A. **107**(3): p. 981-6.
144. Dai, H., *Carbon Nanotubes: Synthesis, Integration, and Properties.* Accounts of Chemical Research, 2002. **35**(12): p. 1035-1044.
145. Dresselhaus, M.S., H. Dai, and Editors, *Advances in Carbon Nanotubes. [In: MRS Bull., 2004; 29(4)]*. 2004. 59 pp.
146. Iijima, S., *Helical microtubules of graphitic carbon.* Nature, 1991. **354**: p. 56-58.
147. Dmitri Golberg, P.M.F.J.C., Masanori Mitome and Yoshio Bando, *Nanotubes in a gradient electric field as revealed by STM TEM technique* Nano Research, 2008. **1**(2): p. 166-175.
148. Weiwei Zhou, C.R.a.P.J.B., *Wafer scale synthesis of dense aligned arrays of single-walled carbon nanotubes.* Nano Research, 2008. **1**(2): p. 158-165.
149. Sander J. Tans, M.H.D., Hongjie Dai, Andreas Thess, Richard E. Smalley, L. J. Geerligs & Cees Dekker, *Individual single-wall carbon nanotubes as quantum wires.* Nature, 1997. **386**: p. 474-477.
150. Kam, N.W., et al., *Carbon nanotubes as multifunctional biological transporters and near-infrared agents for selective cancer cell destruction.* Proc Natl Acad Sci U S A, 2005. **102**(33): p. 11600-5.
151. Chakravarty, P., et al., *Thermal ablation of tumor cells with antibody-functionalized single-walled carbon nanotubes.* Proceedings of the National Academy of Sciences of the United States of America, 2008. **105**(25): p. 8697-8702.
152. Marches, R., et al., *Specific thermal ablation of tumor cells using single-walled carbon nanotubes targeted by covalently-coupled monoclonal antibodies.* Int J Cancer, 2009. **125**(12): p. 2970-7.
153. De la Zerda, A., et al., *Carbon nanotubes as photoacoustic molecular imaging agents in living mice.* Nat Nanotechnol, 2008. **3**(9): p. 557-62.

154. Cherukuri, P., et al., *Near-infrared fluorescence microscopy of single-walled carbon nanotubes in phagocytic cells.* Journal of the American Chemical Society, 2004. **126**(48): p. 15638-15639.
155. Welsher, K., et al., *Selective Probing and Imaging of Cells with Single Walled Carbon Nanotubes as Near-Infrared Fluorescent Molecules.* Nano Letters, 2008. **8**(2): p. 586-590.
156. O'Connell, M.J., et al., *Band gap fluorescence from individual single-walled carbon nanotubes.* Science, 2002. **297**(5581): p. 593-596.
157. Heller, D.A., et al., *Single-walled carbon nanotube spectroscopy in live cells: Towards long-term labels and optical sensors.* Advanced Materials (Weinheim, Germany), 2005. **17**(23): p. 2793-2799.
158. Cherukuri, P., et al., *Mammalian pharmacokinetics of carbon nanotubes using intrinsic near-infrared fluorescence.* Proc Natl Acad Sci U S A, 2006. **103**(50): p. 18882-6.
159. Leeuw, T.K., et al., *Single-Walled Carbon Nanotubes in the Intact Organism: Near-IR Imaging and Biocompatibility Studies in Drosophila.* Nano Letters, 2007. **7**(9): p. 2650-2654.
160. Jin, H., D.A. Heller, and M.S. Strano, *Single-Particle Tracking of Endocytosis and Exocytosis of Single-Walled Carbon Nanotubes in NIH-3T3 Cells.* Nano Letters, 2008. **8**(6): p. 1577-1585.
161. Barone, P.W., et al., *Near-infrared optical sensors based on single-walled carbon nanotubes.* Nature Materials, 2005. **4**(1): p. 86-92.
162. Barone, P.W., R.S. Parker, and M.S. Strano, *In vivo fluorescence detection of glucose using a single-walled carbon nanotube optical sensor: design, fluorophore properties, advantages, and disadvantages.* Anal Chem, 2005. **77**(23): p. 7556-62.
163. Jeng, E.S. and M.S. Strano, *The use of single walled carbon nanotubes for detection of DNA hybridization: Kinetics, thermodynamics, and applications.* Abstracts of Papers, 233rd ACS National Meeting, Chicago, IL, United States, March 25-29, 2007, 2007: p. INOR-085.
164. Rao, A.M., et al., *Diameter-selective Raman scattering from vibrational modes in carbon nanotubes.* Science (Washington, D. C.), 1997. **275**(5297): p. 187-191.
165. Heller, D.A., et al., *Using Raman Spectroscopy to Elucidate the Aggregation State of Single-Walled Carbon Nanotubes.* Journal of Physical Chemistry B, 2004. **108**(22): p. 6905-6909.
166. Niyogi, S., et al., *Chemistry of Single-Walled Carbon Nanotubes.* Accounts of Chemical Research, 2002. **35**(12): p. 1105-1113.
167. Coleman, K.S., et al., *Functionalization of single-walled carbon nanotubes via the Bingel reaction.* J Am Chem Soc, 2003. **125**(29): p. 8722-3.
168. Georgakilas, V., et al., *Organic functionalization of carbon nanotubes.* J Am Chem Soc, 2002. **124**(5): p. 760-1.
169. Tagmatarchis, N., et al., *Sidewall functionalization of single-walled carbon nanotubes through electrophilic addition.* Chem Commun (Camb), 2002(18): p. 2010-1.
170. Rosca, I., Watari, F, Uo, M, Akaska, T, *Oxidation of multiwalled carbon nanotubes by nitric acid.* Carbon, 2005. **43**(15): p. 3124-3131.
171. Liling Zeng, L.B.A., Christopher L. Edwards and Andrew R. Barron, *Demonstration of covalent sidewall functionalization of single wall carbon nanotubes by NMR spectroscopy: Side chain length dependence on the observation of the sidewall sp3 carbons* Nano Research, 2008. **1**(1): p. 72-88.
172. Lee KM, L.L., Dai L, *Asymmetric end-functionalization of multi-walled carbon nanotubes.* J Am Chem Soc., 2005. **27**(12): p. 4122-4123.
173. Minoo J. Moghaddam, S.T., Mei Gao, Shaoming Huang, Liming Dai, and Maxine J. McCall, *Highly Efficient Binding of DNA on the Sidewalls and Tips of Carbon Nanotubes Using Photochemistry.* Nano Letters, 2004. **4**(1): p. 89-93.

174. Tomokazu Umeyama, N.T., Mitsuru Fujita, Yoshihiro Matano,Norihiko Takeda, Kei Murakoshi, Kaname Yoshida, Seiji Isoda, and Hiroshi Imahori, *Retention of Intrinsic Electronic Properties of Soluble Single-Walled Carbon Nanotubes after a Significant Degree of Sidewall Functionalization by the Bingel Reaction.* J. Phys. Chem. C, 2007. **111**(27): p. 9734-9741.
175. Liu, Z., et al., *Preparation of carbon nanotube bioconjugates for biomedical applications.* Nat Protoc, 2009. **4**(9): p. 1372-82.
176. Chen, R.J., et al., *Noncovalent sidewall functionalization of single-walled carbon nanotubes for protein immobilization.* Journal of the American Chemical Society, 2001. **123**(16): p. 3838-3839.
177. Chen, J., et al., *Noncovalent engineering of carbon nanotube surfaces by rigid, functional conjugated polymers.* J Am Chem Soc, 2002. **124**(31): p. 9034-5.
178. Wu, P., et al., *Biocompatible carbon nanotubes generated by functionalization with glycodendrimers.* Angew Chem Int Ed Engl, 2008. **47**(27): p. 5022-5.
179. Kam, N.W.S., et al., *Carbon Nanotubes as multifunctional biological transporters and near-infrared agents for selective cancer cell destruction.* Proceedings of the National Academy of Science, 2005. **102**(33): p. 11600-11605.
180. Zheng, M., et al., *DNA-assisted dispersion and separation of carbon nanotubes.* Nature Materials, 2003. **2**(5): p. 338-342.
181. Zheng, X.T.a.M., *A DNA-based approach to the carbon nanotube sorting problem* Nano Research, 2008. **1**(3): p. 185-194.
182. Moon, H.K.C., C. I.; Lee, D. -K.; Choi, H. C, *Effect of nucleases on the cellular internalization of fluorescent labeled DNA-functionalized single-walled carbon nanotubes.* Nano Res., 2008. **1**: p. 351-360.
183. Chen, J. and C.P. Collier, *Noncovalent functionalization of single-walled carbon nanotubes with water-soluble porphyrins.* J Phys Chem B, 2005. **109**(16): p. 7605-9.
184. dirk m guldi, h.t., g.m.aminur rahman, nikos tagmatarchis, maurizio prato, *novel photoactive single-walled carbon nanotube-porphyrin polymer wraps: efficient and long-lived intracomplex charge separation.* Adv. Mater., 2005. **17**(7): p. 871-875.
185. Chen, R.J., et al., *Noncovalent functionalization of carbon nanotubes for highly specific electronic biosensors.* Proc Natl Acad Sci U S A, 2003. **100**(9): p. 4984-9.
186. Shim, M., et al., *Functionalization of carbon nanotubes for biocompatibility and biomolecular recognition.* Nano Letters, 2002. **2**(4): p. 285-288.
187. Richard, C., et al., *Supramolecular self-assembly of lipid derivatives on carbon nanotubes.* Science, 2003. **300**(5620): p. 775-8.
188. Howard Wang, W.Z., Derek L. Ho, Karen I. Winey, John E. Fischer, Charles J. Glinka, and Erik K. Hobbie, *Dispersing Single-Walled Carbon Nanotubes with Surfactants: A Small Angle Neutron Scattering Study.* Nano Letters, 2004. **4**(9): p. 1789-1793.
189. Liu, Z., et al., *Supramolecular Chemistry on Water-Soluble Carbon Nanotubes for Drug Loading and Delivery.* ACS Nano, 2007. **1**(1): p. 50-56.
190. Kam, N.W.S., Z. Liu, and H. Dai, *Functionalization of Carbon Nanotubes via Cleavable Disulfide Bonds for Efficient Intracellular Delivery of siRNA and Potent Gene Silencing.* Journal of the American Chemical Society, 2005. **127**(36): p. 12492-12493.
191. Liu, Z., et al., *siRNA delivery into human T cells and primary cells with carbon-nanotube transporters.* Angewandte Chemie, International Edition, 2007. **46**(12): p. 2023-2027.
192. Liu, Z., et al., *siRNA delivery into human T cells and primary cells with carbon-nanotube transporters.* Angew Chem Int Ed Engl FIELD Full Journal Title:Angewandte Chemie (International ed. in English), 2007. **46**(12): p. 2023-7.
193. Liu, Z., et al., *Circulation and long-term fate of functionalized, biocompatible single-walled carbon nanotubes in mice probed by Raman spectroscopy.* Proceedings of the National Academy of Sciences of the United States of America, Early Edition, 2008(Jan 29 2008): p. 1-6, 6 pp.

194. Liu, Z., et al., *In vivo biodistribution and highly efficient tumour targeting of carbon nanotubes in mice.* Nature Nanotechnology, 2007. **2**(1): p. 47-52.
195. Zhuang Liu, K.C., Corrine Davis, Sarah Sherlock, Qizhen Cao, Xiaoyuan Chen and Hongjie Dai, *Drug Delivery with Carbon Nanotubes for In vivo Cancer Treatment.* Cancer Research, 2008. **68**: p. 6652.
196. Zhuo Chen, S.M.T., Andrew P Goodwin, Michael G Kattah, Dan Daranciang, Xinran Wang, Guangyu Zhang, Xiaolin Li, Zhuang Liu, Paul J Utz, Kaili Jiang, Shoushan Fan & Hongjie Dai, *Protein microarrays with carbon nanotubes as multicolor Raman labels.* Nature Biotechnology, 2008. **26**: p. 1285-1292.
197. Zorbas, V., et al., *Preparation and Characterization of Individual Peptide-Wrapped Single-Walled Carbon Nanotubes.* Journal of the American Chemical Society, 2004. **126**(23): p. 7222-7227.
198. Dieckmann, G.R., et al., *Noncovalent functionalization of carbon nanotubes with designed amphiphilic peptides.* Abstracts of Papers, 227th ACS National Meeting, Anaheim, CA, United States, March 28-April 1, 2004, 2004: p. IEC-241.
199. Chin, S.-F., et al., *Amphiphilic helical peptide enhances the uptake of single-walled carbon nanotubes by living cells.* Experimental Biology and Medicine (Maywood, NJ, United States), 2007. **232**(9): p. 1236-1244.
200. Yehia, H.N., et al., *Single-walled carbon nanotube interactions with HeLa cells.* J. Nanobiotechnol., 2007. **5**(8): p. 8-58.
201. Yang, S.T., et al., *Long-term accumulation and low toxicity of single-walled carbon nanotubes in intravenously exposed mice.* Toxicol Lett, 2008. **181**(3): p. 182-9.
202. Chin, S.-F., et al., *Amphiphilic helical peptide enhances the uptake of single-walled carbon nanotubes by living cells.* Exp. Biol. Med., 2007. **232**: p. 1236-1244.
203. Chen, X., et al., *Interfacing Carbon Nanotubes with Living Cells.* Journal of the American Chemical Society, 2006. **128**(19): p. 6292-6293.
204. Chen, X., et al., *Biomimetic engineering of carbon nanotubes by using cell surface mucin mimics.* Angew Chem Int Ed Engl, 2004. **43**(45): p. 6111-6.
205. Wu, W., et al., *Targeted delivery of amphotericin B to cells by using functionalized carbon nanotubes.* Angewandte Chemie, International Edition, 2005. **44**(39): p. 6358-6362.
206. Schipper, M.L., et al., *A pilot toxicology study of single-walled carbon nanotubes in a small sample of mice.* Nat Nanotechnol, 2008. **3**(4): p. 216-21.
207. Dumortier, H., et al., *Functionalized carbon nanotubes are non-cytotoxic and preserve the functionality of primary immune cells.* Nano Letters, 2006. **6**(7): p. 1522-8.
208. Kam, N.W.S., et al., *Nanotube molecular transporters: internalization of carbon nanotube-protein conjugates into mammalian cells.* Journal of the American Chemical Society, 2004. **126**(22): p. 6850-6851.
209. Yang, S.T., et al., *Covalently PEGylated carbon nanotubes with stealth character in vivo.* Small, 2008. **4**(7): p. 940-4.
210. Ding, L., et al., *Molecular Characterization of the Cytotoxic Mechanism of Multiwall Carbon Nanotubes and Nano-Onions on Human Skin Fibroblast.* Nano Letters, 2005. **5**(12): p. 2448-2464.
211. Cui, D., et al., *Effect of single wall carbon nanotubes on human HEK293 cells.* Toxicology Letters, 2005. **155**(1): p. 73-85.
212. Muller, J., et al., *Respiratory toxicity of multi-wall carbon nanotubes.* Toxicology and Applied Pharmacology, 2005. **207**(3): p. 221-231.
213. Poland, C.A., et al., *Carbon nanotubes introduced into the abdominal cavity of mice show asbestos-like pathogenicity in a pilot study.* Nat Nanotechnol, 2008. **3**(7): p. 423-8.

214. Shvedova, A.A., et al., *Unusual inflammatory and fibrogenic pulmonary responses to single-walled carbon nanotubes in mice.* American Journal of Physiology, 2005. **289**(5, Pt. 1): p. L698-L708.
215. Warheit, D.B., et al., *Comparative Pulmonary Toxicity Assessment of Single-wall Carbon Nanotubes in Rats.* Toxicological Sciences, 2004. **77**(1): p. 117-125.
216. Lam, C.W., et al., *Pulmonary toxicity of single-wall carbon nanotubes in mice 7 and 90 days after intratracheal instillation.* Toxicol Sci, 2004. **77**(1): p. 126-34.
217. Lifeng Dong, K.L.J., Colette M Witkowski and Michael M Craig, *Cytotoxicity of single-walled carbon nanotubes suspended in various surfactants.* Nanotechnology 2008. **19**.
218. D L Plata, P.M.G.a.C.M.R., *Industrially synthesized single-walled carbon nanotubes: compositional data for users, environmental risk assessments, and source apportionment.* Nanotechnology, 2008. **19**.
219. A. Casey, E.H., M. Davoren, F.M. Lyng, H.J. Byrne and G. Chambers, *Spectroscopic analysis confirms the interactions between single walled carbon nanotubes and various dyes commonly used to assess cytotoxicity.* Carbon, 2007. **45**(7): p. 1425-1432.
220. Worle-Knirsch, J.M., K. Pulskamp, and H.F. Krug, *Oops they did it again! Carbon nanotubes hoax scientists in viability assays.* Nano Letters, 2006. **6**(6): p. 1261-8.
221. Salvador-Morales, C., et al., *Complement activation and protein adsorption by carbon nanotubes.* Molecular Immunology, 2006. **43**(3): p. 193-201.
222. Kam, N.W.S. and H. Dai, *Carbon Nanotubes as Intracellular Protein Transporters: Generality and Biological Functionality.* J. Am. Chem. Soc., 2005. **127**(16): p. 6021-6026.
223. Pantarotto, D., et al., *Translocation of bioactive peptides across cell membranes by carbon nanotubes.* Chemical Communications (Cambridge, United Kingdom), 2004(1): p. 16-17.
224. Kostarelos, K., et al., *Cellular uptake of functionalized carbon nanotubes is independent of functional group and cell type.* Nature Nanotechnology, 2007. **2**(2): p. 108-113.
225. Bianco, A., et al., *Biomedical applications of functionalized carbon nanotubes.* Chemical Communications (Cambridge, United Kingdom), 2005(5): p. 571-577.
226. Ali-Boucetta, H., et al., *Multiwalled carbon nanotube-doxorubicin supramolecular complexes for cancer therapeutics.* Chemical Communications (Cambridge, United Kingdom), 2008(4): p. 459-461.
227. Murakami, T., et al., *Solubilization of single-wall carbon nanohorns using a PEG-doxorubicin conjugate.* Mol Pharm, 2006. **3**(4): p. 407-14.
228. Marshall, E., *Clinical research. Gene therapy a suspect in leukemia-like disease.* Science, 2002. **298**(5591): p. 34-5.
229. Feazell, R.P., et al., *Soluble Single-Walled Carbon Nanotubes as Longboat Delivery Systems for Platinum(IV) Anticancer Drug Design.* Journal of the American Chemical Society, 2007. **129**(27): p. 8438-8439.
230. Pastorin, G., et al., *Double functionalization of carbon nanotubes for multimodal drug delivery.* Chemical Communications (Cambridge, United Kingdom), 2006(11): p. 1182-1184.
231. Liu, Z., et al., *PEGylated nanographene oxide for delivery of water-insoluble cancer drugs.* J Am Chem Soc, 2008. **130**(33): p. 10876-7.
232. Xiaoming Sun, Z.L., Kevin Welsher, Joshua Tucker Robinson, Andrew Goodwin, Sasa Zaric and Hongjie Dai *Nano-graphene oxide for cellular imaging and drug delivery* Nano Research, 2008. **1**(3): p. 203-212.
233. Li, L.J., et al., *Diameter-selective encapsulation of metallocenes in single-walled carbon nanotubes.* Nat Mater, 2005. **4**(6): p. 481-5.
234. H. Kataura, Y.M., T. Kodama, K. Kikuchi, K. Hirahara, K. Suenaga, S. Iijima, S. Suzuki, Y. Achiba and W. Krätschmer, *High-yield fullerene encapsulation in single-wall carbon nanotubes* Synthetic Metals, 2001. **121**(1-3): p. 1195-1196.

235. G. -H. Jeong, A.A.F., R. Hatakeyama, T. Hirata, T. Yaguchi, K. Tohji, H. Mizuseki, and Y. Kawazoe, *Cesium encapsulation in single-walled carbon nanotubes via plasma ion irradiation: Application to junction formation and ab initio investigation.* Phys. Rev. B, 2003. **68**(7).
236. T. Kaneko , T.O., R. Hatakeyama, *DNA Encapsulation Inside Carbon Nanotubes Using Micro Electrolyte Plasmas.* Contributions to Plasma Physics, 2007. **47**(1-2): p. 57-63.
237. Gao, L., et al., *Carbon nanotube delivery of the GFP gene into mammalian cells.* ChemBioChem, 2006. **7**(2): p. 239-42.
238. Singh, R., et al., *Binding and Condensation of Plasmid DNA onto Functionalized Carbon Nanotubes: Toward the Construction of Nanotube-Based Gene Delivery Vectors.* Journal of the American Chemical Society, 2005. **127**(12): p. 4388-4396.
239. Pantarotto, D., et al., *Functionalized carbon nanotubes for plasmid DNA gene delivery.* Angewandte Chemie, International Edition, 2004. **43**(39): p. 5242-5246.
240. Mello, C.C. and D. Conte, Jr., *Revealing the world of RNA interference.* Nature, 2004. **431**(7006): p. 338-42.
241. Zhang, Z., et al., *Delivery of telomerase reverse transcriptase small interfering RNA in complex with positively charged single-walled carbon nanotubes suppresses tumor growth.* Clin Cancer Res, 2006. **12**(16): p. 4933-9.
242. Dhar, S., et al., *Targeted single-wall carbon nanotube-mediated Pt(IV) prodrug delivery using folate as a homing device.* J Am Chem Soc, 2008. **130**(34): p. 11467-76.
243. McDevitt, M.R., et al., *Tumor targeting with antibody-functionalized, radiolabeled carbon nanotubes.* J Nucl Med, 2007. **48**(7): p. 1180-9.
244. Liu, Z., et al., *Multiplexed multicolor Raman imaging of live cells with isotopically modified single walled carbon nanotubes.* J Am Chem Soc, 2008. **130**(41): p. 13540-1.
245. Villa, C.H., et al., *Synthesis and biodistribution of oligonucleotide-functionalized, tumor-targetable carbon nanotubes.* Nano Lett, 2008. **8**(12): p. 4221-8.
246. McDevitt, M.R., et al., *PET imaging of soluble yttrium-86-labeled carbon nanotubes in mice.* PLoS One, 2007. **2**(9): p. e907.
247. Singh, R., et al., *Tissue biodistribution and blood clearance rates of intravenously administered carbon nanotube radiotracers.* Proceedings of the National Academy of Sciences of the United States of America, 2006. **103**(9): p. 3357-3362.
248. L. Lacerda, A.S., R. Singh, G. Pastorin, K. T. Al-Jamal, J. Turton, P. Frederik, M. A. Herrero, S. Li, A. Bao, D. Emfietzoglou, S. Mather, W. T. Phillips, M. Prato, A. Bianco, B. Goins, K. Kostarelos *Dynamic Imaging of Functionalized Multi-Walled Carbon Nanotube Systemic Circulation and Urinary Excretion.* Advanced Materials, 2007. **20**(2): p. 225-230.
249. Guo, J., et al., *Biodistribution of functionalized multiwall carbon nanotubes in mice.* Nucl Med Biol, 2007. **34**(5): p. 579-83.
250. Lacerda, L., et al., *Carbon-nanotube shape and individualization critical for renal excretion.* Small, 2008. **4**(8): p. 1130-2.
251. Jing Wang, X.D., Shengtao Yang, Haifang Wang, PhD, Yuliang Zhaoand Yuanfang Liu, *Rapid translocation and pharmacokinetics of hydroxylated single-walled carbon nanotubes in mice.* Nanotoxicology, 2008. **2**(1): p. 28-32.
252. Wang H, W.J., Deng X, Sun H, Shi Z, Gu Z, Liu Y, Zhao Y., *Biodistribution of carbon single-wall carbon nanotubes in mice.* J Nanosci Nanotechnol., 2004. **4**(8): p. 1019-1024.
253. Yang, S.-T., et al., *Biodistribution of Pristine Single-Walled Carbon Nanotubes In Vivo.* Journal of Physical Chemistry C, 2007. **111**(48): p. 17761-17764.
254. X. Deng, G.J., H. Wang, H. Sun, X. Wang, S. Yang, T. Wang and Y. Liu, *Translocation and fate of multi-walled carbon nanotubes in vivo* Carbon, 2007. **45**(7): p. 1419-1424.

255. Xiaoyong Deng, S.Y., Haiyu Nie, Haifang Wang and Yuanfang Liu, *A generally adoptable radiotracing method for tracking carbon nanotubes in animals.* Nanotechnology, 2008. **19**.
256. Georgin, D., et al., *Preparation of (14)C-labeled multiwalled carbon nanotubes for biodistribution investigations.* J Am Chem Soc, 2009. **131**(41): p. 14658-9.
257. Schnyder A, K.S., Torok M, Drewe J, Huwyler J, *Targeting of skeletal muscle in vitro using biotinylated immunoliposomes.* Biochem J, 2004. **377**: p. 61-67.
258. Ghetie V, T.P., Ghetie MA,Knowles P,Uhr JW,Vitetta ES, *The GLP large scale preparation of immunotoxins containing deglycosylated ricin A chain and a hindered disulfide bond.* J Immunol Methods, 1991. **142**: p. 223-230.
259. Engert A, M.G., Amlot P,Wijdenes J,Diehl V,Thorpe P, *Immunotoxins constructed with anti-CD25 monoclonal antibodies and deglycosylated ricin A-chain have potent anti-tumour effects against human Hodgkin cells in vitro and solid Hodgkin tumours in mice.* Int J Cancer, 1991. **49**: p. 450-456.
260. Hoff, J., *Methods of blood collection in the mouse.* Lab Animal, 2000. **29**(10): p. 47-53.
261. Diamandis, E.P. and T.K. Christopoulos, *The biotin-(strept)avidin system: principles and applications in biotechnology.* Clin Chem, 1991. **37**(5): p. 625-36.
262. Gobin, A.M., et al., *Near-Infrared Resonant Nanoshells for Combined Optical Imaging and Photothermal Cancer Therapy.* Nano Letters, 2007. **7**(7): p. 1929-1934.
263. Weissleder, R., *A clearer vision for in vivo imaging.* Nat Biotechnol, 2001. **19**(4): p. 316-7.
264. ning shao, s.l., eric wickstrom, balaji panchapakesan, *Integrated molecular targeting of IGf1R and Her2 surface receptors and destruction of breast cancer cells using single wall carbon nanotubes.* Nanotechnology, 2007. **18**.
265. Chakravarty, P., et al., *Thermal ablation of tumor cells with antibody-functionalized single-walled carbon nanotubes.* Proc Natl Acad Sci U S A, 2008. **105**(25): p. 8697-702.
266. Tasis, D., et al., *Soluble carbon nanotubes.* Chem. Eur. J., 2003. **9**(17): p. 4000-8.
267. Tasis, D., et al., *Chemistry of carbon nanotubes.* Chemical Reviews, 2006. **106**(3): p. 1105-36.
268. Lin, Y., et al., *Advances toward bioapplications of carbon nanotubes.* J. Mater. Chem., 2004. **14**(4): p. 527-541.
269. Bahr, J.L. and J.M. Tour, *Covalent chemistry of single-wall carbon nanotubes.* Journal of Materials Chemistry, 2002. **12**(7): p. 1952-1958.
270. Sun, Y.-P., et al., *Functionalized carbon nanotubes: properties and applications.* Accounts of Chemical Research, 2002. **35**(12): p. 1096-1104.
271. Kostarelos, K., et al., *Carbon nanotube-mediated delivery of peptides and genes to cells: Translating nanobiotechnology to therapeutics.* Journal of Drug Delivery Science and Technology, 2005. **15**(1): p. 41-47.
272. Alexis, F., et al., *Factors affecting the clearance and biodistribution of polymeric nanoparticles.* Mol Pharm, 2008. **5**(4): p. 505-15.
273. Frautschi JR, E.R., Hubbell JA, *Alkylated cellulosic membranes with enhanced albumin affinity: influence of competing proteins.* J Biomater Sci Polym Ed., 1995. **7**(7): p. 12.
274. ROBERT C. EBERHART, MICHAEL E. LYNCH, , FERTAC H. BILGE, , JOHN F. WISSINGER2, , MARK S. MUNRO, , STEPHEN R. ELLSWORTH, and , ALFRED J. QUATTRONE, *Protein Adsorption on Polymers*

Visualization, Study of Fluid Shear and Roughness Effects, and Methods to Enhance Albumin Binding, in *Biomaterials: Interfacial Phenomena and Applications*. 1982. p. 22.
275. Kagan, V.E., et al., *Direct and indirect effects of single walled carbon nanotubes on RAW 264.7 macrophages: role of iron.* Toxicol Lett, 2006. **165**(1): p. 88-100.
276. Pulskamp, K., S. Diabate, and H.F. Krug, *Carbon nanotubes show no sign of acute toxicity but induce intracellular reactive oxygen species in dependence on contaminants.* Toxicol Lett, 2007. **168**(1): p. 58-74.

277. Massimo Bottini, S.B., Konstantina Nika, Nunzio Bottini, Stefano Bellucci, Andrea Magrini, Antonio Bergamaschi and Tomas Mustelin, *Multi-walled carbon nanotubes induce T lymphocyte apoptosis.* Toxicology Letters, 2006. **160**(2): p. 121-126.
278. Manna, S.K., et al., *Single-Walled Carbon Nanotube Induces Oxidative Stress and Activates Nuclear Transcription Factor-kB in Human Keratinocytes.* Nano Letters, 2005. **5**(9): p. 1676-1684.
279. Monteiro-Riviere, N.A., et al., *Multi-walled carbon nanotube interactions with human epidermal keratinocytes.* Toxicology Letters, 2005. **155**(3): p. 377-384.
280. al., W.e., *The degree and kind of agglomeration affect carbon nanotube cytotoxicity.* Toxicology Letters, 2007. **168**: p. 121-131.
281. al., R.e., *Impact of carbon nanotube exposure, dosage and aggregation on smooth muscle cells.* Toxicology Letters, 2007. **169**: p. 51-63.
282. al., D.e., *Molecular characterization of the cytotoxic mechanism of multiwalled carbon nanotubes and nano-onions on human skin fibroblast.* Nano Letters, 2005. **5**(12): p. 2448-2464.
283. Sayes, C.M., et al., *Functionalization density dependence of single-walled carbon nanotubes cytotoxicity in vitro.* Toxicology Letters, 2006. **161**(2): p. 135-142.
284. al, T.e., *Cytotoxicity of single-wall carbon nanotubes on human fibroblasts.* Toxicology in vitro, 2006. **20**(7): p. 1202-1212.
285. Magrez, A., et al., *Cellular Toxicity of Carbon-Based Nanomaterials.* Nano Letters, 2006. **6**(6): p. 1121-1125.
286. Kagan, V.E., et al., *Direct and indirect effects of single walled carbon nanotubes on RAW 264.7 macrophages: Role of iron.* Toxicology Letters, 2006. **165**(1): p. 88-100.
287. Ou, Z., et al., *Functional single-walled carbon nanotubes based on an integrin alpha v beta 3 monoclonal antibody for highly efficient cancer cell targeting.* Nanotechnology, 2009. **20**(10): p. 105102.
288. Zhou, F., et al., *Cancer photothermal therapy in the near-infrared region by using single-walled carbon nanotubes.* J Biomed Opt, 2009. **14**(2): p. 021009.
289. Prato, N.T.a.M., *Functionalization of carbon nanotubes via 1,3-dipolar cycloadditions.* J. Mater. Chem., 2004. **14**: p. 437-439.
290. Zijiong Lia, B.Z., Ping Liu, Bo Zhao, Da Chen and Yafei Zhang, *Synthesis of high-quality single-walled carbon nanotubes by high-frequency-induction heating.* Physica E: Low-dimensional Systems and nanostructures, 2008. **40**(3): p. 5.
291. Davoren, M. and A.M. Fogarty, *In vitro cytotoxicity assessment of the biocidal agents sodium o-phenylphenol, sodium o-benzyl-p-chlorophenol, and sodium p-tertiary amylphenol using established fish cell lines.* Toxicol In Vitro, 2006. **20**(7): p. 1190-201.
292. Monteiro-Riviere, N.A. and A.O. Inman, *Challenges for assessing carbon nanomaterial toxicity to the skin.* Carbon, 2006. **44**(6): p. 1070-1078.
293. Bianco, A., et al., *Cationic carbon nanotubes bind to CpG oligodeoxynucleotides and enhance their immunostimulatory properties.* Journal of the American Chemical Society, 2005. **127**(1): p. 58-59.
294. Marquis, B.J., et al., *Analytical methods to assess nanoparticle toxicity.* Analyst, 2009. **134**(3): p. 425-39.
295. Ghetie, M.A., et al., *Anti-CD19 inhibits the growth of human B-cell tumor lines in vitro and of Daudi cells in SCID mice by inducing cell cycle arrest.* Blood, 1994. **83**(5): p. 1329-36.
296. Marches, R., R.H. Scheuermann, and J.W. Uhr, *Cancer dormancy: role of cyclin-dependent kinase inhibitors in induction of cell cycle arrest mediated via membrane IgM.* Cancer Res, 1998. **58**(4): p. 691-7.
297. Pommier, Y., et al., *Apoptosis defects and chemotherapy resistance: molecular interaction maps and networks.* Oncogene, 2004. **23**(16): p. 2934-49.

298. Gottesman, M.M., *Mechanisms of cancer drug resistance.* Annu Rev Med, 2002. **53**: p. 615-27.
299. Nikfarjam, M., V. Muralidharan, and C. Christophi, *Mechanisms of focal heat destruction of liver tumors.* J Surg Res, 2005. **127**(2): p. 208-23.
300. Huang, X., et al., *Plasmonic photothermal therapy (PPTT) using gold nanoparticles.* Lasers Med Sci, 2008. **23**(3): p. 217-28.
301. Biris AS, B.D., Palmer J, Monroe WT, Mahmood M, Dervishi E, Xu Y, Li Z, Galanzha EI, Zharov VP., *Nanophotothermolysis of multiple scattered cancer cells with carbon nanotubes guided by time-resolved infrared thermal imaging.* J Biomed Opt, 2009. **14**(2).
302. Moreira, J.N., R. Gaspar, and T.M. Allen, *Targeting Stealth liposomes in a murine model of human small cell lung cancer.* Biochim Biophys Acta, 2001. **1515**(2): p. 167-76.
303. Hashizume, H., et al., *Openings between defective endothelial cells explain tumor vessel leakiness.* Am J Pathol, 2000. **156**(4): p. 1363-80.
304. Xiao, Y., et al., *Anti-HER2 IgY antibody-functionalized single-walled carbon nanotubes for detection and selective destruction of breast cancer cells.* BMC Cancer, 2009. **9**: p. 351.
305. Bhirde, A.A., et al., *Targeted killing of cancer cells in vivo and in vitro with EGF-directed carbon nanotube-based drug delivery.* ACS Nano, 2009. **3**(2): p. 307-16.
306. Elena Heistera, V.N., Carmen Tîlmaciu, Kamil Lipert, Vanesa Sanz Beltrán, Helen M. Coley, S. Ravi P. Silva and Johnjoe McFadden, *Triple functionalisation of single-walled carbon nanotubes with doxorubicin, a monoclonal antibody, and a fluorescent marker for targeted cancer therapy* Carbon, 2009. **47**(9): p. 2152-2160.
307. Denardo, S.J., et al., *111In-LLP2A-DOTA Polyethylene Glycol-Targeting {alpha}4{beta}1 Integrin: Comparative Pharmacokinetics for Imaging and Therapy of Lymphoid Malignancies.* J Nucl Med, 2009. **50**(4): p. 625-34.
308. Elkin, T., et al., *Immuno-carbon nanotubes and recognition of pathogens.* ChemBioChem, 2005. **6**(4): p. 640-643.
309. Kang, B., et al., *Cancer-cell targeting and photoacoustic therapy using carbon nanotubes as "bomb" agents.* Small, 2009. **5**(11): p. 1292-301.
310. Zuckier, L.S., L.D. Rodriguez, and M.D. Scharff, *Immunologic and pharmacologic concepts of monoclonal antibodies.* Semin Nucl Med, 1989. **19**(3): p. 166-86.
311. http://www.medscape.com/viewarticle/550008_3.
312. Derycke, A.S. and P.A. de Witte, *Liposomes for photodynamic therapy.* Adv Drug Deliv Rev, 2004. **56**(1): p. 17-30.
313. Gu, F., et al., *Precise engineering of targeted nanoparticles by using self-assembled biointegrated block copolymers.* Proc Natl Acad Sci U S A, 2008. **105**(7): p. 2586-91.
314. Dai, H., *Carbon nanotubes: opportunities and challenges.* Surface Science, 2002. **500**(1-3): p. 218-241.
315. Owens, D.E., 3rd and N.A. Peppas, *Opsonization, biodistribution, and pharmacokinetics of polymeric nanoparticles.* Int J Pharm, 2006. **307**(1): p. 93-102.
316. Moghimi, S.M., A.C. Hunter, and J.C. Murray, *Nanomedicine: current status and future prospects.* FASEB J, 2005. **19**(3): p. 311-30.
317. Hak Soo Choi, W.L., Fangbing Liu, Khaled Nasr, Preeti Misra, Moungi G. Bawendi & John V. Frangioni, *Design considerations for tumour-targeted nanoparticles.* Nature Nanotechnology, 2010. **5**: p. 6.
318. al, K.e., *Carbon nanotubes degraded by neutophil myeloperoxidase induce less pulmonary inflammation.* Nature Nanotechnology, 2010.

BIOGRAPHICAL STATEMENT

Pavitra Chakravarty was born in Chennai, India on October 19, 1973. After graduating from Mount Carmel College in Bangalore, India in 1991, she entered R. V. College of Engineering in Bangalore, India. In Fall 1995, she earned a Bachelor of Engineering (B.E.) degree in Computer Science Engineering (CSE). Following this, she worked in software industry in India, Switzerland and U.S for six and a half years on Enterprise Resource Planning (ERP) and Enterprise Application Integration (EAI) packages.

In Summer 2002, Pavitra started as a research technician in the Center for Biomedical Inventions (CBI) under Dr Stephen Johnston at UT Southwestern Medical Center. She worked with a postdoc Dr Tsukasa Oyama on isolating lung tumor-specific peptides from a peptide library using the phage display approach in Dr Kathlynn Brown's laboratory.

In Summer 2003 Pavitra entered the Biomedical Engineering graduate program at the University of Texas at Arlington in Dallas, Texas, and began her work in Dr. Ellen Vitetta's laboratory in December 2004. Her collaborative research led to two journal articles.

During her time in Dr Vitetta's laboratory, Pavitra served as a conference leader for the immunology module of the Medical Microbiology course in 2006, and she mentored two students in the SURF program.

Pavitra has no siblings. In February 1999, Pavitra married Srinath Chakravarty of Bangalore, India. They have one child, a son Raman, born on September 7, 2009.